Nanoscale force sensors to study supramolecular systems

E. Hande CINGIL

Thesis committee

Promotor

Prof. Dr Martien A. Cohen Stuart

Emeritus professor of Physical Chemistry and Colloid Science

Wageningen University

Co-promotor

Dr Joris H.B. Sprakel

Assistant professor, Physical Chemistry and Soft Matter

Wageningen University

Other members

Prof. Dr Aldrik H. Velders, Wageningen University

Prof. Dr A.M. Brouwer, University of Amsterdam, the Netherlands

Dr Alexander J.C. Kühne, DWI-Liebniz Institute for Interactive Materials, Aachen University, Germany

Prof. Dr Rint P. Sijbesma, Eindhoven University of Technology, the Netherlands

This research was conducted under the auspices of the Graduate School VLAG (Advanced studies in Food Technology, Agrobiotechnology, Nutrition and Health Sciences).

Nanoscale force sensors to study supramolecular systems

E. HANDE CINGIL

Thesis

submitted in fulfillment of the requirements for the degree of doctor
at Wageningen University
by the authority of the Rector Magnificus
Prof. Dr A.P.J. Mol,
in the presence of the
Thesis Committee appointed by the Academic Board
to be defended in public
on Tuesday 26 April 2016
at 4 p.m. in the Aula.

E. Hande CINGIL
Nanoscale Force Sensors to Study Supramolecular Systems
136 pages.

PhD thesis, Wageningen University, Wageningen, NL (2016)
With references and summary in English

ISBN: 978-94-6257-697-1

"I'm not leaving a spiritual legacy of dogmas, unchangeable petrified directives. My spiritual legacy is science and reason... What I wanted to and what I tried to achieve for the Turkish nation is quite evident. If those people who wish to follow me after I'm gone take the ***'reason'*** *and* ***'science'*** *as their guides they will be my true spiritual heirs."*

"Ben, manevî miras olarak hiç bir ayet, hiçbir dogma, hiçbir donmuş ve kalıplaşmış kural bırakmıyorum. Benim manevî mirasım ilim ve akıldır… Benim Türk milleti için yapmak istediklerim ve başarmaya çalıştıklarım ortadadır. Benden sonra beni benimsemek isteyenler, bu temel eksen üzerinde ***akıl*** *ve* ***ilmin*** *rehberliğini kabul ederlerse, manevî mirasçılarım olurlar."*

Mustafa Kemal ATATURK (1933)

Contents

CHAPTER 1

Introduction

1.1 Supramolecular Systems

Supramolecular systems are solutions, suspensions or solids, 'beyond' classical molecular systems, where cohesion is provided through noncovalent forces.[1] Classical molecular chemistry deals with making and breaking of covalent bonds, often to develop higher-order and complex molecular structures. By contrast, supramolecular chemistry concerns itself with weak bonds, formed by physical and non-covalent interactions. It is these weak and dynamic bonds that drive molecular self-assembly in nature, leading to high-precision formation of complex ordered structures. Supramolecular chemistry aims to bring this approach to the realm of synthetic materials. Compared to molecular chemistry, which has been developing since the synthesis of urea in 1828, supramolecular chemistry is a relatively young field of study which gained popularity since the Nobel Prize in Chemistry was awarded to researchers in the field in 1987.[1] Standing at the crossroads of biology, chemistry and physics, it has received considerable interest from various scientific fields in a short period of time.

One of the main advantages of supramolecular chemistry to classical approaches is that the formation of noncovalent interactions can occur spontaneously and does not require complex organic synthesis. When the conditions are pre-adjusted, mixing the pre-arranged components in the appropriate stoichiometry and conditions, lead to ordered materials at thermodynamic equilibrium.[2] This spontaneous process is known as self-assembly and occurs in atomic, molecular and colloidal systems like, for example, in protein folding, the formation of bilayers from lipids and the spontaneous ordering of rod-like molecules into liquid crystals.[3] By contrast, self-organization is an analogous process of structure formation from smaller building blocks in which continuous energy input is required. It relies on dissipation of energy to drive the system away from thermodynamic equilibrium.[4] Dissipative self-organization is the basis for many of natures' functions such as adaptation, evolution of intelligent behavior and replication. More specifically, it can be observed for example during mitosis of the cell, in signaling pathways for protein aggregation, when cells organize into tissues and organs, bacteria into colonies as well as higher organisms into transient structures such as bird swarms or schools of fish.[3-4]

Even though understanding dynamic self-assembly is crucial to unravel and mimic many processes occurring in nature, the challenge cannot be easily addressed as it involves many dynamic interactions which are difficult to capture.[5] Moreover, the complexity of these systems, especially the biological ones, stems from the multitude of possible interaction routes which may cooperatively, noncooperatively or competitively generate a complex manifold of interaction pathways.[6] Thus, advances in understanding self-assembly and co-assembly derive mostly from studies done on static systems.

Self-assembly requires mobility of the pre-arranged components; driven by thermal fluctuations, a fluid environment or smooth surface is required to allow components to come together and form supramolecular bonds. The building blocks for this process carry the information which later determines the type of interaction that will take place in the system and ultimately the structure it will create.[3] Due to their reversible character, being broken and reformed at some characteristic rate by thermal activation, supramolecular materials, once formed, do not require high energy input to disassemble and reassemble.[2] This results in their high receptivity to environmental perturbations and the spontaneous annealing of structural defects. This allows us to manipulate the state of the environment to change the interactions between components. Similarly, templates or boundaries can be employed to increase the level of control of the structures to be formed.

Noncovalent intermolecular interactions, such as electrostatic, van der Waals, hydrophobic or π-π interactions and hydrogen and coordination bonds, are individually weak and dynamic, often insufficient to stabilize a molecular complex against rapid dissociation.[2-3, 7] However, when several of them act cooperatively, their combined bond strength can reach levels comparable to those of covalent bonds (100 -400 kJ mol^{-1}) (Table 1).[8]

Supramolecular interactions and forces can be considered as 'specific' when there is cooperativity and directionality between interacting components.[6] Strong non-covalent bonds such as ionic and hydrogen bonds fall under this category (Table 1). One frequently encounters descriptions such as 'complementary' and 'recognition' interactions referring to 'specific' noncovalent interactions.[6] The remaining interactions are considered as 'non-specific', and occur between various different types of atoms, molecules and surfaces.

Table 1. Strength of noncovalent intermolecular interactions.

Type of interaction or bonding	Strength (kJ mol^{-1})
van der Waals	< 2
Coulomb	5 – 100
hydrogen bonding	4 – 25
ion - dipole	20 – 80
dipole – dipole	2 – 20
cation – π	2 – 30
π – π	0 – 20
metal ligand	0 – 160
hydrophobic	-

Van der Waals interactions: The most abundant non-specific noncovalent interaction is Van der Waals forces, a term which covers various dispersion forces arising from the electric dipole character of molecules. Keesom and Debye forces arise between two permanent dipoles, and between a permanent dipole and an induced dipole, respectively; they are considered as types of van der Waals forces. Additionally, there is the London dispersion force that acts between two fluctuating dipoles. The strength of these non-directional central van der Waals forces depends only on the distance between molecules.

Electrostatic interactions, on the other hand, occur only among charged species or surfaces. This force can either be attractive or repulsive, depending on the sign of the charges on the interacting parties. The interaction between two charges in a vacuum follows the Coulomb's Law, ($F \approx q_1 * q_2$ (the magnitude of charges of each atom)/ r^2 (distance between the charges)): the force is inversely proportional to the square of the distance between the charged groups. In aqueous solutions, electrostatic interactions are significantly more complex. This is due to the presence of hydration water and additional ions which screen the electrostatic interactions and lead to exponential decay of the interaction energy with separation distance.[9-10] Moreover, as attractive electrostatic bonds form between oppositely charged species, counter-ions can be released into the aqueous solution which provides an entropic contribution to the strength of electrostatic bonds. Finally, these ionic bonds, when formed between a pair of oppositely charged macroions such as polyelectrolytes, tend to cause rearrangements or conformational changes of flexible molecules or surfaces to align

themselves in such a way that collectively all the bonds can be attractive. This combination of factors can lead to very strong binding and a moderate degree of directionality. However, due to the strong dependency of the bond strength on the ionic strength of the medium, these charge interactions are highly tunable and often employed in nature to create dynamic structures such as the DNA-histone complex in the cellular nucleus.

Hydrogen bonding, which is maybe the most important noncovalent interaction found in biological systems, arises between a hydrogen atom and two strongly electronegative atoms; where one of them is the "H-bond donor" and the other is the "H-bond acceptor".[11] The donor and acceptor character can be tuned by changing the acidity and basicity of the system. The strength of hydrogen bonds is usually weaker than covalent bonds but stronger than van der Waals interactions, and tends to vary in different solvents.[8, 12] If one of the components involved in a hydrogen bond has ionic character, the bond strength will be even stronger.[13] Hydrogen bonds are very critical secondary interactions for the construction of supramolecular assemblies due to their high selectivity and directionality.[8] Hydrogen bonds are formed in natural dyes and pigments, organic semiconductors and in biomaterials (Figure 1.1). They are responsible for keeping the base pairs together in double stranded (ds) -DNA, and to stabilize protein secondary structures, like *a*-helices and *β*-sheets. In these systems, hydrogen bonds are highly specific and directional between amine proton donors (-NH_2 or-NH) and carbonyl group (=O) acceptors.[14] Hydrogen bonds in polysaccharides such as cellulose and chitin occur between –OH groups.[14] Obviously, hydrogen bonds are one of the key components in self-assembly and self-organization of complex supramolecular systems. They also contribute to the semiconducting character of DNA,[15] melanin[16] and natural indigo pigment[17]. Hydrogen bonds are also utilized to construct highly ordered supramolecular polymers from π-conjugated monomeric building blocks.[18]

π - π stacking is a crucial secondary interaction which plays a role in the self-assembly of π-conjugated materials.[8] This is an attractive force between two aromatic rings. The strength of this noncovalent interaction varies significantly from one system to another and is subject to an ongoing debate in the scientific community.[19] The stacking of aromatic molecules in water is often also driven by nonspecific hydrophobic interactions.[6] π – interactions are

also found in biological systems, often mediated by aromatic amino acids such as tryptophan or tyrosine, and play a crucial role in protein-ligand interactions for example during transmission of neural signals.

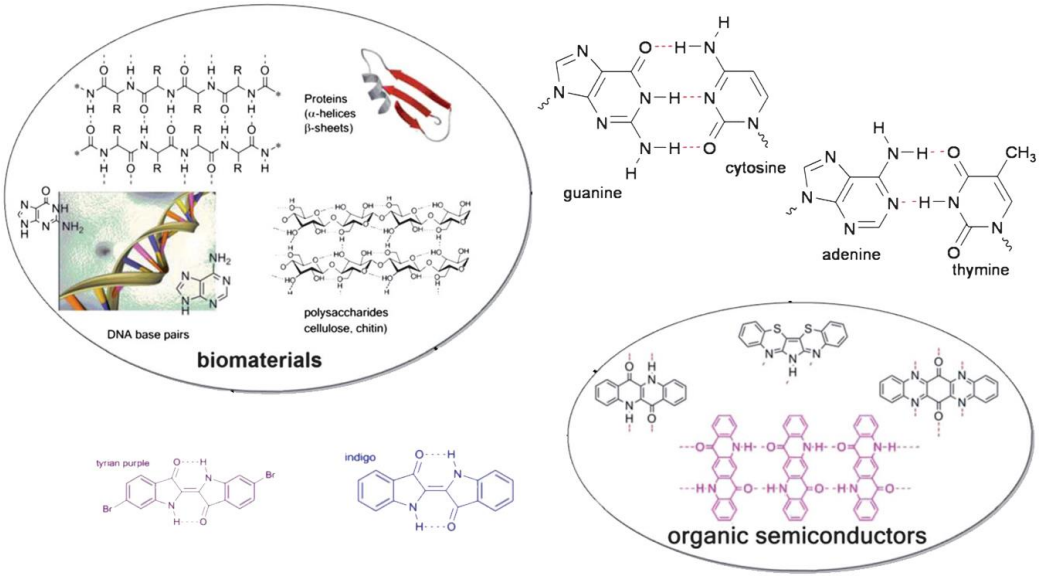

Figure 1.1 Examples of hydrogen-bonding in biomaterials and organic semiconductors with schematic illustrations of directionality of hydrogen bonding in DNA building blocks, in dyes and pigments. Adapted from ref 14 with permission of The Royal Society of Chemistry.

The above mentioned non-covalent interactions play their pivotal and complex role to construct supramolecular systems such as virus-like particles,[20-23] micelles,[24] fibers,[25-26] hydrogels,[27-29] nanoparticles,[30] liquid crystals,[31] π-conjugated polymers[8] and many more[7]. The high level of complexity in such systems does not make it easier for the scientist to control and elucidate the mechanisms of co- and self-assembly of natural as well as synthetic materials. Nevertheless, supramolecular chemistry progresses in various directions and opens new perspectives in materials science to create new smart materials. There is already substantial progress in biomedical applications, regenerative medicine and tissue engineering, where diagnostics, sensors, gene and drug delivery benefit from self-assembled nanomaterials.[7]

In this thesis, we explore two optical methods to gain new, in-depth understanding of the dynamics and mechanics during supramolecular assembly at the nanoscale: (*i*) superposition microrheology and (*ii*) molecular mechanosensing.

1.2 Microrheology with Optical Microscopy

Soft materials which consist of polymers, colloids, amphiphilic molecules, biomaterials or any other type of supramolecular structures are almost never purely solid or liquid. Rather, virtually all soft matter is viscoelastic.[32] When exposed to mechanical stress, they exhibit viscous as well as elastic behavior depending on time, extent of deformation and even the direction of the applied stress. One example of this is cytoplasm: at long timescales or low frequencies it flows as a viscous fluid, while at short timescales or high frequencies it shows elastic behavior.[33] Passive microrheology (multiple particle tracking microrheology) is a method, first introduced in 1995,[34] to measure the viscoelastic properties of these highly complex soft materials, by analyzing the motion of embedded colloids (beads) driven purely by thermal motion and without any external force applied. Submicron sized beads (< 1 μm) suspended in a viscous liquid such as water are affected by two types of forces (when inertial forces are neglected): a random force caused by collisions with solvent molecules, giving the particle a kinetic energy equal to the thermal energy k_BT, and the counteracting frictional and elastic forces dictated by the viscoelastic properties of the medium.[33] This results in random displacements of the particles within the medium whose specific features can be used to deduce the medium properties. This random walk of the beads is known as Brownian motion, which is described for simple liquids by Einstein's diffusion equation:

$$\mathrm{MSD} = \langle\, \Delta \mathrm{r}^2(\tau) \,\rangle \;=\; \langle\, \left|\, \vec{r}(t \,+\, \tau\,) \,-\, \vec{r}(t) \,\right|^2 \,\rangle = 2dD\tau \tag{1.1}$$

Here r is the bead position, τ is the correlation lag time, d the dimensionality of the system and D the diffusion coefficient of the bead. The brackets $\langle\ \rangle$ indicate an average over all beads and starting times, t. For two-dimensional diffusion, as we consider here, the prefactor $2d = 4$. The diffusion coefficient of a bead in a liquid can be derived from the Stokes-Einstein relationship as

$$D = k_BT/\xi \quad \text{and} \quad \xi = 6\pi\eta\alpha \tag{1.2}$$

where ξ is the friction coefficient of the bead in the liquid, η is the viscosity of the liquid and α is radius of the bead. Hence, the viscosity of the fluid can be obtained from MSDs collected via multiple particle tracking:

$$\eta = \frac{2k_BT}{3\pi\alpha} = \frac{\tau}{\langle \Delta r^2(\tau) \rangle} \tag{1.3}$$

Multiple particle tracking microrheology requires video recordings of thermally driven random motion of beads suspended in the liquid by an optical microscopy equipped with high speed camera over significantly long times. To obtain adequate statistics, trajectories of many beads (>100) need to be tracked and analyzed to obtain good quality ensemble-averaged MSD $\langle\langle\, \Delta\vec{r}^2(\tau)\, \rangle\rangle$.

The MSDs of beads in an elastic solid exhibit a time-independent plateau with amplitude that indicates the extent to which the bead, driven by thermal energy, is able to deform its elastic surroundings. However, most soft materials are viscoelastic and their rheological response depends on time (or frequency). Microrheology allows determining those frequency-dependent mechanical properties such as elastic or viscous modulus of the medium of interest from the MSD obtained by using the generalized Stokes-Einstein Relation (GSER):

$$\langle \Delta\tilde{r}^2(s) \rangle = \frac{k_BT}{\pi\alpha s\tilde{G}(s)} \tag{1.4}$$

here $\Delta\tilde{r}^2(s)$ is the Laplace transform of $\Delta r^2(\tau)$ as a function of Laplace frequency s and $\tilde{G}(s)$ is the frequency-dependent shear modulus. If the medium is homogenous at the length scale of the bead radius α, then the Fourier transformed GSER can be used to obtain the complex shear modulus $G^*(\omega)$, a conventional bulk rheological property, with this relation:

$$G^*(\omega) = G'(\omega) + iG''(\omega) \tag{1.5}$$

where the storage modulus G' characterizes the elastic contribution to the material behavior and the loss modulus G'' the contribution due to dissipative, viscous stresses. Even though MSDs obtained from microrheology measurements can be utilized to get bulk (average)

properties by using the given equations above, microrheology is a unique tool to investigate local viscoelastic properties, which cannot be determined by conventional rheology. Variation in local viscoelastic properties can reveal heterogeneities in the system; studying those heterogeneities is especially important for biological systems such as cells.[35] Moreover, microrheology enables probing of important characteristics in other soft materials, such as polymeric solutions and networks, at the micrometer length scale and below; this enables the study of properties at length scales otherwise unreachable in the range of interchain separation or mesh size for gels.[35]

However, despite the versatility of this technique, forces at the molecular scale remain out of reach due to the resolution of 5-10 nm in determining the position of the tracer particles. Unveiling forces at the smallest relevant scale in supramolecular systems requires a different approach.

1.3. Conjugated Polymers as Force Sensors

Conjugated polymers or intrinsically (semi)conducting polymers are, as described in the Nobel Lecture by Alan J. Heeger, "materials which exhibit the electrical and optical properties of metals or semiconductors and which retain the attractive mechanical properties and processing advantages of polymers".[36] Since their discovery [37-38] in 1976 by a group of researchers under supervision of Alan G. MacDiarmid, Alan J. Heeger and Hideki Shirakawa in University of Pennsylvania, they attracted attention from scientific and industrial communities in various fields due to their unique combination of properties.

The electronic configuration of conjugated polymers differs from conventional (saturated) polymers. Conventional polymers have all the valence electrons of carbon atoms in the backbone engaged in sigma orbitals. By contrast, conjugated polymers have one unpaired electron (π-electron) for each carbon atom (Figure 1.2). The π-bonding, in which consecutive carbon orbitals in sp^2p_z configuration overlap along the backbone, results in electronic delocalization.[36]

This characteristic delocalized electronic structure of the polymer backbone brings unique optoelectronic properties to conjugated polymers and makes them attractive materials for a

variety of applications in organic (opto-) electronics such as in LEDs, displays, memories and solar cells.[39-40]

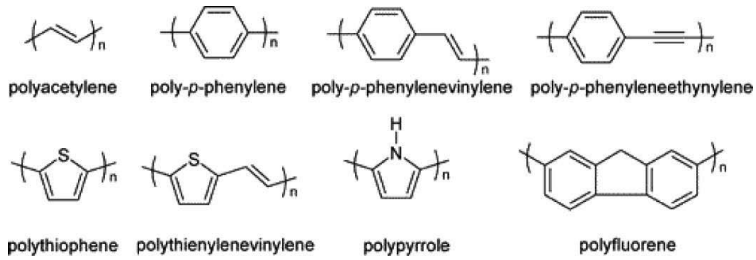

Figure 1.2. Chemical structures of several conjugated polymers. Reproduced with permission from ref 8. Copyright 2005 American Chemical Society.

Conjugated polymers can also be used as sensitive sensors[41]; the underlying mechanism which makes conjugated polymers such versatile building blocks for sensor applications is that any change occurring at a site along the conjugated backbone, e.g. due to environmental changes or analyte binding, affects the optoelectronic properties of the entire polymer because electrons can travel significant distances along the conjugated backbone.[42] The typical conjugation length along which electronic delocalization occurs can be from several to tens of nanometers. The optoelectronic response to such changes can easily be probed in the fluorescence spectra of the polymer as an enhancement or quenching in photoluminescence intensity or a distinct wavelength shift. While such a optoelectronic response can be pronounced in the luminescence spectra, often absorption spectra remain relatively unaffected as they do not exhibit such a sensitivity to low degrees of analyte binding. The reason for this is that in conjugated polymers only a small number of repeat units, up to the effective chain conjugation length, determine the optical band gap; extending the chain beyond this specific number of repeat units has no further effect. For example for dihexyl-substituted polyfluorenes, no further changes in luminescence are observed when the chain extends beyond 6 monomeric units.[43] Due to this signal amplification of a binding event makes conjugated polymers more sensitive than most small-molecule fluorophores, which give only single chromophore response. This is especially important for biosensor applications where the analyte of interest exists in low concentrations.

Conjugated polymers without further functionalization are mostly insoluble in polar solvents due to their highly hydrophobic and rigid aromatic backbone. To overcome this solubility limitation, various functional groups can be attached to the conjugated backbone. To enable their application in biological or biologically-relevant aqueous systems, most commonly charged moieties are introduced, such as carboxylate, phosphonate, sulfonate or quaternary ammonium moieties. These pendant substituents with ionic functionality can make conjugated polymers water-soluble under appropriate conditions of pH and ionic strength. Conjugated polymers with water-solubilizing ionic groups are known as conjugated polyelectrolytes (CPEs). CPEs uniquely combine the properties of having delocalized conjugated backbone, with being water-soluble and able to interact with multivalent ions or oppositely charged (biological) molecules via electrostatic interactions. These powerful functionalities of CPEs open many possibilities for emerging technologies not only in biosensing[44] but also in imaging[45] and in electronics[46-47].

In addition to these above mentioned properties, which make CPEs desirable as sensor materials, several types of CPEs also exhibit variable chromism, which is the sensitivity of optoelectronic properties to chain conformation and vibrational degrees of freedom. Polydiacetylene (PDA) is one of the mostly studied chromic CPE; its backbone conformation is very sensitive to environmental perturbations such as pH, temperature, solvent, mechanical force and analyte binding. Environmental triggers induce backbone twisting, which directly affects the optical response. PDA goes through a chromic transition from non-fluorescent to fluorescent, and a colorimetric change from blue to red (Figure 1.3).[48] PDAs in the form of liposomes, vesicles and wires have been used for colorimetric detection of ions, glucose, DNA and bacteria such as E. coli or influenza virus.[49-50] Similarly, upon analyte binding, polythiophenes (PTs) go through a conformational change from a random-coil nonplanar conformation which emits yellow, to a planarized extended conformation with red emission. This coupling between the emission color of a dye (macro) molecule and a mechanically-induced change in conformation is known as mechanochromism and can be utilized to quantify forces or force-induced conformation changes. Simultaneously, analyte binding can induce a transition from isolated single objects to an aggregated state, which can be observed by strong fluorescence quenching in conjunction with the color change.

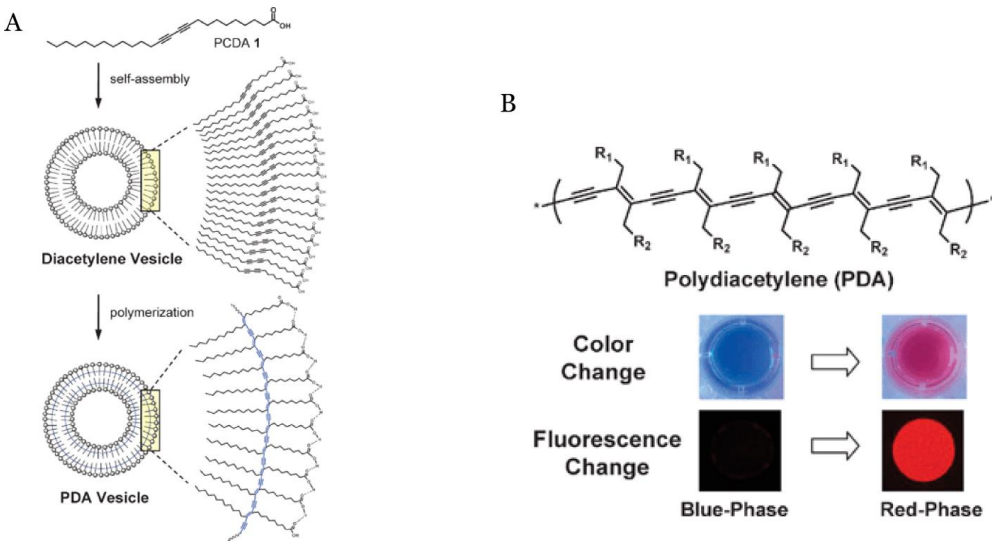

Figure 1.3 Schematic representation of pathways to obtain polydiacetylene vesicles from 10,12-pentacosadiynoic acid (PCDA) which in aqueous solution self assembles into diacetylene vesicles that can be polymerized by UV irradiation (A). The structure of PDA and its typical fluorescent and colorimetric response to any trigger (B). Adapted from ref 48 with permission of The Royal Society of Chemistry.

Thus, PTs function as sensors for their own conformation, for example the conjugated backbone of polythiophene acetic acid stretches and planarizes upon binding to amyloid fibrils (orange solution), whereas nonplanarization and chain separation occurs upon binding to native bovine insulin (yellow solution).[51] Cationic PT derivatives exhibit the same mechanochromic response upon complexing with structurally similar diamines,[52] adenosine triphosphate,[53] as well as ss- and ds-oligonucleotides[54-55].

Multicolor sensing can also be achieved by tailoring the conjugated backbone of CPEs with donor-acceptor units. The delocalized conjugated backbone of CPEs can exhibit intrachain and interchain exciton migration pathways.[56] The main energy transfer mechanism in dilute, well-dissolved systems, where energy transfer between molecules is suppressed, is via intrachain exciton migration that happens along the isolated polymer chain as a one-dimensional random walk.[57-58] However, in concentrated systems where polymers aggregate, due to solvent evaporation, analyte binding and etc., isolated polymer chains come in close proximity, which allows Förster (fluorescence) resonance energy transfer (FRET) via

interchain exciton migration. This more efficient energy transfer pathway is a three-dimensional random walk over multiple conjugated chains.[57-59] FRET occurs when there are donor-acceptor units within close proximity (2 - 10 nanometers).[60] The mechanism of FRET is described in the highly schematic illustration below (Figure 1.4).

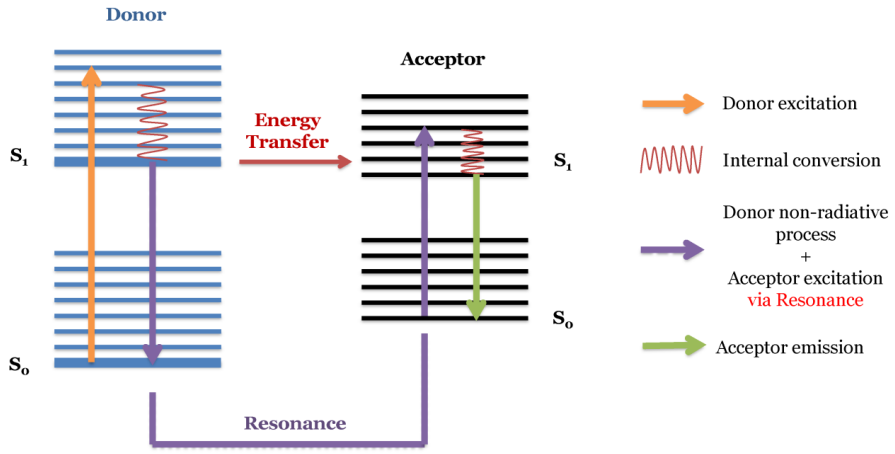

Figure 1.4 Schematic diagram of Förster Resonance Energy Transfer (FRET)

While the excited donor returns back to the ground state (S_0), by first relaxing to the lowest excited singlet state (S_1) as a natural outcome of Kasha's rule, the energy being released simultaneously excites the acceptor group via non-radiative transfer (resonance). If the emission spectrum of a donor group overlaps with the absorption spectrum of the acceptor, energy transfer becomes more efficient. CPEs that contain FRET donor-acceptor pairs utilize the intermolecular energy transfer and act as multicolor sensors for interpolyelectrolyte complexation. The polycationic poly (fluorene-alt-phenylene) which contains a small fraction of benzothiadiazole (BT) units as acceptor domain in its conjugated backbone emits blue fluorescence in its native, well-dissolved state. Aggregation of conjugated chains upon complexing with polyanionic DNA enhances the interchain energy transfer from the fluorene segments (donor) to the low-energy emissive BT sites (acceptor) (Figure 1.5). As a result, the complex emits green fluorescence. By using this and similar CPEs, and utilizing the multicolor response from blue to green or red, researchers detected [61-62] and quantified [62-63] dsDNA and differentiated heparin from its structural analogue hyaluronic acid [64].

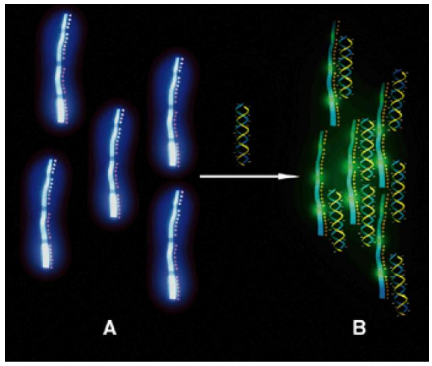

Figure 1.5 Isolated chains of a polycationic poly(fluorene-alt-phenylene) with BT substitution emit blue light in the absence of DNA (A). The change in emission color upon addition of dsDNA via FRET (B). Reproduced with permission from ref 63. Copyright 2006 Wiley-VCH Verlag Gmbh & Co. KGaA.

A similarly designed polyanionic polyfluorene derivative with BT constituents in the conjugated backbone has been shown to exhibit multicolor responses from blue to yellow, green and dark (no emission) in the presence of lysozyme, bovine serum albumin (BSA) and cytochrome c, respectively (Figure 1.6).[65]

P2-BT$_x$ x = 7.5, 15, 30

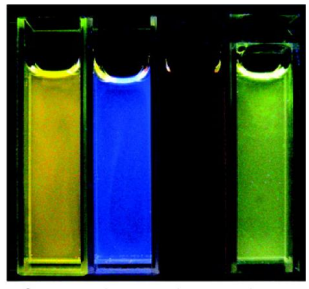

P2-BT$_{30}$ P2-BT$_{30}$ P2-BT$_{30}$ P2-BT$_{30}$
-Lysozyme + Cyt *c* + BSA

Figure 1.6 The structure of polyanionic polyfluorene with BT substitution (left). Multicolor response of P2-BT$_{30}$ to lysozyme, cyt c and BSA add imaged in quartz cuvettes under UV excitation (λ = 365 nm) (right). Adapted with permission from Ref 65. Copyright 2008 American Chemical Society.

Another CPE, anthryl-doped polyanionic poly (p-phenylene ethynylene) selectively detects natural amines such as spermine, spermidine, as well as small molecule analytes such as neomycin with a change in emission color from blue to green.[58]

Special Focus: Polyfluorene

Polyfluorenes (PFs) are the simplest step-ladder type polyphenylenes. They are intrinsically blue-light emitting conjugated polymers; however they can be tuned to emit light throughout the entire visible spectrum via chromophore incorporation in the main chain or substitutions of side chains in the 9,9-position of the fluorene unit.[66] Due to their high quantum efficiency in the solid state, excellent chemical and thermal stability, as well as color tunability, PFs are the primary blue-light source for polymer-based light-emitting device applications.[67-68]

Well-structured polyfluorene derivatives can be synthesized via transition-metal catalyzed couplings such as palladium-catalyzed aryl-aryl cross couplings of aryldiboronic acids and dihaloaryls in Suzuki couplings; or distannylaryls and dihaloaryls in Stille couplings. For higher molecular weight and precise end-group functionality one would typically employ nickel-catalyzed aryl-aryl couplings of dihaloaryls (Yamamoto coupling). It is essential to use very pure monomers and oxygen-depleted reaction conditions to achieve defect-free polyfluorene derivatives.

PFs have complex photophysical properties which strongly depend on the morphology of their conjugated chains.[69] In solution under dilute conditions, PFs display an absorption maximum at 380 nm which is independent from the alkyl chain substitution. Their photoluminescence (PL) exhibits well-resolved vibronic bands attributed to 0-0, 0-1 and 0-2 vibronic transitions with the 0-0 transition band at ~315 nm. Alkyl-substituted PFs go through a conformational change from regular amorphous state to a state called β-phase[70]; this happens upon thermal quenching in poor solvent conditions,[71-73] in aligned thin films,[74] during particle formation[75] and through physical confinement in ionogels[76]. This mostly solid state-attributed conformation exhibits an extended[77] and planarized conjugated backbone conformation, which leads to a bathochromic shift and well-resolved vibronic progression in its absorption and fluorescence spectrum.[74, 78] While β-phase formation of polyfluorene backbone is widely reported for linear alkyl (most favorably *octyl*-) chain-substituted PFs, it is fully suppressed in the presence of branched alkyl chain substituted ones. The underlying mechanism is attributed to the Van der Waals bonding force

between appropriate alkyl chains that overcomes the steric hindrance of the conjugated backbone and causes it to planarize.[73]

1.4 Outline of the thesis

In this thesis, we employ two distinct methods to monitor the dynamics of supramolecular assemblies at the nanoscale (*i*) multiple particle tracking microrheology and (*ii*) conjugated polymer mechanosensors.

Chapter 2 discusses the use of multiple particle tracking microrheology to study the melting and gelation dynamics of a thermoreversible collagen-inspired recombinant polypeptide in the form of a triblock copolymer gel former. Upon cooling, the end blocks assemble into short triple-helices and form an elastic network. To investigate the transition from a viscous liquid to a gel and back from a gel to a viscous liquid, we apply time-cure superposition to one-point microrheology data. Since this method sensitively probes changes in mechanical properties at the critical transition regimes, it provides information on the gel- and melting point, the critical relaxation exponent and the dynamic scaling exponents. This allows a direct comparison of the melting and gelation pathways and dynamics, which occur in the same system.

Chapter 3 reports on the novel use of mechanochromic polymers to sense supramolecular assembly. We describe a water-soluble anionic polyfluorene homopolymer which undergoes a conformational change upon electrostatic complexation with a recombinant cationic-neutral polypeptide diblock inspired by natural protein capsid formers. Since the structure of the conjugated backbone and the optoelectronic properties of the polyfluorene are directly related, any conformational alterations result in changes of the vibronic bands which are monitored by fluorescence spectroscopy. When the protein encapsulates the polymer in a bottle-brush structure, steric hindrance between the proteins in the brush induce mechanical stress on the conjugated backbone which then transforms into a planarized and stretched conformation. By utilizing this stretching response, we show that the conjugated polymer is not only a mechanosensor for its own conformational change but can also enable quantitative detection of low degrees of protein binding as well as the reverse (capsid disintegration).

In Chapter 4, we investigate the functionality of same mechanosensor by electrostatic complexation with a synthetic cationic-neutral diblock copolymer which forms micelles in aqueous conditions. In this charge-driven co-assembly, planarization of the conjugated backbone is again observed, at low charge stoichiometries. However, as charge compensation is approached, the vibronic bands of the homopolymer signal a possible molecular aggregation with a loss of spectral features. To probe how the transition beyond this point from single molecule complexes to multimolecular micelles occurs, we introduce a new conjugated polymer which is tailored specifically to probe chain proximity, in addition to possessing all properties of the previous polymer. Integrating a donor-acceptor unit within the polyfluorene backbone improves interchain electron migration between optical partners provided the chains come into close proximity. When the conditions are met, the fluorescence emission of the polymer not only shifts but also generates a new low energy emission band of the acceptor unit which can easily be seen as a different color under UV illumination. By using this mechanochromic sensor we probe backbone planarization and stretching at low charge ratios and condensed, multimolecular micelle formation around charge stoichiometry. This multifunctional mechanochromic conjugated polymer sensor allows detection of analyte binding as well as release; it monitors its own conformational alteration by sensing the mechanical stress from the environment and probes chain proximity which indicates accumulations during supramolecular structure formations.

The last experimental chapter of this thesis, Chapter 5, explores the potential use of these previously introduced mechanosensors to monitor the highly cooperative, templated self-assembly of a complex recombinant coat protein. This recombinant protein differs from the previously studied minimal design coat protein in Chapter 3 by having an additional polypeptide block which is responsible of lateral self-assembly by stacking into a characteristic β-roll conformation. Since this is a dynamic self-assembling system we monitor the complex formation by measuring the evolution of the fluorescence emission spectrum in time. The spectral changes observed for planarized conformation of polyfluorene appear again, due to the self-assembly of the coat protein along the conjugated backbone. This allows us to study the dynamics of this supramolecular system in the course of self-assembly. Our mechanosensors also shed light on the previously hypothesized but not yet experimentally proven possibility that there is competition between the templated self-assembly (which

happens on the backbone of the mechanosensors) and non-templated self-assembly (which happens in solution).

Finally, in the General Discussion (Chapter 6), we review the outcomes of this thesis with a special focus on mechanochromism of polyfluorene. We will discuss the factors which influence β-phase formation in polyfluorene, as well as a potential use of mechanochromic sensors in more complex thermoresponsive protein systems, supported by preliminary experimental data. We will conclude with prospects for future research, followed by a Summary of the thesis.

References

[1] J.-M. Lehn, *Science* **1993**, *260*, 1762-1763.

[2] K. Liu, Y. Kang, Z. Wang, X. Zhang, *Adv Mater* **2013**, *25*, 5530-5548.

[3] G. M. Whitesides, B. Grzybowski, *Science* **2002**, *295*, 2418-2421.

[4] M. Fialkowski, K. J. M. Bishop, R. Klajn, S. K. Smoukov, C. J. Campbell, B. A. Grzybowski, *J Phys Chem B* **2006**, *110*, 2482-2496.

[5] A. V. Davis, R. M. Yeh, K. N. Raymond, *Proc Natl Acad Sci U S A* **2002**, *99*, 4793-4796.

[6] D. Leckband, J. Israelachvili, *Q Rev Biophys* **2001**, *34*, 105-267.

[7] E. Busseron, Y. Ruff, E. Moulin, N. Giuseppone, *Nanoscale* **2013**, *5*, 7098-7140.

[8] F. J. M. Hoeben, P. Jonkheijm, E. W. Meijer, A. P. H. J. Schenning, *Chem Rev* **2005**, *105*, 1491-1546.

[9] E. Spruijt, S. A. Van Den Berg, M. A. Cohen Stuart, J. Van Der Gucht, *Acs Nano* **2012**, *6*, 5297-5303.

[10] R. A. L. Jones, *Soft Condensed Matter*, Oxford University Press Inc., New York, **2002**.

[11] P. Atkins, *General Chemistry*, Scientific American Books, New York, **1989**.

[12] C. B. Aakeroy, K. R. Seddon, *Chem Soc Rev* **1993**, *22*, 397-407.

[13] M. Meot-Ner, *Chem Rev* **2005**, *105*, 213-284.

[14] E. D. Glowacki, M. Irimia-Vladu, S. Bauer, N. S. Sariciftci, *J Mater Chem B* **2013**, *1*, 3742-3753.

[15] B. Giese, J. Amaudrut, A. K. Köhler, M. Spormann, S. Wessely, *Nature* **2001**, *412*, 318-320.

[16] M. Irimia-Vladu, N. S. Sariciftci, S. Bauer, *J Mater Chem* **2011**, *21*, 1350-1361.

[17] M. Irimia-Vladu, E. D. Gåowacki, P. A. Troshin, G. Schwabegger, L. Leonat, D. K. Susarova, O. Krystal, M. Ullah, Y. Kanbur, M. A. Bodea, V. F. Razumov, H. Sitter, S. Bauer, N. S. Sariciftci, *Adv Mater* **2012**, *24*, 375-380.

[18] A. El-Ghayoury, A. P. H. J. Schenning, P. A. Van Hal, J. K. J. Van Duren, R. a. J. Janssen, E. W. Meijer, *Angew Chem Int Ed* **2001**, *40*, 3660-3663.

[19] C. R. Martinez, B. L. Iverson, *Chem Sci* **2012**, *3*, 2191-2201.

[20] K. Matsuura, K. Watanabe, T. Matsuzaki, K. Sakurai, N. Kimizuka, *Angew Chem Int Ed* **2010**, *49*, 9662-9665.

[21] Y.-B. Lim, E. Lee, Y.-R. Yoon, M. S. Lee, M. Lee, *Angew Chem Int Ed* **2008**, *47*, 4525-4528.

[22] F. Boato, R. M. Thomas, A. Ghasparian, A. Freund-Renard, K. Moehle, J. A. Robinson, *Angew Chem Int Ed* **2007**, *46*, 9015-9018.

[23] A. Hernandez-Garcia, D. J. Kraft, A. F. J. Janssen, P. H. H. Bomans, N. a. J. M. Sommerdijk, D. M. E. Thies-Weesie, M. E. Favretto, R. Brock, F. A. De Wolf, M. W. T. Werten, P. Van Der Schoot, M. A. Cohen Stuart, R. De Vries, *Nat Nanotechnol* **2014**, *9*, 698-702.

[24] M. A. Cohen Stuart, B. Hofs, I. K. Voets, A. De Keizer, *Curr Opin Colloid Interface Sci* **2005**, *10*, 30-36.

[25] L. H. Beun, I. M. Storm, M. W. T. Werten, F. A. De Wolf, M. A. Cohen Stuart, R. De Vries, *Biomacromolecules* **2014**, *15*, 3349-3357.

[26] H. C. Fry, J. M. Garcia, M. J. Medina, U. M. Ricoy, D. J. Gosztola, M. P. Nikiforov, L. C. Palmer, S. I. Stupp, *J Am Chem Soc* **2012**, *134*, 14646-14649.

[27] M. Ikeda, T. Yoshii, T. Matsui, T. Tanida, H. Komatsu, I. Hamachi, *J Am Chem Soc* **2011**, *133*, 1670-1673.

[28] A. Wada, S.-I. Tamaru, M. Ikeda, I. Hamachi, *J Am Chem Soc* **2009**, *131*, 5321-5330.

[29] I. Yoshimura, Y. Miyahara, N. Kasagi, H. Yamane, A. Ojida, I. Hamachi, *J Am Chem Soc* **2004**, *126*, 12204-12205.

[30] R. De Larica, R. M. Fratila, A. Szarpak, J. Huskens, A. H. Velders, *Angew Chem Int Ed* **2011**, *50*, 5704-5707.

[31] J.-M. Lehn, *Polym Int* **2002**, *51*, 825-839.

[32] D. T. N. Chen, Q. Wen, P. A. Janmey, J. C. Crocker, A. G. Yodh, in *Annu Rev Condens Matter Phys, Vol 1,* (Ed.: J. S. Langer), Annual Reviews, Palo Alto, **2010**, pp. 301-322.

[33] D. Wirtz, *Annu Rev Biophys, Vol. 38*, Annual Reviews, Palo Alto, **2009**, pp. 301-326.

[34] T. G. Mason, D. A. Weitz, *Phys Rev Lett* **1995**, *74*, 1250-1253.

[35] F. C. Mackintosh, C. F. Schmidt, *Curr Opin Colloid Interface Sci* **1999**, *4*, 300-307.

[36] A. J. Heeger, *Angew Chem Int Ed* **2001**, *40*, 2591-2611.

[37] C. K. Chiang, C. R. Fincher, Y. W. Park, A. J. Heeger, H. Shirakawa, E. J. Louis, S. C. Gau, A. G. Macdiarmid, *Phys Rev Lett* **1977**, *39*, 1098-1101.

[38] H. Shirakawa, E. J. Louis, A. G. Macdiarmid, C. K. Chiang, A. J. Heeger, *J Chem Soc, Chem Commun* **1977**, 578-580.

[39] A. Duarte, K. Y. Pu, B. Liu, G. C. Bazan, *Chem Mater* **2011**, *23*, 501-515.

[40] C. J. Brabec, N. S. Sariciftci, J. C. Hummelen, *Adv Funct Mater* **2001**, *11*, 15-26.

[41] S. W. Thomas Iii, G. D. Joly, T. M. Swager, *Chem Rev* **2007**, *107*, 1339-1386.

[42] T. M. Swager, *Acc Chem Res* **1998**, *31*, 201-207.

[43] G. Klaerner, R. D. Miller, *Macromolecules* **1998**, *31*, 2007-2009.

[44] H. A. Ho, A. Najari, M. Leclerc, *Acc. Chem Res* **2008**, *41*, 168-178.

[45] C. Zhu, L. Liu, Q. Yang, F. Lv, S. Wang, *Chem Rev* **2012**, *112*, 4687-4735.

[46] C. V. Hoven, A. Garcia, G. C. Bazan, T. Q. Nguyen, *Adv Mater* **2008**, *20*, 3793-3810.

[47] H. Jiang, P. Taranekar, J. R. Reynolds, K. S. Schanze, *Angew Chem Int Ed* **2009**, *48*, 4300-4316.

[48] B. Yoon, S. Lee, J. M. Kim, *Chem Soc Rev* **2009**, *38*, 1958-1968.

[49] J. Lee, H. J. Kim, J. Kim, *J Am Chem Soc* **2008**, *130*, 5010-5011.

[50] S. Seo, J. Lee, E. J. Choi, E. J. Kim, J. Y. Song, J. Kim, *Macromol Rapid Commun* **2013**, *34*, 743-748.

[51] K. P. R. Nilsson, A. Herland, P. Hammarström, O. Inganäs, *Biochemistry* **2005**, *44*, 3718-3724.

[52] T. L. Nelson, C. O'sullivan, N. T. Greene, M. S. Maynor, J. J. Lavigne, *J Am Chem Soc* **2006**, *128*, 5640-5641.

[53] C. Li, M. Numata, M. Takeuchi, S. Shinkai, *Angew. Chem. Int. Ed.* **2005**, *44*, 6371-6374.

[54] H. A. Ho, M. Boissinot, M. G. Bergeron, G. Corbeil, K. Doré, D. Boudreau, M. Leclerc, *Angew. Chem. Int. Ed.* **2002**, *41*, 1548-1551.

[55] H. A. Ho, M. Leclerc, *J Am Chem Soc* **2004**, *126*, 1384-1387.

[56] K. Y. Pu, L. Cai, B. Liu, *Macromolecules* **2009**, *42*, 5933-5940.

[57] I. A. Levitsky, J. Kim, T. M. Swager, *J Am Chem Soc* **1999**, *121*, 1466-1472.

[58] A. Satrijo, T. M. Swager, *J Am Chem Soc* **2007**, *129*, 16020-16028.

[59] D. Beljonne, G. Pourtois, C. Silva, E. Hennebicq, L. M. Herz, R. H. Friend, G. D. Scholes, S. Setayesh, K. Müllen, J. L. Brédas, *Proc Natl Acad Sci U S A* **2002**, *99*, 10982-10987.

[60] X. You, A. W. Nguyen, A. Jabaiah, M. A. Sheff, K. S. Thorn, P. S. Daugherty, *Proc Natl Acad Sci U S A* **2006**, *103*, 18458-18463.

[61] B. Liu, G. C. Bazan, *J Am Chem Soc* **2004**, *126*, 1942-1943.

[62] C. Chi, A. Mikhailovsky, G. C. Bazan, *J Am Chem Soc* **2007**, *129*, 11134-11145.

[63] J. W. Hong, W. L. Hemme, G. E. Keller, M. T. Rinke, G. C. Bazan, *Adv Mater* **2006**, *18*, 878-882.

[64] K. Y. Pu, B. Liu, *Macromolecules* **2008**, *41*, 6636-6640.

[65] D. Yu, Y. Zhang, B. Liu, *Macromolecules* **2008**, *41*, 4003-4011.

[66] A. C. Grimsdale, K. Müllen, in *AdvPolym Sci, Vol. 212* (Eds.: U. Scherf, D. Neher), **2008**, pp. 1-48.

[67] M. C. Hung, J. L. Liao, S. A. Chen, S. H. Chen, A. C. Su, *J Am Chem Soc* **2005**, *127*, 14576-14577.

[68] S. A. Chen, H. H. Lu, C. W. Huang, in *AdvPolym Sci, Vol. 212* (Eds.: U. Scherf, D. Neher), **2008**, pp. 49-84.

[69] U. Scherf, E. J. W. List, *Adv Mater* **2002**, *14*, 477-487.

[70] M. Grell, D. D. C. Bradley, X. Long, T. Chamberlain, M. Inbasekaran, E. P. Woo, M. Soliman, *Acta Polymerica* **1998**, *49*, 439-444.

[71] F. B. Dias, J. Morgado, A. L. Maçanita, F. P. Da Costa, H. D. Burrows, A. P. Monkman, *Macromolecules* **2006**, *39*, 5854-5864.

[72] M. Knaapila, F. B. Dias, V. M. Garamus, L. Almásy, M. Torkkeli, K. Leppänen, F. Galbrecht, E. Preis, H. D. Burrows, U. Scherf, A. P. Monkman, *Macromolecules* **2007**, *40*, 9398-9405.

[73] D. W. Bright, F. B. Dias, F. Galbrecht, U. Scherf, A. P. Monkman, *Adv Funct Mater* **2009**, *19*, 67-73.

[74] A. J. Cadby, P. A. Lane, H. Mellor, S. J. Martin, M. Grell, C. Giebeler, D. D. C. Bradley, M. Wohlgenannt, C. An, Z. V. Vardeny, *Phys RevB: Condens Mater Phys* **2000**, *62*, 15604-15609.

[75] A. J. C. Kuehne, M. Kaiser, A. R. Mackintosh, B. H. Wallikewitz, D. Hertel, R. A. Pethrick, K. Meerholz, *Adv Funct Mater* **2011**, *21*, 2564-2570.

[76] R. C. Evans, P. C. Marr, *Chem Commun* **2012**, *48*, 3742-3744.

[77] M. Grell, D. D. C. Bradley, G. Ungar, J. Hill, K. S. Whitehead, *Macromolecules* **1999**, *32*, 5810-5817.

[78] E. Da Como, K. Becker, J. Feldmann, J. M. Lupton, *Nano Lett* **2007**, *7*, 2993-2998.

CHAPTER 2

Equivalent pathways in melting and gelation of well-defined biopolymer networks

We use multiple particle tracking microrheology to study the melting and gelation behaviour of well-defined collagen-inspired designer biopolymers expressed by the transgenic yeast *P. Pastoris*. The system consists of a hydrophilic random coil-like middle block and collagen-like end blocks. Upon cooling, the end blocks assemble into well-defined transient nodes with exclusively three-fold functionality. We apply the method of time-cure superposition of the mean-square displacement of tracer beads embedded in the biopolymer matrix to study the kinetics and thermodynamics of approaching the gel point from both the liquid and the solid side. The melting point, gel point and critical relaxation exponents are determined from the shift factors of the mean-square displacement and we discuss the use of dynamic scaling exponents to correctly determine the critical transition. Critical relaxation exponents obtained for different concentrations in both systems are compared with the currently existing dynamic models in literature. In our study, we find that, while the time scales of gelation and melting are different by orders of magnitude, and show inverse dependence on concentration, that the pathways followed are completely equivalent.

This chapter is published as

Hande E. Cingil, Wolf H. Rombouts, Jasper van der Gucht, Martien A. Cohen Stuart, and Joris Sprakel. *Biomacromolecules*, 2015, 16 (1), 304–310, DOI: 10.1021/BM5015014.

2.1 Introduction

Multiple particle tracking microrheology is an ideal method to determine the mechanical properties of soft biomaterials due to its highly sensitive, non-invasive nature while requiring only very small sample volumes of less than 10 μL. The technique is particularly advantageous for studying sol-gel transitions where moduli changes rapidly with time, because within short acquisition times it can obtain dynamic mechanical information spanning several decades in frequency. Passive microrheology, introduced[1] in 1995, has been applied to the characterization of many biomaterial systems especially to identify the sol-gel transition and gelation kinetics of peptides,[2-4] proteins and DNA solutions.[5-7]

Time-cure superposition was first applied by Larsen and Furst[8] to microrheological data as a new analysis method for investigating the transition from a viscous liquid to a gel, both in chemically cross-linked gels and physical peptide hydrogels, 18 years after having been first introduced.[9] This analysis provides information on the gel point, the critical relaxation exponent and dynamic scaling exponents. The method of time-cure superposition relies on the fact that a growing network in which cross-links are formed in time approaches a critical percolation point at where characteristic length and time scales diverge. On approaching this critical point, the size of polymer clusters, and associated relaxation times exhibit self-similarity. As the method sensitively probes changes in mechanical properties around the critical point, it is believed to be ideal to shed light on the universal properties of percolating systems. Following the work of Larsen and Furst, time cure superposition has been applied successfully to different systems such as fibrillar protein gels,[10-11] covalently cross-linked hydrogels[12-13] and peptides,[14] as well as the reverse percolation of a hydrogel.[15] Surprisingly however the approach has never been applied to a thermoreversible gel system.

The principal goal of the present work is to study the dynamics of a thermoreversible gel system, that not only undergoes a sol-gel transition (gelation), but also the reverse transition from a gel to a viscous liquid (melting) upon heating and to compare these two pathways. As our system of choice, we select a well-defined collagen-inspired polypeptide[16] for which the thermodynamics and kinetics of crosslink formation is very well defined and known in detail.[16-19] On this system, we apply time-cure superposition analysis, using

multiple particle tracking one-point microrheology data. The selected system is a polymer of 400 amino acids, with a triblock structure having a random coil central block, with a radius of gyration (R_g) of 10-11 nm radius, which acts as a hydrophilic spacer and prevents bundling or further assembly of triple helices such that mesh sizes do not exceed the R_g of the biopolymer; and short (2-3 nm) triple-helix forming *(Pro-Gly-Pro)*$_9$ repeat units at either end. These end blocks are responsible for the thermoreversible crosslinks formed by the system. Upon cooling they assemble into junctions with a multiplicity of exactly three. This well-studied biopolymer offers an ideal system to test the use of time-cure superposition analysis on a thermoreversible gel network system. In this context, we also intend to critically test and compare various methods to determine the critical point and the numerical values of exponents.

2.2 Experimental Section

Materials Carboxyl latex microspheres with diameter 0.4 μm are used as tracer particles in each passive microrheology experiment (Molecular Probes by Life Technologies). Prior to use, particles are diluted to a final weight to volume fraction of 0.12 % and sonicated to break up any agglomerates.

Triblock Copolymer TR4T Thermoreversible physical polymer gels are prepared from a collagen-inspired polypeptide (TR4T) which consists of a random coil central block, capped with a short triple-helix forming sequence at either end. Central block has same amino acid composition as collagen but different sequence, to prevent the higher-order structure of collagen leading to large length scales. A fed-batch fermentation of a transgenic *Pishia pastoris* strain expressing the TR4T (~42 kDa) is carried out in a 3-1 Bioflo 3000 reactor (New Brunswick Scientific) at 30 °C and pH 3 as reported previously.[16] The purification process of the protein from the cell-free broth is also performed as described before.[16] Sodium dodecyl sulfate polyacrylamide gel electrophoresis (SDS-PAGE) is performed using the NuPAGE Novex system (Invitrogen, Carlsbad, CA). Matrix-assisted laser desorption/ionization time of flight (MALDI-TOF) mass spectrometry is carried out in an Ultraflex mass spectrometer (Bruker, Billerica, MA).

Sample Preparation Five different concentrations of triblock copolymer TR4T are prepared, ranging from 0.9 mM up to 1.3 mM, in mixtures of 45 vol% 10mM phosphate buffer (pH=7) and 55 vol% D_2O, chosen to match the density of the tracer particles to minimize sedimentation. The protein solution is prepared by dissolving it at 50 ^oC for 30 mins. Tracer particles are introduced into the system at a final weight to volume fraction of 0.12% and mixed with the protein solution by vortexing. Immediately after preparation, samples are loaded into microscope chambers made of a microscope slide and coverslips attached with UV-curable epoxy (Norland). To eliminate water evaporation, the two open ends of the microscope chamber are hermetically sealed with the same UV-curable epoxy.

Multiple particle tracking microrheology Each sample is imaged using optical microscopy in bright-field mode with a 100x oil immersion objective. The thermal motion of more than 100 beads in each image are captured by using a high speed camera (Phantom V9.1, Vision Research) in 2400 consecutive frames recorded at 100 Hz. Images are collected in 2-3 mins intervals during several hours, spanning the entire melting or gelation process. The temperature of the system is controlled with an Instec TSA02i temperature control stage mounted on the microscope, with 0.01 °C accuracy. The trajectories of the beads are determined with standard particle tracking algorithms implemented in MATLAB.[20] The centroid positions of tracked beads are determined, with a measured accuracy of 11 nm, in each consecutive frame to generate individual 2D trajectories, from which the ensemble-averaged mean-squared displacement (MSD) is computed as

$$\langle \Delta r^2(\tau) \rangle = \langle \left| \vec{r}(\mathrm{t} + \tau) - \vec{r}(\mathrm{t}) \right|^2 \rangle \tag{2.1}$$

2.3. Results and Discussion

2.3.1 Mean-Squared Displacements

Using time-resolved multiple particle tracking, we follow the gelation and melting process of the biopolymer TR4T at 1.0 mM concentration on the microscopic scale, as shown in the ensemble-averaged mean-squared displacements (MSD) in Figure 2.1. Note that here we only show a fraction of all MSDs we obtained, for clarity.

We start by quenching the system from a molten state at 45 °C to 23 °C, where the system will gradually form a gel. The rapid drop in temperature initiates the formation of physical nodes in the biopolymer solution due to self-assembly of the end-blocks of TR4T into triple helices, which can be followed from the time-progression of the MSDs as shown in Figure 2.1A. The uppermost curve displays purely diffusive behavior, with a linear dependence of mean-square displacement on time. As time progresses after the quench, the MSD begins to exhibit subdiffusive behavior ($MSD \sim \tau^{\alpha}, \alpha \leq 1$) at short lag times; this is indicative of the formation of an, initially weak, viscoelastic material. The dashed line indicates the crossover from diffusive behavior into subdiffusive and eventually elastic behavior at long lag times. As the formation of trimeric nodes continues to evolve within the system, MSDs begin to exhibit plateaus. These plateaus in the mean-squared displacement indicate the emergence of an elastic modulus in the system.

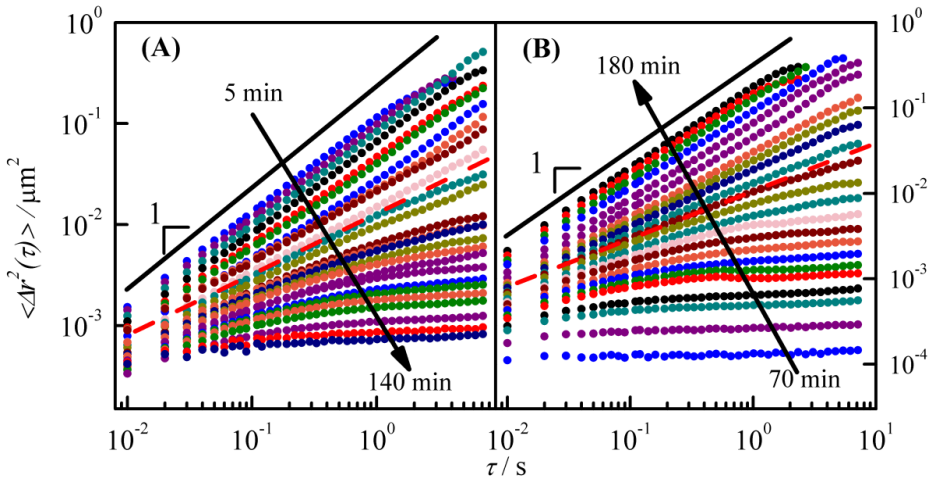

Figure 2.1 Mean-squared displacements of carboxyl polystyrene microspheres with diameter 0.4 µm, embedded in 1.0 mM TR4T is plotted versus lag time (***τ***). Individual curves corresponds to MSDs of particles obtained at discrete times (A) after gelation is initiated by quenching the temperature of the system from a molten state 45 °C to 23 °C, (B) after melting is triggered by rapidly increasing the temperature of a gel equilibrated at 23 °C to 45 °C. Dashed lines indicate the critical transition point which corresponds to gel point in (A) and melting point in (B). For clarity, not all collected MSDs are plotted.

Ultimately, at sufficiently long lag times, these nodes will relax with a node relaxation time of the order of 3000-4000 seconds,[21] which is well outside of the temporal range we explore here. As gelation progresses, the elastic modulus of the system increases; at some point the modulus becomes so high that the motion of the particles is restricted to very small displacements which cannot be detected with our particle tracking algorithm. From the generalized Stokes-Einstein relation[22] and our particle tracking accuracy of 11 nm, we estimate an upper limit of the elastic modulus we can probe of approximately 10 Pa. Hence, by using this method we can only accurately probe the near-critical stage of the gelling system. However, due to the thermoreversible, triple-helix forming nature of end blocks, we can do this not only for gelation but also for melting. By rapidly increasing the temperature of the gel that is equilibrated at 23 °C to 45 °C, nodes start to dissociate and the gel melts into a liquid state, as illustrated by the MSDs in Figure 2.1B. Here we observe qualitatively the same phenomena as for gelation, but in reverse order: the initial elastic response gradually transforms into subdiffusive, and eventually into diffusive behaviour. Clearly, biopolymer TR4T indeed features a fully thermoreversible mechanism; the melting process follows qualitatively the same trends as gelation.

2.3.2 The method: Time-cure superposition

The time-cure superposition method[9] relies on the fact that a polymer system in which crosslinks are formed in time approaches a critical percolation point in which length and time scales diverge. It has been proposed that in the neighbourhood of this critical point, the size of polymer clusters, and associated relaxation times, exhibit self-similarity.

Furthermore, the method assumes that the distance to the critical point, ε, expressed in these experiments as a time t_c is equivalent to the classical expression in terms of the connectivity p:

$$\varepsilon = |p - p_c|/p_c = |t - t_c|/t_c \tag{2.1}$$

To explore this approach, we shift the MSD curves obtained at discrete times during the course of the process by multiplying the horizontal and vertical axis with shift factors a and b, respectively, so as to construct a master curve of the mean-square displacements,[8] in direct analogy to time-temperature superposition in conventional rheological measurements.

The time shift factor, a, corresponds to the scaling of the longest relaxation time in the gelling system, while the MSD shift factor, b, corresponds to changes in the steady-state creep compliance. As noted previously,[14] static and dynamic errors that inherently arise in particle tracking analysis may affect the accuracy of MSD data at short lag times, resulting in misleading scaling of the shift factors. Therefore, data obtained around lag times (τ) ~ 1 s and above are selected from each MSD curves (representing a discrete time), and used to construct the master curves. Collecting sufficient data close to the critical regime is important to get acceptable statistics and a clear, reliable picture of the gelation kinetics; however, we are limited here by the video recording capacity. To overcome the limitations, we choose the shortest time interval compatible with the recording capacity, which is 2-3 mins. The time-cure superposition method has been successfully applied earlier[8, 10, 14] to determine the critical gel point in several systems. We noted while attempting the re-shifting for our system that some degree of ambiguity existed in choosing the shift factors to construct the master curves for both regimes. This may be troublesome because the shift factors, which are manually assigned to obtain the best superposition, are later used to determine the critical gel point or melting point, and the distance from the critical point ε. Moreover, they influence the results found for the dynamic scaling exponents, y and z, that in the critical region are expected to exhibit power-law behavior: $a \sim \varepsilon^{y}$ and $b \sim \varepsilon^{z}$, and eventually the critical relaxation exponent, n, from the relation $n = z/y$. In the following we therefore describe in detail our approach to obtaining superposition for our experimental system and our attempt to extract the gel times as accurately as possible.

One possible criterion to distinguish between the liquid and gel regimes, may be to take the logarithmic slope $\alpha = d[\log\langle \Delta r^2(\tau)\rangle] \,/\, d\,[\log \tau\,]$ of the master curve for the liquid regime between unity and a value in the range $0.55 \leq \alpha \leq 0.60$, and to assign MSD curves which have lower values of logarithmic slope than 0.55, to the second master curve, associated with the gel regime.[8] Also here, some ambiguity in precisely determining the gel point remains.

In the original paper by Larsen and Furst,[8] which first described the approach we apply to the thermoreversible gels in this paper, the dynamic scaling exponents, y and z, are extracted separately for liquid and gel regimes. From these dynamic scaling exponents, y and z,

the critical relaxation exponent ($n = z/y$) can then be determined. From their pioneering work, the critical relaxation exponents were found to be either consistent with Rouse dynamics of fractal polymers ($n = 2/3$) for hydrogels of stiff peptide fibers, while significant deviations were observed for gels of flexible polyacrylamide [8] ($n = 0.45$). It has also been proposed[11, 14] that the critical gel point can be determined by assuming, *a priori,* a value for the critical exponent of 0.60 and adjusting the superposition shift factors until this value is met; as we do not know what critical exponent to expect for the system we investigate here, this approach is not applicable.

In an alternative method, proposed by Corrigan and Donald[10], the shift factors obtained for pre-gel and post-gel are combined and the power-law relationship of shift factors with ε is simplified as $a \sim \varepsilon^y$, $b \sim \varepsilon^z$ so to $b \sim a^{z/y}$. Thus, from the shift factors alone, without knowledge of the exact gel point, the critical relaxation exponent can be determined, however, to determine dynamic scaling exponents y and z separately, the gel/melt point needs to be known *a priori*. For the system under study here, in which we do not know the gel point or critical scaling exponent *a priori*, we describe below our method to first construct the master curves and then extract the numerical values for the critical points and exponents.

We include all MSD curves, also the ones that, for clarity reasons, are not plotted in Figure 2.1, into our time-cure superposition analysis. The MSD curves that span the course of gelation should form two master curves, separated by the critical gelation time; we label them liquid and gel. To determine the critical gelation regime and construct the master curves accurately, we first plot the logarithmic slope of the MSD curves as a function of experimental time, as shown in Figure 2.2A. For the experimental system we use here, the long-time relaxation occurs at several hundreds of seconds; on the time scale we probe during these short "snapshot" microrheology measurements, terminal relaxation does not occur, and as such we may treat the network, within the experimental frequency range, as non-transient. We therefore adopt the approach used previously[14] to extract a subdiffusive slope from the final decade in the MSD ($\tau > 1$ s) in which short-term (caged) diffusion is negligible.

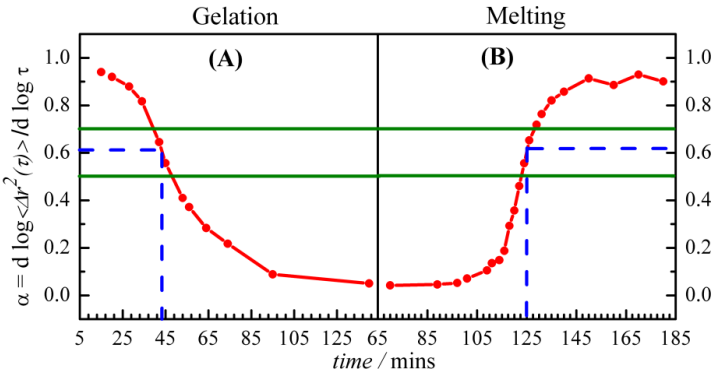

Figure 2.2 Logarithmic slope obtained from each MSD curve ($\boldsymbol{\tau} > 1$ s) is plotted as a function of actual experimental time for gelation (A) and for melting (B). The horizontal dashed lines depicting the predicted values for critical relaxation exponents from earlier analysis and from the intersection with x-axis, critical gelation time and melting time are determined. Solid horizontal lines indicate the limits of theoretical predictions of fractal-like polymer growth.

This relies on the assumption that node relaxation is unimportant at these time scales. The horizontal solid lines here indicate the limits of theoretical predictions of the critical gel regime $0.50 \leq \alpha \leq 0.70$ for fractal-like polymer growth[14] which we expect for the self-assembly of filamentous peptide network. While we superpose MSD curves by assigning horizontal, a, and vertical, b, shift factors, we follow the method of Corrigan and Donald[10] and at the same time plot the shift factors, b versus a, in Figure 2.3.

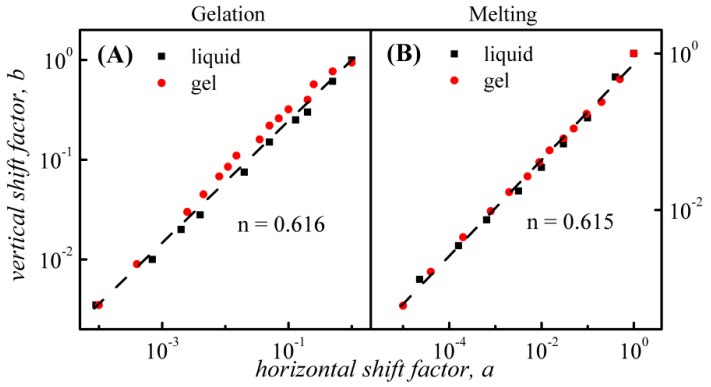

Figure 2.3 The values of vertical shift factor, $\boldsymbol{b}$, related to steady-state creep compliance are plotted with respect to the values of horizontal shift factor, $\boldsymbol{a}$, related to the longest relaxation time for gela-

tion (A) and for melting (B). The exponent from the power-law relation, $\boldsymbol{b \sim a^{z/y}}$, is the critical relaxation exponent.

The exponent from the power-law relation, $b \sim a^{z/y}$ is the critical relaxation exponent, n. In this way, the evolution of the value for the critical relaxation exponent can be followed while new shift factors are included. This method gives us more control while we assign the shift factors, thus reducing the ambiguity of the method, and resulting in a consistent superposition of the mean-square displacements. The value of n we find to be 0.616, can then be used to accurately determine the critical gel point, for this example at t_c = 43 mins, as indicated by the dashed line in Figure 2.3A. The assigned shift factors are then used to construct the liquid and gel master curves in Figure 2.4A and 2.4B, respectively.

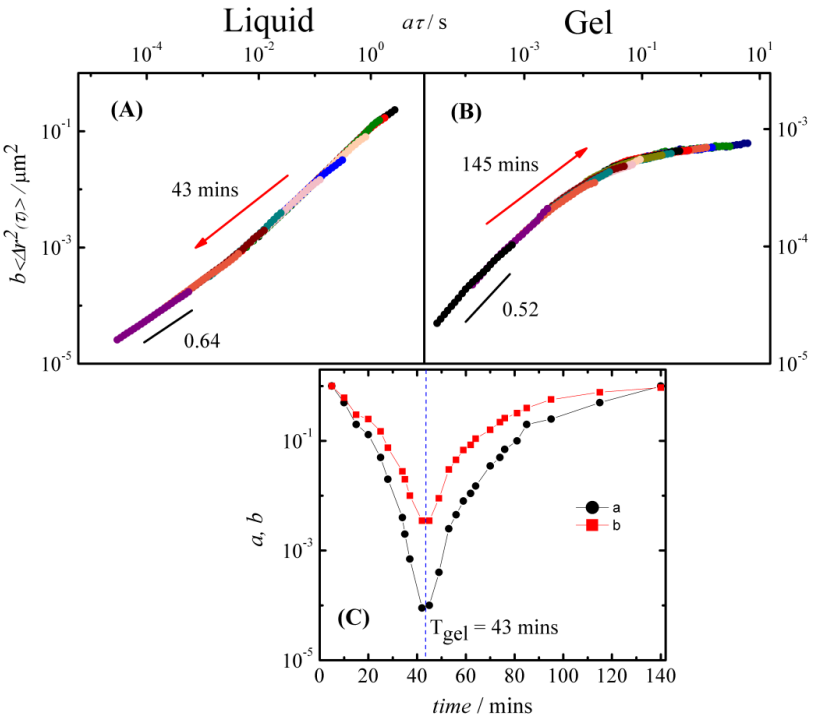

Figure 2.4 Master curves constructed by applying time-cure superposition analysis on MSDs obtained before (A) and after (B) the critical gel transition. (C) Horizontal and vertical axis shift factors $\boldsymbol{a}$ and $\boldsymbol{b}$ respectively plotted as a function of gelation time. Divergence of shift factors identifies the critical gel time indicated by dashed vertical line.

The master curve for the liquid clearly reveals a transition from diffusive to subdiffusive behaviour during the first 42 mins after the quench, with the power-law slope steadily decreasing from 1 to 0.64. Around the critical point, the system changes rapidly, which can be observed in Figure 2.4B as the sudden decrease of logarithmic slope from 0.64 to 0.52 within 3 mins. Subsequent MSD curves that exhibit viscoelastic solid behaviour form the gel master curve, which finally reaches a logarithmic slope of almost zero in 140 mins, indicative of the formation of a solid gel. Figure 2.4C presents the shift factors a, b plotted as a function of experimental time. The sharp cusp signals the critical point; since the spacing of our data is 3 mins, we can locate the critical point with a precision of ±3 mins. However, by interpolation of the two diverging branches forming the cusp we can get t_c more accurately as 43 mins and validate the result of earlier analysis. We follow the same method to construct the master curves for the melting experiment in Figure 2.5. First, we plot the logarithmic slope of MSD curves as a function of actual experimental time in Figure 2.2B. Then during the superposition of MSDs, we also plot the shift factors, b versus a, in Figure 2.3B, and obtain the critical relaxation exponent for melting experiment as n =0.615. This value of n is used to extract the critical melting time to be 123.5 mins, as indicated by the dashed line in Figure 2.2B.

The melting data for 1.0 mM TR4T reveal the same trend, in a reverse manner, as gelation data of the same system see the gel and liquid master curves in Figure 2.5A and 2.5B, respectively. Within 180 min the master curves show a transition from solid-like to purely diffusive behavior. Also here we find the typical cusp-like shape, from which the melting time can be extracted and found to be consistent with the determination from the critical relaxation exponent (Figure 2.5C).

We note that the time to reach the critical melting point, namely 123.5 mins, is a result of the chosen experimental protocol, a sudden increase of the temperature from 23 ^{o}C to 45 ^{o}C; other quench depths result in different melting times. The critical relaxation exponents obtained for TR4T biopolymer system, for both gelation and melting, n ~ 0.6, are meaningful for our peptide network as it is within the predicted range for percolation of a flexible polymer.

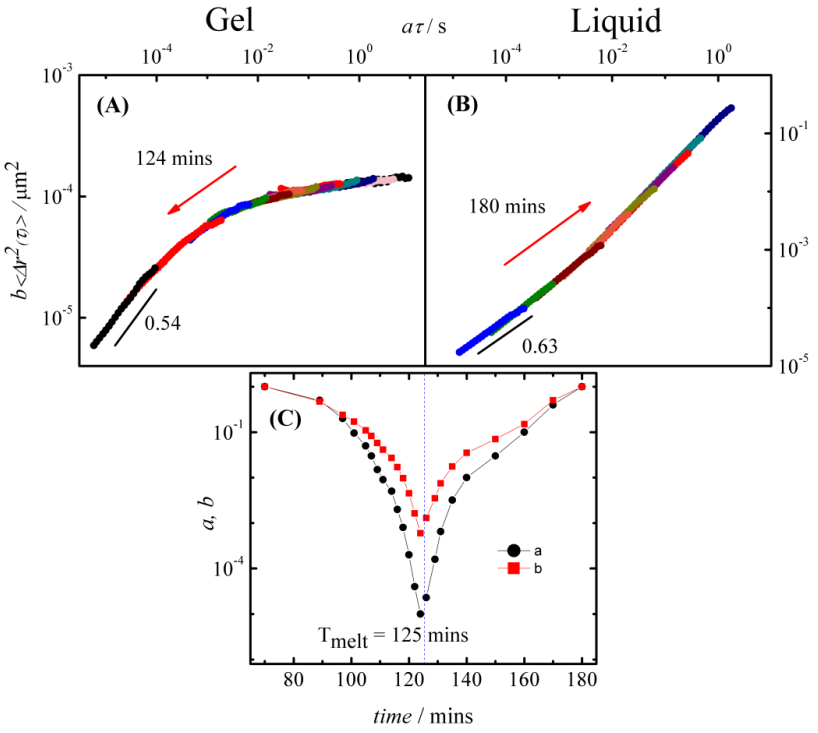

Figure 2.5 Master curves constructed by applying time-cure superposition analysis on MSDs obtained before (A) and after (B) the critical melting transition. Horizontal and vertical axis shift factors ***a***, and ***b***, respectively, plotted as a function of melting time (C). Divergence of shift factors identifies the critical melting point indicated by dashed vertical line.

Both gelation and melting in these systems exhibit the same self-similarity close to the melting point, indicating full thermodynamic reversibility around the gel point. However, the melting and gelation times exhibit a striking difference in their dependence of polymer concentration. The self-consistent time-cure superposition, discussed above, is applied to gelation data for concentrations of 1.0 mM, 1.2 mM and 1.3 mM, as well as to melting data with two additional concentrations, 0.9 mM and 1.1 mM. All critical melting and gelation times determined are shown in Figure 2.6. The gelation time drops over the concentration range 0.9 – 1.3 mM by almost an order of magnitude, whereas the melting time increases over the same concentration range by less than a factor of 3. This observation supports a previously reported kinetic model[21] for melting and gelation of TR4T. This can be under-

stood by considering the molecular details of gelation versus melting of this biopolymer, TR4T.

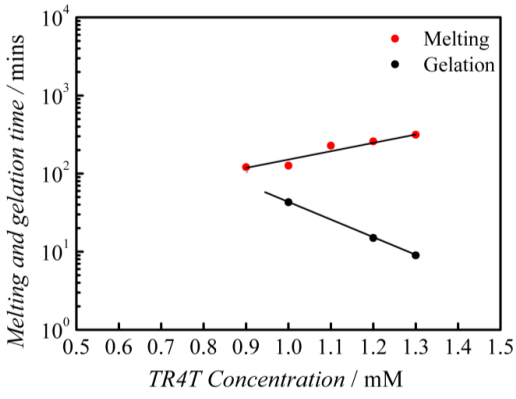

Figure 2.6 Critical melting and gelation times, determined from the time-cure superposition analysis of 1P-MSDs, are plotted versus the concentration of biopolymer TR4T.

For gelation, as described in detail in a previous study[22], individually dispersed nodes need to meet in pairs of three to form a stable triple helix. Thus, it is required that three chain ends are in close proximity, and this reaction is known to be between 1st and 3rd order kinetics.[17] This diffusion limited process depends strongly on concentration due to the collision frequency of the chain ends, scaling as the concentration cubed. For melting, already existing nodes need to disintegrate and it is 1st order kinetics. Depending on the quench depth, this will occur linearly in time during this entire node melting process.

2.3.3 The dynamic scaling exponents: a comparison

Different methods have been applied for obtaining dynamic scaling exponents from time-cure superposition method as described above. We therefore performed a sensitivity analysis on those methods, using the melting data of 1.0 mM TR4T as an example. First, we determine y and z for two different, but equally plausible values of ε, where ε is the distance to the critical point, as described by Larsen and Furst.[8] By using the shift factors already assigned during our analysis, we obtain dynamic scaling exponents for the liquid and gel regimes and present these in Figure 2.7A and Figure 2.7A*, respectively.

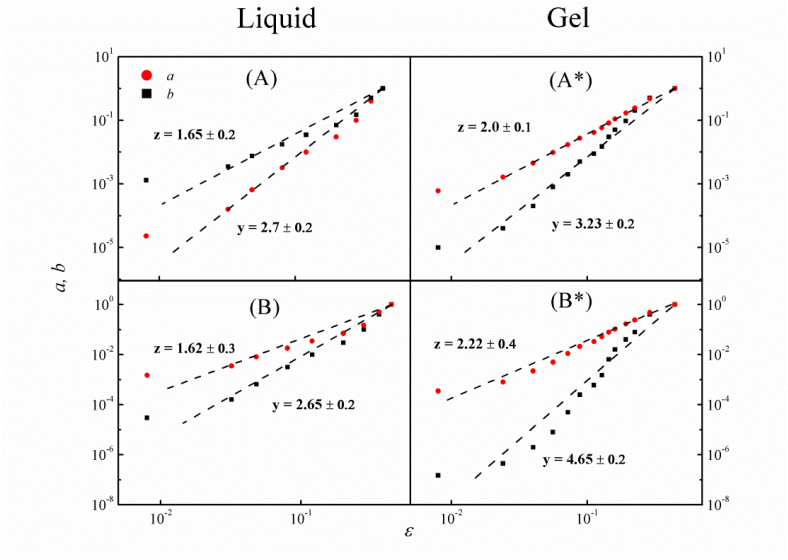

Figure 2.7 Shift factors, ***a*** and ***b***, obtained to construct master curves in Figure 2.5, are plotted versus the distance from the melting point, ε, for liquid (A) and gel (A*) regimes. The same MSD curves are superposed with slightly different shift factors to obtain second set of master curves and those shift factors are used to plot (B) and (B*). Dynamic scaling exponents, ***y*** and ***z***, obtained from the power-law relation are shown on each plot.

Then we construct a second set of master curves, this time not being guided by the evolution of critical relaxation exponent, in Figure 2.3, but visually, as is commonly done.[8] We show the dynamic scaling exponents obtained for the second set of analysis in Figure 2.7B and 2.7B*. Although the dynamic exponents, y and z, are similar in the liquid state (Figures 7A and B), those for the gel state are significantly different. It is also obvious from the curvature that experimental results do not present a perfect power law. We think of two possible reasons; ε is very sensitive to the exact value of the gel point so small errors in assigning the gel point can lead to large error in ε for its lowest value; or power law dependence is only expected to be valid close to solid-liquid (or percolation) transition, may not need to extend entirely into the fully developed system. In this example, the value of n varies between 0.61 and 0.48 which makes a comparison with theory hardly meaningful. Since there are some methods rely on the critical gel time to determine the numerical values of exponents, we also checked the change in values of dynamic scaling exponents and critical relaxation exponents by slightly varying the possible critical melt times. In this way, we show

in Table 2.1, how slight variations in critical melt / gel time can change the dynamic scaling exponents; we find large variations in both z (2.3 to 1.4, and 1.6 to 2.2) and y (3.7 to 2.3 and 2.6 to 3.6). Yet n remains almost the same, 0.607 – 0.616, and consistent with Rouse dynamics.

Table 2.1 Dynamic Scaling Exponents and Critical Relaxation Exponents for 1.0 mM TR4T Obtained from Power-law Relation with Shift Factors, a and b, at Melting Times Close to the Critical Transition.

t_{melt} (mins)	z_{liquid}	y_{liquid}	n_{liquid}	z_{gel}	y_{gel}	n_{gel}
122.5	2.30	3.73	0.616	1.60	2.60	0.611
123	2.20	3.56	0.615	1.73	2.83	0.613
123.5	2.09	3.40	0.615	1.65	2.68	0.615
124.5	1.82	2.97	0.612	1.71	2.78	0.616
125	1.65	2.70	0.611	2.00	3.23	0.616
125.5	1.41	2.33	0.607	2.20	3.56	0.616

2.4 Conclusions

We introduce the use of time-cure superposition analysis on multiple particle tracking microrheology data of a reversible gel network system. We critically test and compare the already proposed methods to determine the critical transition points and the numerical values of exponents from time-cure superposition analysis. We show how slight variations in shift factors and in possible critical points lead to significant differences in numerical values of exponents. Eventually, we propose a clear and straightforward approach on first, how to construct the master curves and then extract the numerical values for the critical points and exponents. Additionally, we study and compare the dynamics of this reversible system that undergoes a sol-gel transition (gelation) as well as the reverse transition from a gel to a viscous liquid (melting). MSDs obtained for gelation and melting exhibit the same-self similarity close to the critical point while confirming the fully thermoreversible mechanism of collagen-inspired polypeptide, TR4T. We determine the critical relaxation exponent of our filamentous peptide network for both pathways as $n \sim 0.60$ consistent with those reported

for Rouse dynamics. The concentration dependence of each pathway exhibit a striking difference while supporting a previously reported kinetic model, as node formation (gelation) being a third-order diffusion limited process depends stronger on concentration than node melting that scales linearly with the polymer concentration.

References

[1] T. G. Mason, D. A. Weitz, *Phys Rev Lett* **1995**, *74*, 1250-1253.

[2] C. Veerman, K. Rajagopal, C. S. Palla, D. J. Pochan, J. P. Schneider, E. M. Furst, *Macromolecules* **2006**, *39*, 6608-6614.

[3] T. Savin, P. S. Doyle, *Soft Matter* **2007**, *3*, 1194-1202.

[4] C. Xu, V. Breedveld, J. Kopeček, *Biomacromolecules* **2005**, *6*, 1739-1749.

[5] Y. Tseng, K. M. An, D. Wirtz, *J Biol Chem* **2002**, *277*, 18143-18150.

[6] Y. Tseng, D. Wirtz, *Biophys J* **2001**, *81*, 1643-1656.

[7] I. A. Hasnain, A. M. Donald, *Phys Rev E: Stat, Nonlinear, Soft Matter Phys* **2006**, *73*.

[8] T. H. Larsen, E. M. Furst, *Phys Rev Lett* **2008**, *100*.

[9] D. Adolf, J. E. Martin, *Macromolecules* **1990**, *23*, 3700-3704.

[10] A. M. Corrigan, A. M. Donald, *Langmuir* **2009**, *25*, 8599-8605.

[11] A. M. Corrigan, A. M. Donald, *Eur Phys J E* **2009**, *28*, 457-462.

[12] K. M. Schultz, A. D. Baldwin, K. L. Kiick, E. M. Furst, *Soft Matter* **2009**, *5*, 740-742.

[13] K. M. Schultz, A. D. Baldwin, K. L. Kiick, E. M. Furst, *Macromolecules* **2009**, *42*, 5310-5315.

[14] T. H. Larsen, M. C. Branco, K. Rajagopal, J. P. Schneider, E. M. Furst, *Macromolecules* **2009**, *42*, 8443-8450.

[15] K. M. Schultz, A. D. Baldwin, K. L. Kiick, E. M. Furst, *ACS Macro Lett* **2012**, *1*, 706-708.

[16] M. W. T. Werten, H. Teles, A. P. H. A. Moers, E. J. H. Wolbert, J. Sprakel, G. Eggink, F. A. De Wolf, *Biomacromolecules* **2009**, *10*, 1106-1113.

[17] P. J. Skrzeszewska, F. A. De Wolf, M. A. Cohen Stuart, J. Van Der Gucht, *Soft Matter* **2010**, *6*, 416-422.

[18] P. J. Skrzeszewska, J. Sprakel, F. A. De Wolf, R. Fokkink, M. A. Cohen Stuart, J. D. Van Gucht, *Macromolecules* **2010**, *43*, 3542-3548.

[19] C. I. F. Silva, P. J. Skrzeszewska, M. D. Golinska, M. W. T. Werten, G. Eggink, F. A. De Wolf, *Biomacromolecules* **2012**, *13*, 1250-1258.

[20] Y. X. Gao, M. L. Kilfoil, *Opt Express* **2009**, *17*, 4685-4704.

[21] P. J. Skrzeszewska, F. A. De Wolf, M. W. T. Werten, A. P. H. A. Moers, M. A. Cohen Stuart, J. Van Der Gucht, *Soft Matter* **2009**, *5*, 2057-2062.

[22] T. G. Mason, T. Gisler, K. Kroy, E. Frey, D. A. Weitz, *J Rheol* **2000**, *44*, 917-928.

CHAPTER 3

Monitoring protein capsid assembly with conjugated polymer strain sensor

Semiconducting polymers owe their optoelectronic properties to the delocalised electronic structure along their conjugated backbone. Their spectral features are therefore uniquely sensitive to the conformation of the polymer, where mechanical stretching of the chain leads to distinct vibronic shifts. Here we demonstrate how the optomechanical response of conjugated polyelectrolytes can be used to detect their encapsulation in a protein capsid. Coating of the sensor polymers by recombinant coat proteins induces their stretching due to steric hindrance between the proteins. The resulting mechanical planarizations lead to pronounced shifts in the vibronic spectra, from which the process of capsid formation can be directly quantified. These results show how the coupling between vibronic states and mechanical stresses inherent to conjugated polymers can be used to non-invasively measure strains at the nanoscale.

This chapter is published as

Hande E. Cingil, Ingeborg M. Storm, Yelda Yorulmaz, Diane W. te Brake, Renko de Vries, Martien A. Cohen Stuart, and Joris Sprakel. *J Am Chem Soc*, 2015, 137,9800-9803, DOI: 10.1021 /jacs.5b05914.

3.1 Introduction

Conjugated polymers derive their unique optoelectronic properties from the characteristic delocalized electronic structure of the polymer backbone. For well-defined conjugated polymers, fluorescence spectra exhibit distinct vibronic bands, which are uniquely sensitive to the backbone conformation. These effects are often employed in the solid state to manipulate the band structure and optoelectronic properties of conjugated polymer films.[1-3] The transition from amorphous to semi-crystalline order in the β-phase of polyfluorenes, is attributed to the planarization of the backbone that gives rise to distinct vibronic transitions of the molecule and a red-shifted emission.[4] Due to the mechanochromism which is widely reported also for polydiacetylene,[5-7] the conjugated polymer acts as a sensitive optical sensor for its own conformation.[8-9] This planarized β-phase of polyfluorenes is typically found and studied in the solid state.[10-13] In principle, this coupling between induced planarization and vibronic states may also occur when single molecules in solution are forced into an extended state. This holds the promise of using conjugated chains as molecular strain sensors to probe how supramolecular assembly triggers conformational changes or to probe strains in polymer networks at the single-molecule level.[14] One striking example of how supramolecular assembly can lead to mechanical stresses is the stiffening of polymers upon their grafting with side chains into so-called bottlebrush structure.[15] This is for example encountered when DNA is encapsulated by viral coat proteins in the formation of rod-like viruses.[16] As the local concentration of coat proteins increases, lateral interactions between these individual building blocks increase the effective persistence length of the co-assembled structure, upon which the DNA template stretches.[17] While binding processes can be studied directly using FRET,[18] the changes in the conformation of the macromolecules it encapsulates can only be deferred indirectly, and are especially difficult to evaluate during early stages of capsid formation when stretching is modest.

In this chapter, we show how a water-soluble conjugated polyelectrolyte (CPE) can be used as a mechanosensor for the conformational changes it undergoes upon encapsulation in a protein capsid. The electrostatic complexation of a recombinant coat protein with an anionic polyfluorene derivative induces stretching of the template, resulting in distinct vibronic shifts in the fluorescence spectra of the polymer. Through calibration we demonstrate that

this single molecule strain sensor shows high sensitivity even for low degrees of protein binding. Finally, we show how the same probe can be used to quantitatively determine capsid disintegration upon gradual weakening of the binding energy.

We start from a carboxylated polyfluorene derivative, poly[9,9'-bis(3'-propanoate) fluoren-2,7-yl] sodium salt (CP1), synthesized by Yamamoto coupling[19] (Figure 3.1A), which is soluble in water at pH > 7, with M_w = 16.7 kg/mol (PDI = 2.4), see Appendix for detailed information. Similar anionic conjugated polymers have been studied extensively for sensitive detection of multivalent charged species by superquenching.[20-21]

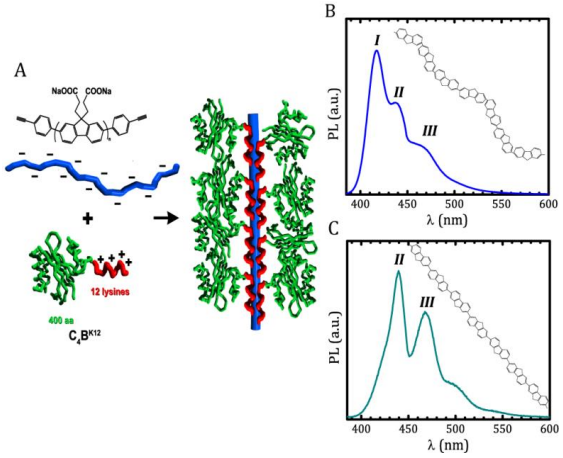

Figure 3.1 Schematic illustration of the structure of the polyfluorene-based sensor polyelectrolyte CP1 and the coat protein C_4B^{K12} (A). PL spectra of bare and flexible CP1 (B) and of stretched CP1 after coating with C_4B^{K12} (C).

While this approach offers excellent detection thresholds, measurement of quantum efficiency does not provide direct insight into the resulting chain conformation. Rather, we note that when these polymers are synthesized to be well-defined with few defects, their photoluminescence (PL) spectra exhibit distinct vibronic bands (Figure 3.1B), which are highly sensitive to the chain conformation.

To induce stretching of the CP1 we use a neutral-cationic polypeptide diblock C_4B^{K12} (Figure 3.1A), which is inspired by natural protein capsid formers and biosynthetically produced in a recombinant *Pichia pastoris* host. It is a minimal design for a coat protein composed of two blocks; the weakly-zwitterionic and hydrophilic, stabilizing coil block (C_4)

consists of 400 amino acids, maintains a random coil structure with a radius of gyration of 7 nm and ensures colloidal stability; and the cationic binding block (B^{K12}) consisting of 12 lysine residues. C_4B^{K12} has previously shown capable of physically attaching to single DNA molecules forming a stable coat [22] while inducing an effective stiffening of the chain.[15, 17, 23] The mixing ratio between CP1 and protein is expressed as the molar ratio of cationic charges to the total number of charges $f+ = [+]/([-] + [+])$. For all experiments we work under dilute conditions of the CP1 (0.6 μM) to avoid intramolecular radiative transfer; unless stated otherwise, in absence of added salt, at pH=8.5, at 22 °C.

The bare CP1 in its native and dissolved state exhibits significant chain flexibility that allows out-of-plane rotations of the backbone which reduce its effective conjugation length. In this scenario we observe three distinct vibronic bands in its fluorescence spectra (Figure 3.1B), with a main band *I* at 418 nm, and two weaker bands, *II* and *III* at 436 and 465 nm, respectively. These bands correspond to the 0-0, 0-1 and 0-2 vibronic transition within the Franck-Condon description. In its coated state, after complexation with the coat protein, a bathochromic shift of ~ 3 nm occurs. More distinctly, we observe distinct changes in the vibronic peaks, where band *I* is significantly quenched, except for a small shoulder at ≈ 415 nm, a shoulder corresponding to the 0-3 transition is discernible around 505 nm.

Upon titrating C_4B^{K12} to CP1 in small increments, we observe a distinct broadening of the absorption spectra towards lower energies (Figure 3.2A). More pronouncedly, the binding that ensues triggers a gradual transition from the PL spectrum of the bare CP1 to the fully coated state (Figure 3.2B). The intensity from the lowest vibronic transition decays smoothly and simultaneously, bands *II* and *III* grow in intensity with increasing $f+$ (inset Figure 3.2B). This characteristic change in the vibronic states is also observed when amorphous polyfluorene transforms into a planarized state known as the β-phase.[4, 9-10, 24] In this ordered state, observed in the solid state of well-defined alkyl-functionalized polyfluorenes, intramolecular chain interactions force the polymers to stretch, reducing rotational degrees of freedom and thereby increasing the effective conjugation length.

This raises the intriguing possibility that the vibronic shifts we observe upon protein binding are the direct result of the stretching and planarization of the conjugated polyelectrolyte due to electrostatic complexation with the coat protein.

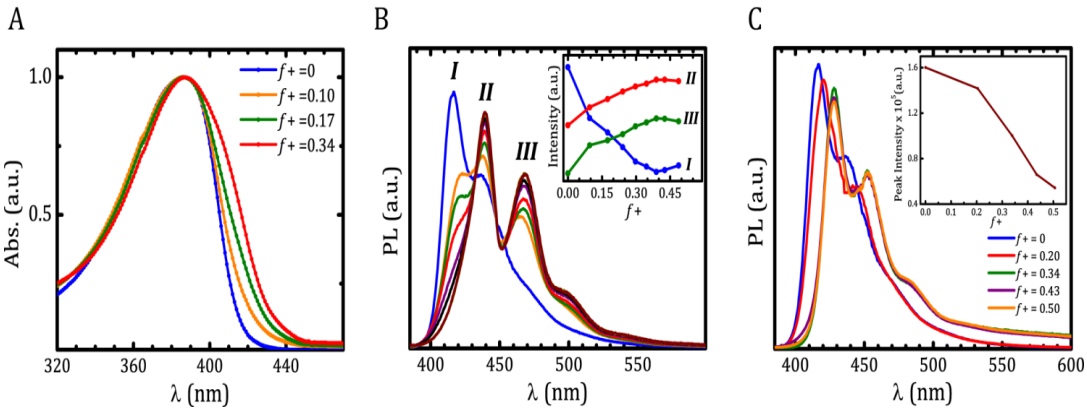

Figure 3.2 Absorption spectra for CP1 at different mixing ratios $f+$ with the diblock protein C_4B^{K12} (A); corresponding normalized PL spectra with inset showing the intensity change of vibronic bands *I, II* and *III* (B); Normalized PL spectra of bare CP1 compared to its complex formed with poly(lysine) homopolymer at mixing ratio $f+ = 0.5$ with inset showing the corresponding maximum peak intensity as a function of mixing ratio, illustrating the superquenching effect (C).

Interestingly, the previously reported effect of superquenching,[17,18] which detects binding rather than chain stretching, is also observed here (Figure A3.1); thus, suggesting the possibility that binding and stretching can be detected independently with the same molecular sensor. To confirm that the observed vibronic shifts are due to stretching of the chain and not due to the charge compensation itself, we repeat the experiment above with a polylysine homopolymer. This polypeptide binds to the anionic polyfluorene but lacks the stabilizing block which is responsible for the lateral interactions between grafts that lead to an increase in main-chain persistence length. Upon mixing the anionic polyfluorene with polylysine a liquid-like coacervate forms, in which chains adopt a largely screened coil-like conformation.[25] While we observe strong quenching of the PL (inset Figure 3.2C), reported previously to result from binding,[17,18] the characteristic vibronic shifts, which we attribute to stretching, remain absent (Figure 3.2C). This indeed suggests that vibronic spectroscopy can be used to sensitively monitor conformational changes in single conjugated chains in solution. While the sensor polymer exhibits significant polydispersity, the vibronic spectra are mostly sensitive to local effects at the scale of the conjugation length; since the average local protein density is independent of CP1 length, polydispersity effects are expected not to be of major significance.

We further verify this by determining the structure of the complexes by means of synchrotron small-angle x-ray scattering. For dilute solutions of scatterers with typical dimension R, the Guinier regime, found at small scattering vectors $qR < 1$, exhibits a power law decay $I(q) \propto q^{-\alpha}$. The exponent α is related to the structure of the scattering objects; $\alpha = 0$ indicates an isotropic coil-like conformation while $\alpha > 0$ signals a stretched and anisotropic conformation.[8, 26] The bare CP1 exhibits a slope of $\alpha \approx 0.6$, indicating a semi-flexible chain intermediate between rod and coil, which can be explained by the relatively high Kuhn length of 7-9 nm,[27] compared to its contour length of $l_c \approx 45$ nm (Figure 3.3A). As protein binds to the polymer, we indeed observe stiffening and stretching of the CP1 chains as the exponent increases significantly. The fact that α becomes larger than unity indicates the formation of a ribbon-like structure when the CP, together with its physically grafted protein side chains, extends and planarizes. This has also been observed for alkyl-functionalized polyfluorenes during β-phase formation.[28]

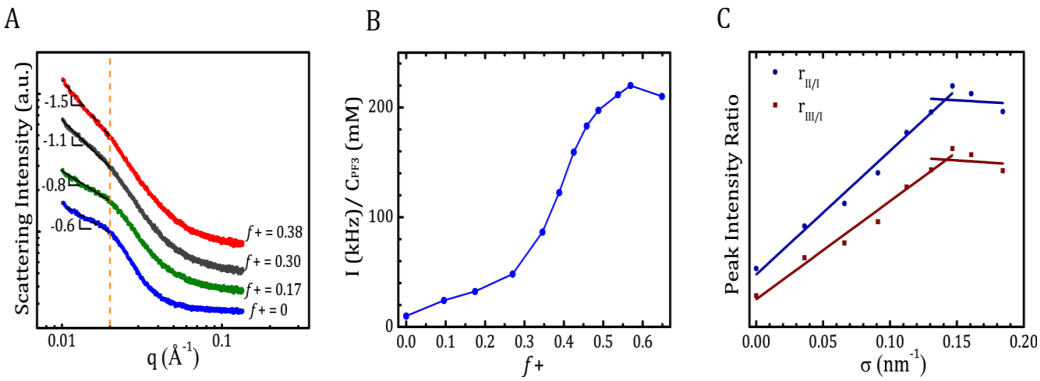

Figure 3.3 Small angle x-ray scattering intensity as a function of wave vector q, the dotted line indicates the limits of the Guinier regime where $I(q) \propto q^{-\alpha}$, with the slope $\boldsymbol{\alpha}$ indicated for each mixing ratio $f+ = 0$ ($\sigma = 0$), $f+ = 0.17$ ($\sigma = 0.066$), $f+ = 0.30$ ($\sigma = 0.112$), $f+ = 0.38$ ($\sigma = 0.146$) (A); light scattering intensity, corrected for dilution, as a function of mixing ratio indicating saturation of binding at charge compensation $f+ \approx 0.5$ (B); sensor calibration given as the ratio of peak intensities $r_{II/I}$ and $r_{III/I}$ as a function of the estimated grafting density σ.

For flexible polymers, such electrostatic interactions would lead to the formation of spherical objects, driven by coacervate surface tension; however, the intrinsic stiffness of the CP1 causes anisotropic objects. To calibrate the strain sensor, we use light scattering to confirm

that binding saturates at full charge compensation, seen as a plateau in concentration-corrected scattering intensity at $f+ \approx 0.5$ (Figure 3.3B). From this, assuming tight binding, we estimate that at $f+ \approx 0.5$, on average 8.5 proteins with 12 cationic groups bind to each CP1 chain which has ≈ 100 negative charges. This allows us to construct a calibration curve of the ratio of vibronic band intensities, $r_{II/I}$ and $r_{III/I}$, as a function of grafting density σ, which is the number of side grafts per unit length of the backbone (Figure 3.3C). We find a linear relation between $r_{II/I}$ and $r_{III/I}$, and grafting density for $\sigma < 0.14$ nm^{-1}. In this regime, we can thus accurately detect and quantify the protein binding on the CP1 backbone from the stretching it induces. Interestingly, at grafting densities $\sigma > 0.14$ nm^{-1}, below the maximum grafting density $\sigma_{max} = 0.19$ nm^{-1} at full charge compensation, the vibronic signal saturates (Figure 3.3C). This saturation effect can be explained by considering how binding of the coat protein induces an effective stiffening of the CP1. The polymeric sensor is composed of $N_s \approx 50$ statistical segments of dimension $a_s = 0.9$ nm, with a contour length $l_c = N_s\, a_s \approx 45$ nm. This backbone is decorated with pendant protein grafts, consisting of the C_4 block composed of $N_g = 400$ amino acids with dimension $a_g \approx 0.3$ nm. The grafting density σ is related to the number of bound protein grafts n_g, as $\sigma = n_g / N_s\, a_s$. The presence of the grafted chains provides additional resistance to bending of the backbone, leading to an effective increase in persistence length $l_p \approx {N_g}^2 v {a_g}^3 \sigma^2 = {N_g}^2 v {a_g}^3 \sigma^2 {n_g}^2 / {N_s}^2 {a_s}^2$, where v is the dimensionless second virial coefficient, which is 0.5 in a good solvent.[12] At saturation, $\sigma = 0.14$ nm^{-1}, the effective persistence length of the grafted CP1 $l_p \approx 42$ nm becomes almost equal to the contour length of the sensor polymer. Saturation of the vibronic shift thus occurs when $l_p \approx l_c$; binding of additional proteins beyond this point no longer induces further stretching, which results in a plateau in the ratio of vibronic peak intensities. This indicates that sensitivity and saturation threshold of the conformation sensors can be tailored in the sensor design by means of, for example, its degree of polymerization N_g.

The binding between C_4B^{K12} and CP1 is the result of electrostatic interactions. Consequently, the binding strength should depend sensitively on the ionic strength of the aqueous solution due to screening of the Coulombic interactions between the oppositely charged polyelectrolytes. The conformational changes upon binding of the protein should be reversible

upon addition of salt. We start with complexes formed at $f+ = 0.2$, in absence of added salt, and gradually titrate the solution with a 5 M NaCl solution. As the ionic strength increases, resulting in weakening of the electrostatic bonds, we observe a reversal of the vibronic shifts reported above; the intensity of the first vibronic peak *I* increases, while band *II* and *III* gradually quench (Figure 3.4A). This trend can be followed in the inset of Figure 3.4A which shows the change in the vibronic signature of CP1 with increasing salt concentration.

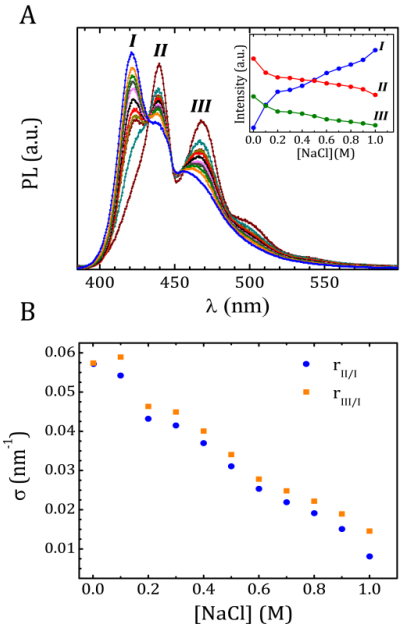

Figure 3.4 Reversibility assay where a pre-assembled electrostatic complex of capsid forming protein C_4B^{K12} and CP1 is titrated with indifferent electrolyte: the normalized PL spectra with the inset showing the corresponding change in normalized vibronic band intensities (A); grafting density as a function of ionic strength is determined from the sensor calibration given above (B).

This confirms that upon addition of salt, binding is gradually suppressed, thereby CP1 returns to its semi-flexible, uncoated state. Using the calibration curve in Figure 3.3C, we also directly quantify the protein binding density along the polymer backbone as a function of ionic strength. With increasing salt concentration, the density of bound proteins decreases linearly (Figure 3.4B); the data suggests that the electrostatic complexes disintegrate com-

pletely at [NaCl] ~ 1.2 M, which is consistent with the observed dissolution of complexes between oppositely charged synthetic polymers.[29]

These results highlight how vibronic spectroscopy on simple π-conjugated polyelectrolytes can be used to directly and non-invasively detect their conformational state in solution. The coupling of vibrational and electronic states in anionic polyfluorenes, resulting in distinct vibronic fingerprints, allows sensitive and quantitative detection of how supramolecular interactions lead to changes in the configuration of a single polymer chain. Combined with their superquenching ability, this offers a complete tool to study the kinetics of binding and resulting shape transformations in the supramolecular assemblies. Moreover, we envision that the intimate connection between the stretching of single chains with spectral response, as demonstrated here, opens new possibilities to measure local strains in mechanical testing of bulk materials, such as gels or elastomers, to give molecular insight into the mechanisms of deformation and failure.

References

[1] A. J. C. Kuehne, M. Kaiser, A. R. Mackintosh, B. H. Wallikewitz, D. Hertel, R. A. Pethrick, K. Meerholz, *Adv Funct Mater* **2011**, *21*, 2564-2570.

[2] C. Rothe, F. Galbrecht, U. Scherf, A. Monkman, *Adv Mater* **2006**, *18*, 2137-+.

[3] A. L. T. Khan, P. Sreearunothai, L. M. Herz, M. J. Banach, A. Kohler, *Phys Rev B* **2004**, *69*.

[4] A. J. Cadby, P. A. Lane, H. Mellor, S. J. Martin, M. Grell, C. Giebeler, D. D. C. Bradley, M. Wohlgenannt, C. An, Z. V. Vardeny, *Phys Rev B: Condens Mater Phys* **2000**, *62*, 15604-15609.

[5] R. A. Nallicheri, M. F. Rubner, *Macromolecules* **1991**, *24*, 517-525.

[6] R. W. Carpick, D. Y. Sasaki, A. R. Burns, *Langmuir* **2000**, *16*, 1270-1278.

[7] D. H. Park, J. Hong, I. S. Park, C. W. Lee, J. M. Kim, *Adv Funct Mater* **2014**, *24*, 5186-5193.

[8] E. Da Como, K. Becker, J. Feldmann, J. M. Lupton, *Nano Lett* **2007**, *7*, 2993-2998.

[9] K. Becker, J. M. Lupton, *J Am Chem Soc* **2005**, *127*, 7306-7307.

[10] F. B. Dias, J. Morgado, A. L. Maçanita, F. P. Da Costa, H. D. Burrows, A. P. Monkman, *Macromolecules* **2006**, *39*, 5854-5864.

[11] M. Knaapila, M. Torkkeli, A. P. Monkman, *Macromolecules* **2007**, *40*, 3610-3614.

[12] R. R. Rosencrantz, K. Rahimi, A. J. C. Kuehne, *J Phys Chem B* **2014**, *118*, 6324-6328.

[13] R. C. Evans, P. C. Marr, *Chem Commun* **2012**, *48*, 3742-3744.

[14] E. Ducrot, Y. L. Chen, M. Bulters, R. P. Sijbesma, C. Creton, *Science* **2014**, *344*, 186-189.

[15] L. Feuz, F. a. M. Leermakers, M. Textor, O. Borisov, *Macromolecules* **2005**, *38*, 8891-8901.

[16] C. M. Knobler, W. M. Gelbart, *Annu Rev Phys Chem* **2009**, *60*, 367-383.

[17] C. Zhang, A. Hernandez-Garcia, K. Jiang, Z. Y. Gong, D. Guttula, S. Y. Ng, P. P. Malar, J. A. Van Kan, L. Dai, P. S. Doyle, R. De Vries, J. R. C. Van Der Maarel, *Nucleic Acids Res* **2013**, *41*.

[18] V. B. Rao, L. W. Black, *Virol J* **2010**, *7*.

[19] S. Y. Cho, A. C. Grimsdale, D. J. Jones, S. E. Watkins, A. B. Holmes, *J Am Chem Soc* **2007**, *129*, 11910-11911.

[20] S. Kumaraswamy, T. Bergstedt, X. B. Shi, F. Rininsland, S. Kushon, W. S. Xia, K. Ley, K. Achyuthan, D. Mcbranch, D. Whitten, *Proc Natl Acad Sci U S A* **2004**, *101*, 7511-7515.

[21] C. H. Fan, S. Wang, J. W. Hong, G. C. Bazan, K. W. Plaxco, A. J. Heeger, *Proc Natl Acad Sci U S A* **2003**, *100*, 6297-6301.

[22] A. Hernandez-Garcia, M. W. T. Werten, M. A. Cohen Stuart, F. A. De Wolf, R. De Vries, *Small* **2012**, *8*, 3491-3501.

[23] I. M. Storm, M. Kornreich, A. Hernandez-Garcia, I. K. Voets, R. Beck, M. A. Cohen Stuart, F. a. M. Leermakers, R. De Vries, *J Phys Chem B* **2015**, *119*, 4084-4092.

[24] M. Grell, D. D. C. Bradley, G. Ungar, J. Hill, K. S. Whitehead, *Macromolecules* **1999**, *32*, 5810-5817.

[25] E. Spruijt, F. a. M. Leermakers, R. Fokkink, R. Schweins, A. A. Van Well, M. a. C. Stuart, J. Van Der Gucht, *Macromolecules* **2013**, *46*, 4596-4605.

[26] M. Knaapila, D. W. Bright, R. Stepanyan, M. Torkkeli, L. Almásy, R. Schweins, U. Vainio, E. Preis, F. Galbrecht, U. Scherf, A. P. Monkman, *Phys Rev E: Stat, Nonlinear, Soft Matter Phys* **2011**, *83*.

[27] G. Fytas, H. G. Nothofer, U. Scherf, D. Vlassopoulos, G. Meier, *Macromolecules* **2002**, *35*, 481-488.

[28] M. Knaapila, F. B. Dias, V. M. Garamus, L. Almásy, M. Torkkeli, K. Leppänen, F. Galbrecht, E. Preis, H. D. Burrows, U. Scherf, A. P. Monkman, *Macromolecules* **2007**, *40*, 9398-9405.

[29] I. K. Voets, A. De Keizer, M. A. Cohen Stuart, *Adv Colloid Interface Sci* **2009**, *147-48*, 300-318.

APPENDIX

A3.1 Materials and Methods

The monomer 2,7-Dibromo-9,9-bis(3-(*tert*-butyl propanoate))fluorene **(MonF3-*t*)** is purchased from SageChem. Poly(L-lysine) hydrochloride ($PLKC_{20}$) with molecular weight 3300 g/mol and PDI 1.05 is purchased from Alamanda Polymers. All reagents were purchased from Sigma-Aldrich and Biosolve and were used as received. Mill-Q water (18.2 MΩ) is used to prepare all polymer and protein polymer solutions. All the measurements are performed at room temperature.

NMR spectra are obtained on a Bruker Avance III 400MHz spectrometer. Fed-batch fermentation of C_4B^{K12} protein polymer is performed in 2.5-L Bioflo 3000 fermentor (New Brunswick Scientific, Edison, NJ).

Sodium dodecyl sulfate polyacrylamide gel electrophoresis (SDS-PAGE) is performed using the NuPAGE Novex system (Invitrogen, Carlsbad, CA).

Matrix-assisted laser desorption/ionization time of flight (MALDI-TOF) mass spectrometry is carried out in an Ultraflex mass spectrometer (Bruker, Billerica, MA).

Shimadzu UV-1601 Spectrophotometer is used to record absorption spectra; data is averaged over 3 scans. Fluorescence emission and excitation measurements are performed on Edinburg Instruments Fluorescent Spectrophotometer FLS920 with 450W xenon lamp; data is averaged over 3 scans.

Dynamic light scattering experiments are performed at fixed angle 90 ^{o} with an ALV light scattering apparatus, equipped with a 400 mW argon ion laser operating at 632.8 nm.

Small-Angle *x*-ray Scattering (SAXS) experiments are performed at the European Synchrotron Radiation Facility (ESRF) in Grenoble, France, at the BM26B DUBBLE beamline. The samples are measured in 2 mm quartz capillaries (Hilgenberg) with an outside diameter of 2 mm and a wall thickness of 0.01 mm. A Pilatus 1M detector with a photon wavelength of 1.54 Å and a sample-to-detector distance of 7 meters are used to reach a *q*-range of 0.0023 – 0.166 $Å^{-1}$. Data is averaged over 10 scans, with the sample acquisition time in the order of 60 s for each sample and is analyzed by using the SasView software.

A3.2 Synthesis and Characterization of Polymer

(1) Poly[9,9′-bis(*tert*-butyl-3″-propanoate)fluoren-2,7-yl] (PF3-*t*)

The synthesis of homopolymer PF3-*t* via the nickel(0)-mediated polymerization reaction, Yamamoto polymerization, has been slightly modified from a previously described method.[1]

$Ni(COD)_2$ (550 mg, 2 mmol) and 2,2′-bipyridyl (312 mg, 2 mmol) are placed in a 50 mL two neck round- bottom flask in the glove box. Dry dimethylformamide (3.5 mL) is added into the flask and purged with nitrogen at 75 °C. COD (245 µL, 2 mmol) is added dropwise and the mixture is stirred for 1 hour. (MonF3-*t*) (0.55 g, 1 mmol) is dissolved in anhydrous toluene (6 mL) in a separate flask and purged with nitrogen, later it is added into the reaction vessel dropwise. The mixture is stirred under nitrogen for 9 hrs.

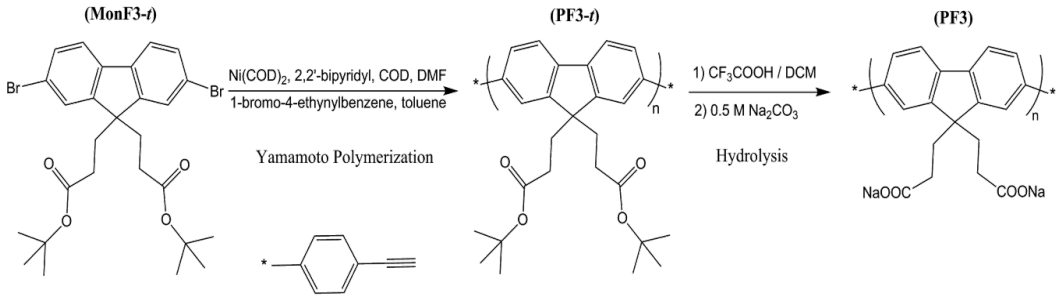

Schematic A3.1 The protocol for Yamamoto polymerization and hydrolysis.

The endcap agent, 1-bromo-4-ethynylbenzene (97%) (181 mg, 1 mmol) is dissolved in anhydrous toluene (2 mL) and injected into the reaction vessel dropwise. The mixture is stirred overnight under the same conditions.

For the purification of the polymer, crude product is stirred in a solvent mixture (methanol: acetone: HCl (0.1M) = 1:1:1) for 2 h. The precipitate is filtered and Soxhlet extracted subsequently with Methanol, Acetone, DCM and obtained as yellow solid (310 mg, 56 %) with M_w =16.7 kg/mol (after correction against polystyrene standards) and PDI = 2.4.

^{1}H NMR (400 MHz, $CDCl_3$, 25 °C): δ 7.79-7.66 (m, 6H), 2.46 (s, 4H, $-CH_2-$), 1.57 (s, 4H,$-CH_2-$), 1.22 (s, 18H) ppm.

(2) Poly[9,9′-bis(3″-propanoate)fluoren-2,7-yl] Sodium Salt (CP1)

PF3-*t* (60 mg) is dissolved in DCM (50 mL) in a 100 mL round bottom flask. Trifluoroacetic acid (TFA) (5 mL) is added dropwise into the reaction flask and the mixture is stirred overnight at room temperature. After the removal of solvent with rotavap, the residue is refluxed with Na_2CO_3 solution (0.5 M, 50 mL) for 24 hrs. The polymer is purified through dialysis units (M_w cutoff: 1000) against Mill-Q water for 3 days. CP1 is obtained after freeze-drying as fibrous yellow solid (31.3 mg, 52 %). ^{1}H NMR (400 MHz, MeOD, 25 ^{o}C): δ 7.83-7.73 (m, 6H), 2.51 (s, 4H), 1.54 (s, 4H) ppm, 1.22 (s, 18H). Conversion efficiency is obtained as 94%.

A3.3 Protein Polymer C_4B^{K12}

Biosynthetic production of neutral-cationic protein diblock copolymer (C_4B^{K12}) is achieved by using recombinant *Pichia pastoris* yeast strains that carry the artificial genes for the desired amino acid sequences:

GPPGEPGNPGSPGNQGQPGNKGSPGNPGQPGNEGQPGQPGQNGQPGEPGSNGPQ

GSQGNPGKNGQPGSPGSQGSPGNQGSPGQPGNPGQPGEQGKPGNQGPAGEPGNP

GSPGNQGQPGNKGSPGNPGQPGNEGQPGQPGQNGQPGEPGSNGPQGSQGNPGKN

GQPGSPGSQGSPGNQGSPGQPGNPGQPGEQGKPGNQGPAGEPGNPGSPGNQGQPG

NKGSPGNPGQPGNEGQPGQPGQNGQPGEPGSNGPQGSQGNPGKNGQPGSPGSQG

SPGNQGSPGQPGNPGQPGEQGKPGNQGPAGEPGNPGSPGNQGQPGNKGSPGNPG

QPGNEGQPGQPGQNGQPGEPGSNGPQGSQGNPGKNGQPGSPGSQGSPGNQGSPG

QPGNPGQPGEQGKPGNQGPAGG-KKKKKKKKKKKKG

A previously described protocol is followed for both biosynthesis and purification.[2] The protein diblock copolymer consists of a stabilizing coil (C_4) block and a binding (B^{K12}) block. The stabilizing block consists of 400 amino acids with the same composition as collagen but a different sequence to suppress self-assembly. The block is hydrophilic and exhibits a random coil structure in solution with a radius of gyration of 7 nm.[3] The cationic binding block consists of 12 lysine residues and is placed at the C terminus of the protein polymer.

The molecular characterization of protein diblock copolymer is done by MALDI-TOF and SDS-PAGE. The molecular weight of C_4B^{K12} obtained with MALDI-TOF (Figure A3.5) is around ~38 kDa. SDS-PAGE is used to check the purity of the protein by loading three different protein concentrations (0.5 $mgml^{-1}$, 1 $mgml^{-1}$ and 2 $mgml^{-1}$). In Figure A3.6 SDS-PAGE gel reveals the band for the protein polymer in all concentrations. The minor upper band visible is due to impurity and it has been observed also in previous studies.[2,4] Hydrophilic C_4 block due to its nature inhibits proper SDS-binding of the protein polymer and cause slow migration on the gel.[2,4-6] This results in apparent molecular weight (~100 kDa) which is not consistent with the MALDI-TOF result.

A3.4 Sample Preparation

Fresh protein and polymer stocks are prepared immediately before every experiment at room temperature. Homogenous solutions of C_4B^{K12} (2 $mgml^{-1}$), poly(L-lysine) (1 $mgml^{-1}$) and CP1 (0.01 $mgml^{-1}$) are prepared in Mill-Q, pH = 8.5 is adjusted by using NaOH. Samples are mixed by using vortex for few seconds. Sonication is never used. For the salt titration, complex formed at pH = 8.5, is titrated with 5M NaCl to the desired ionic strength. For the light scattering experiments, all solutions are filtered through 0.2 µm syringe filters to remove trace quantities of dust.

A3.5 Figures and NMR Spectra

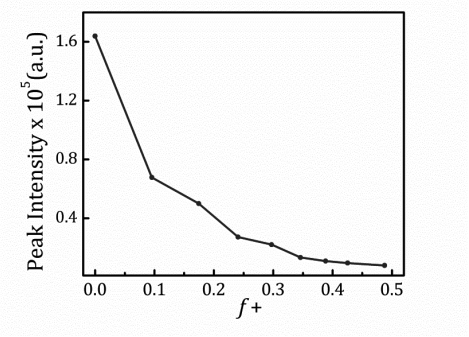

Figure A3.1 Photoluminescence intensity as a function of mixing ratio, illustrating superquenching effect**.**

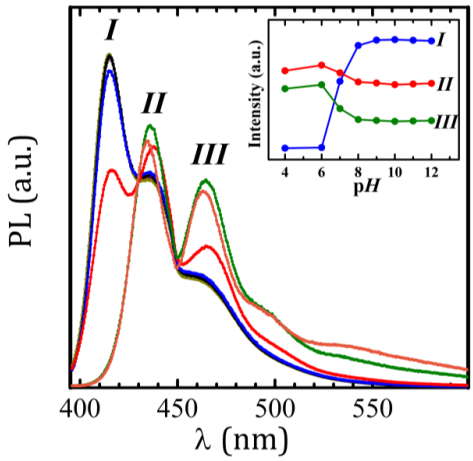

Figure A3.2 Normalized photoluminescence spectra of CP1 at different pH conditions with inset showing the intensity change of vibronic bands *I*, *II* and *III*.

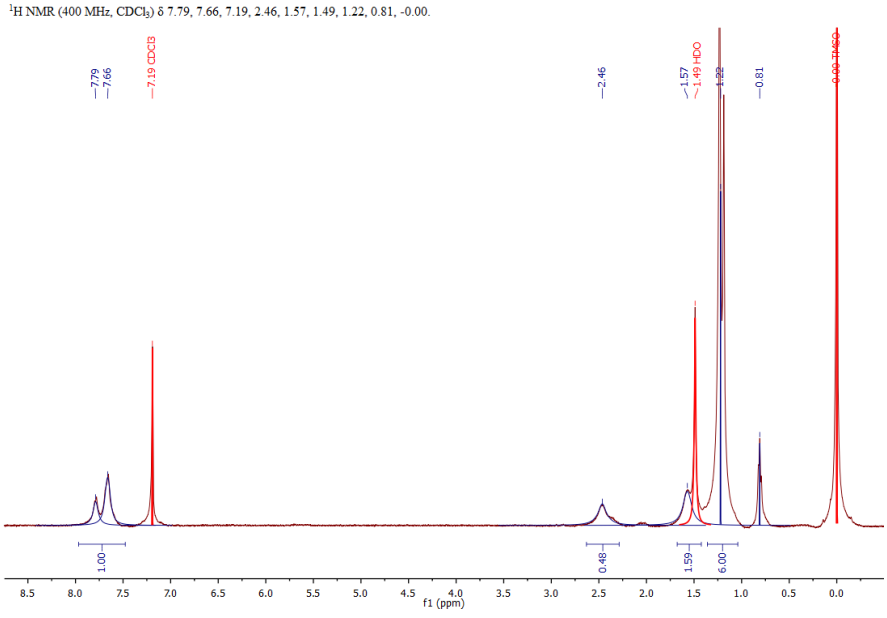

Figure A3.3 ¹H NMR spectrum of PF3-*t*

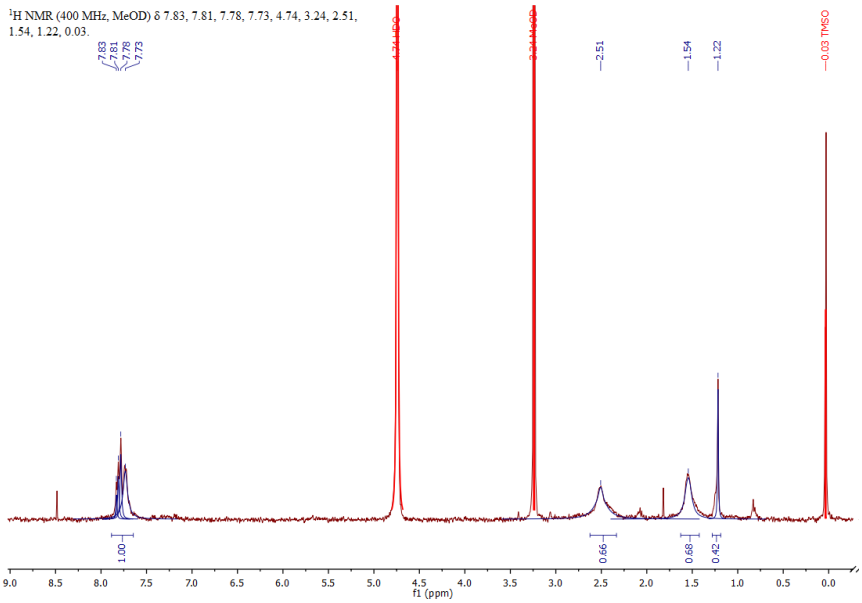

Figure A3.4 ^{1}H NMR spectrum of CP1

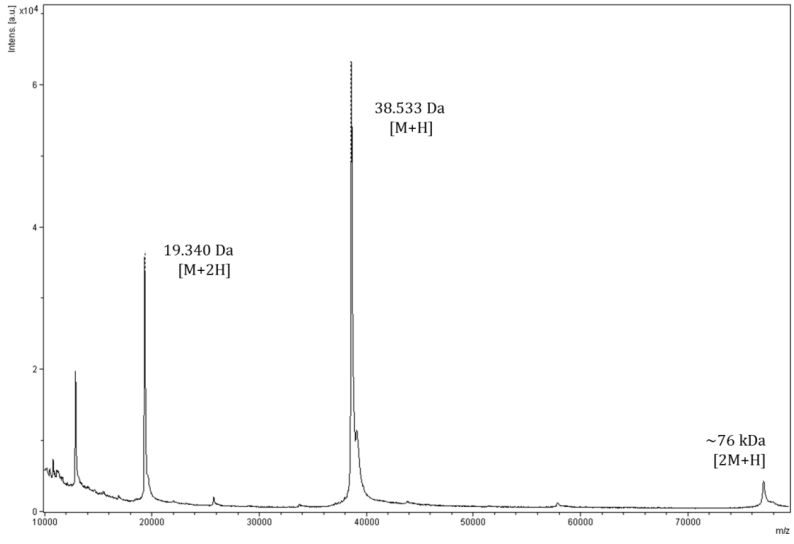

Figure A3.5 MALDI-TOF (Matrix Assisted Laser Desorption/Ionization Time-of-Flight Mass Spectrometry) spectrum of C_4K^{B12}

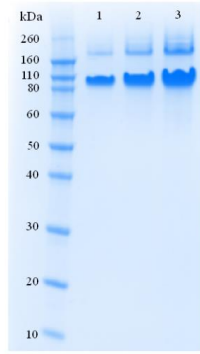

Figure A3.6 SDS-PAGE (Sodium dodecyl sulfate polyacrylamide gel electrophoresis) of C_4K^{B12}. Lane 1: 0.5 mg/mL, lane 2: 1 mg/mL and lane 3: 2 mg/mL C_4K^{B12} loading.

References

[1] S. Y. Cho, A. C. Grimsdale, D. J. Jones, S. E. Watkins, A. B. Holmes, *J Am Chem Soc* **2007**, *129*, 11910-11911.

[2] A. Hernandez-Garcia, M. W. T. Werten, M. A. Cohen Stuart, F. A. De Wolf, R. de Vries, *Small* **2012**, *8*, 3491-3501.

[3] M. W. T. Werten, H. Teles, A. P. H. A. Moers, E. J. H. Wolbert, J. Sprakel, G. Eggink, F. A. De Wolf, *Biomacromolecules* **2009**, *10*, 1106-1113.

[4] L. H. Beun, I. M. Storm, M. W. T. Werten, F. A. De Wolf, M. A. Cohen Stuart, R. De Vries, *Biomacromolecules* **2014**, *15*, 3349-3357.

[5] M. W. T. Werten, W.H. Wisselink, T.J.J. van den Bosch, E.C. de Bruin, F.A. de Wolf, *Protein Eng* **2001,** *14*, 447-454.

[6] A.A. Martens, G. Portale, M. W. T. Werten, R. de Vries, G. Eggink, M. A. Cohen Stuart, F.A. de Wolf, *Macromolecules* **2009,** *42*, 1002-1009.

CHAPTER 4

Probing nanoscale co-assembly with dual mechanochromic sensors

Attractive electrostatic forces between polymers can be exploited to create well-defined and responsive nanoscale structures. In the process of charge-driven co-assembly, the polymers involved undergo subtle conformational changes. However, ascertaining these conformational transitions, and relating this to the nanostructures that are formed, has remained elusive to date. Here we show how the force-optical response of tailored mechanochromic polymers can be used to detect structural transitions that occur at the nanoscale during assembly. We show that at low charge stoichiometry, electrostatic binding causes individual macromolecules to stretch and stiffen. Remarkably, at stoichiometries close to full charge compensation a gradual transition from single molecular complexes to multimolecular micelles is observed. Moreover, the same macromolecular sensors reveal how the assembly pathways are fully reversible as the binding strength is weakened. These results highlight how mechanochromic polymer sensors can be used to detect the molecular transitions occur during supramolecular structure formation with high precision.

This chapter is published as

Hande E. Cingil, Emre B. Boz, Junyou Wang, Martien A. Cohen Stuart, and Joris Sprakel. *Adv Funct Mater* 2016, 26, 1420-1427, doi: 10.1002/adfm.201504632.

4.1 Introduction

Upon mixing two oppositely charged polyelectrolytes, electrostatic complexation leads to associative and macroscopic phase separation known as complex coacervation.[1-3] If an additional stopping mechanism is introduced, this phase-separation can be halted at the nanoscale to yield well-defined co-assembled nanostructures. For example, the electrostatic co-assembly of an ionic-neutral block copolymer and an oppositely charged homopolyelectrolyte results in charged-driven micellar structures known as interpolyelectrolyte complexes[4-5] or complex coacervate core micelles[1]. These responsive nanoscopic complexes are promising delivery systems for drugs, proteins, DNA and RNA segments[1-2, 6-10] or can act as multimodal imaging contrast agents[11]. Depending on ionic strength, charge density and mixing ratio, a range of soluble complexes or condensed nanostructures are hypothesized to occur.[9] However, as charges remain hydrated during assembly, the resulting structures invariable contain significant amounts of water. This result in low contrast in imaging or scattering, such that obtaining detailed insight into the assembly mechanism, and the resulting changes in conformations of the macromolecules involved, is challenging. While indirect evidence can be obtained from scattering or electron microscopy[12-14], subtle changes occurring within the nanostructures are impossible to resolve to date. However, understanding in detail how charge interactions in aqueous media give rise to the formation of well-defined and responsive nanoscopic delivery vehicles is essential to push their design to the next level.

Conjugated polyelectrolytes (CPEs) are water-soluble conjugated polymers whose backbone exhibits a delocalized electronic structure that creates interesting optoelectronic properties. Upon complexation, the optical properties of CPEs change as a result of changes in energy transfer both within the chain and the coupling to its environment.[15] This has been employed for the detection and quantification of DNA,[16-18] sensing of various proteins,[19] natural polyamines,[20] enzyme activities[21] and hydrogen peroxide levels[22]. Moreover, when these chains are prepared in well-defined states without defects, some CPEs exhibit mechanochromism, a unique coupling between electronic states and force-induced changes in polymer conformation. When the conformation of a polyelectrolyte changes due to the intermolecular forces which arise when it binds to an analyte, e.g. by means of electrostat-

ics, the conjugated backbone goes through alterations such as twisting[23] or planarizing[24]. These changes in turn lead to distinct optoelectronic shifts, which can be easily monitored with optical spectroscopy. Mechanochromism has previously been shown to allow the detection and differentiation of amyloid fibrils,[24] influenza A virus,[25] diamines,[26] and ss-/ds-oligonucleotides[27-28]. More recently, we showed that the conjugated backbone of an anionic polyfluorene goes through a conformational change and planarizes upon complexation with a recombinant capsid protein.[29] This mechanical stretching of the conjugated backbone can be monitored from the shifts in distinct vibronic bands in the photoluminescence (PL) spectra of the CPE. We independently verified that the vibronic shifts cannot be explained by binding alone, but must be the result of chain stretching; this is directly analogous to these phenomena in the β-phase formation of solid polyfluorenes.[30-31] In solution, this mechanochromic response can be used, for example, to quantify low degrees of protein binding as well as capsid disintegration.[29]

As the molecular structure of conjugated polymers can be tailored in a modular fashion, the mechanochromic response can be engineered at the molecular level. For example, incorporation of donor-acceptor units within a polymeric backbone utilizes the improved interchain electron migration between optical partners as a result of complexation to achieve multicolor sensing. In principle, this enhanced interchain energy transfer mechanism may also indicate the transition from a single-molecule complex to a condensed one. This holds the promise of using the change in chain proximity to probe co-assembly processes occurring at the nanoscale.

In this chapter, we use mechanochromism of specifically engineered conjugated chains as a tool to study how macromolecular conformations and environments change during electrostatic complexation. We study the complexation of a well-defined CPE with a neutral-cationic diblock copolymer which results in the formation of micelles. We first show how complexation causes vibronic shifts in fluorescence spectra that are due to mechanical stretching of the conjugated backbone. Surprisingly, we find that close to charge stoichiometry, a distinct change in spectral features emerges. The initially sharp vibronic spectra begin to exhibit a featureless, low-energy band, indicative of molecular aggregation. To understand this effect, we engineer our mechanochromic sensor at the molecular level, by in-

cluding donor-acceptor pairs in the chain to introduce proximity-sensing capability. With this multifunctional macromolecular sensor we unveil how electrostatic co-assembly gives rise to a transition from single-molecule soluble complexes to condensed, multimolecular micelles. We believe that this is a verification of the condensation model proposed for complex coacervation close to charge neutrality.[13, 32] These results shed new light onto the molecular mechanisms of nanostructure formation driven by electrostatic forces and highlight how mechanochromism can be utilized to study complex phenomena at the nanoscale.

4.2 Results and Discussion

4.2.1 Mechanochromic sensor 1

We start by synthesizing the mechanochromic homopolymer poly[9,9′-bis(*tert*-butyl-3″-propanoate)fluoren-2,7-yl] (PF3-*tert*) via nickel(0)-mediated Yamamoto coupling[33] (Figure 4.1A) from the monomer 2,7-dibromo-9,9-bis(3-(*tert*-butyl propanoate)) fluorene (Mon-1). The chains are terminated with 4-bromo phenylacetylene as an end-capping agent (ECA) to control the molecular weight.

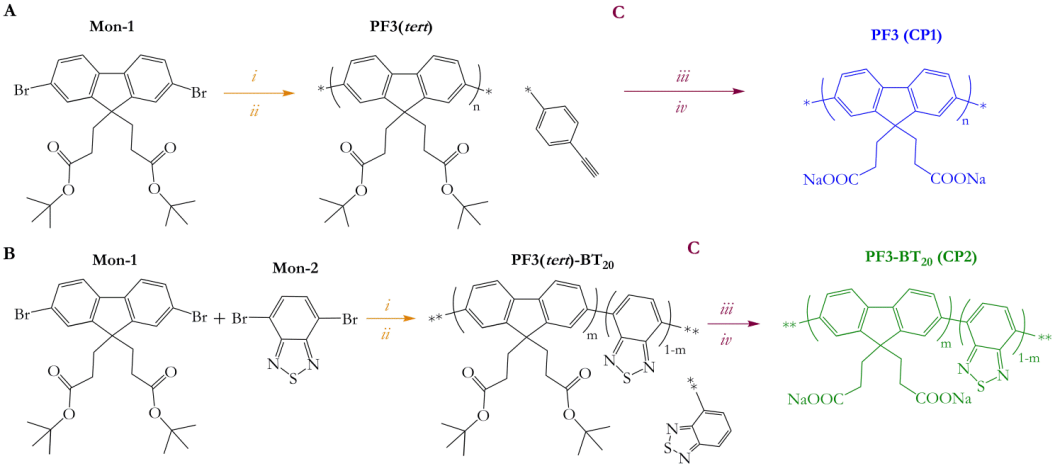

Figure 4.1 Synthesis of mechanochromic polymers via Nickel(0)-mediated Yamamoto coupling; yielding poly[9,9′-bis(tert-butyl-3″-propanoate)fluoren-2,7-yl](PF3*(tert)* with 4-bromo phenylacetylene as end-capping agent (ECA) (A); poly[9,9′-bis(tert-butyl-3″-propanoate)fluorene-co-4,7-(2,1,3-benzothiadiazole)$_{20}$] (PF3*(tert)*-BT$_{20}$) with 4-bromo-2,1,3-benzothiadiazole as ECA (B); ester hydrolysis to obtain PF3*(tert)* sodium salt (CP1) and PF3*(tert)*-BT$_{20}$ sodium salt (CP2) (C); Reagents and con-

ditions: i) $Ni(COD)_2$, 2,2′-bipyridyl, COD/ anhyd. DMF, 75 °C, 9 hrs, under N_2; ii) ECA/toluene, 75°C, 12 hrs under N_2; iii) CF_3COOH/DCM, 23°C, 20 hrs iv) Na_2CO_3/H_2O, 80 °C, 24 hrs.

Carboxylate-functionalized side chains are obtained after hydrolysis of the ester side groups (Figure 4.1C), resulting in polymer CP1 (M_w = 16.7 kgmol^{-1} and PDI = 2.4). The carboxylate charges ensure water solubility at pH > 7 and provide the chain with a high density of anionic charges required for electrostatic complex formation. In solution at pH = 8.5 CP1 exhibits an absorption maximum at 382 nm (Figure A4.1). The photoluminescence spectra show distinct vibronic bands (Figure 4.2B); these allow us to infer the degree of chain stretching, as demonstrated previously[29].

4.2.2 Chain stretching during electrostatic co-assembly

We induce stretching of CP1 by its electrostatic complexation with a neutral-cationic diblock copolymer. For all experiments, unless stated otherwise, we work at pH=9 in absence of added salt at 22 °C and at very dilute polymer concentrations. As a diblock we use poly (*N*-methyl-2-vinylpyridinium)-*b*-poly (ethylene oxide) ($PM2VP_x$-*b*-PEO_y), which is obtained after the quaternization [34] of poly (2-vinylpyridine)-b-poly (ethylene oxide) (Scheme A4.1). It is one of the most commonly studied cationic-neutral diblock copolymers in complex coacervate core micelle systems.[10, 35] We start with $P2VP_{41}$-*b*-PEO_{204} (DP1), which carries almost the same number of cationic charges per chain as a single chain of CP1 (~ 50), complemented by a relatively long neutral block (Table 1). The strongly-charged cationic block binds to the anionic conjugated polyelectrolyte to form a complex coacervate. Macroscopic phase separation is prevented however, by the neutral PEO block, which provides solubility and stability of the complexes formed. The mixing ratio between anionic conjugated polyelectrolytes and cationic-neutral diblock copolymer is expressed as the molar ratio of cationic charges to the total number of charges $f+ = [+] / ([-] + [+])$. Charge stoichiometry thus occurs at $f+ = 0.5$. We introduce DP1 in small increments into the solution of CP1 (0.6 μM). The absorption spectrum of the CP1 at mixing ratio $f+ = 0.40$ shows broadening toward lower energies as a result of complexation (Figure 4.2A). Broadening of the absorption spectra is one of the optical indicators of the planarized conformation of polyfluorene known as β-phase.[30, 36-37] More prominent changes occur in the PL spectrum of CP1 upon

binding to DP1 (Figure 4.2B). The photoluminescence (PL) spectrum of CP1 goes through a gradual vibronic transition, as observed earlier,[29] which signals the change from a bare, semi-flexible polyfluorene to a coated and stretched chain. This transition with increasing $f+$ is observed as a decay in the main band I at 415 nm, which is the 1-0 vibronic transition, and a simultaneous increase in bands II at 436 nm and III at 465 nm, which are the 2-0 and 3-0 transitions, respectively; this is clearly seen in a plot of intensity ratios as a function of $f+$ (inset Figure 4.2B).

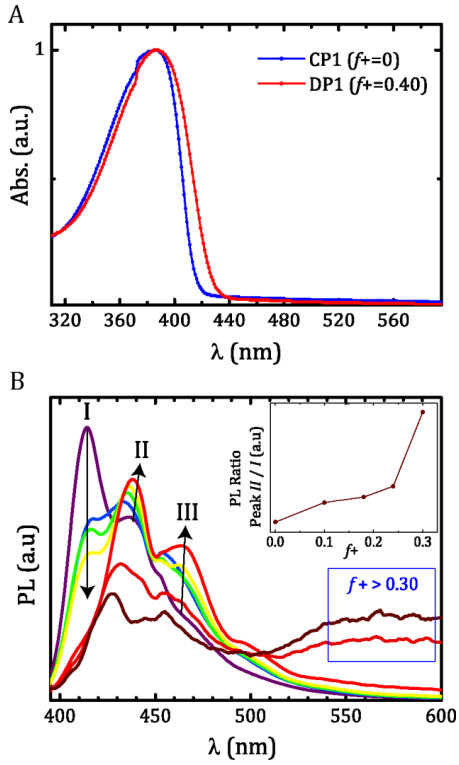

Figure 4.2 Absorption spectra of CP1 with DPs at high mixing ratios ($f+$) (A); Normalized PL spectra of bare CP1 and of the complex formed with DP1 at different $f+$ with inset showing the ratio of intensity of vibronic bands II to I (B). Box highlights the emergence of a low-energy band at mixing ratios $f+> 0.3$.

The effective persistence length of the PF3 with attached ('grafted') diblocks is calculated to become almost equal to the contour length of the sensor polymer at $f+= 0.38$, after which no further stretching occurs at higher mixing ratios; there is saturation of the sensor sig-

nal.[29] However, at $f+>$ 0.30 a new and striking change occurs in the PL spectrum of the complexes formed with DP1. We observe, in addition to the rapid drop in intensity of vibronic bands II and III, the emergence of a broad, featureless low-energy emission band above 500 nm. In the solid state, such a transition is often attributed to an aggregated state of the polyfluorene chains.[30, 37-38] This result rises the intriguing question what process at the nanoscale during the electrostatic co-assembly is responsible for such a sudden spectral shift. Hence we tend to assign this feature to a transition from single molecular objects, at low $f+$, to multimolecular micelles as mixing approaches charge stoichiometry. Such a scenario was predicted to occur theoretically by the so-called condensate model for complex coacervation of homopolymers.[13, 32] At asymmetric stoichiometry, complexes carry a net charge which keeps them soluble and prevents further aggregation. As charge compensation is approached, a transition occurs where neutral droplets, containing many polymer chains, condense and coexist with a small fraction of free chains in excess.

4.2.3 Mechanochromic sensor 2

To verify this hypothesis, we engineer our mechanochromic sensor at the molecular scale. To arrive at a polyfluorene-based sensor that not only detects the mechanical stretching of chains, as we observed earlier,[29] but also the proximity of other chains, we dope the conjugated backbone with a small fraction of benzothiodiazole (BT) acceptor moieties in the conjugated backbone. This creates a "turn-on"/"turn-off" colorimetric response through intermolecular energy migration via FRET.[16, 19, 39-40] We copolymerize 4,7-dibromobenzo[c]-1,2,5-thiadiazole monomer (Mon-2) in a 1:4 ratio with Mon-1, following the same Yamamoto coupling scheme. This results in the statistical copolymer poly[9,9'-bis(tert-butyl-3"-propanoate) fluorene-co-4,7-(2,1,3-benzothiadiazole)$_{20}$] (PF3(*tert*)-BT$_{20}$) (Figure 4.1B). Here we use 4-bromo-2,1,3-benzothiadiazole as the ECA. Ester hydrolysis of the side chains attached to the polyfluorene units is achieved with high yield (93%, Figure 4.1C) resulting in a second mechanochromic polyelectrolyte (CP2) with M_w =12.0 kgmol^{-1} and PDI = 2.2. Like CP1, this chain exhibits the distinct vibronic peaks allowing quantification of the degree of chain extension, when fully dissolved in water at pH = 8.5. However, upon decreasing pH, the chain solubility decreases, leading to increasing intermolecular contacts between fluorene and BT units, giving rise to broadening and red-shift of absorption spectra (Figure

A4.2), while a FRET peak emerges in the photoluminescence (PL) spectra at 550 nm (Figure A4.3).

4.2.4 Chain clustering during electrostatic co-assembly

For an isolated polymer chain, energy transfer between fluorene and BT units within a chain occurs through excited state migration, as a one-dimensional random walk along the backbone.[15, 20] To observe a significant BT peak in the luminescence spectrum, sufficient intrachain energy migration must occur; this requires a relatively high doping of BT units along the backbone. In the synthesis of CP2 we polymerize fluorene and BT in a molar ratio of 4: 1. In the PL spectra of CP2, in a completely dissolved state at pH > 8.5, we only see the polyfluorene emission at 418 nm (Figure A4.3). The absence of a BT emission band at ~ 550 nm illustrates that the doping ratio is insufficient to generate enough energy transfer to give rise to a noticeable BT emission band. This is important, as any BT emission observed during complexation thus must originate from resonant energy transfer between chains in close proximity through the medium. This occurs through a three-dimensional energy transfer [15, 20] which is more efficient and thus gives rise to stronger emission in the BT band. In this way, we can now probe the speculated transition from single-molecule to multimolecular objects with fluorescence spectroscopy.

To study the possible structure transformation in more detail, we perform electrostatic complexation experiments with cationic-neutral diblock copolymers of different architectures (Table 4.1). Additionally, we also use polylysine homopolymer which consists of 20 cations that ensure the binding to the anionic conjugated polyelectrolyte, but lacks the PEO stabilizing block. Figure 4.3A shows the absorption spectra of CP2 with cationic polyelectrolytes at high mixing ratios which show a bathochromic shift, broadening and a prominent increase in the low energy band that can be attributed to BT at 450 - 500 nm. We perform the PL measurements of co-assembled system in more detail by introducing the diblock copolymer in small increments to the CP2 (0.8 μM) solution. We again start with DP1 and observe the change in vibronic bands due to β-phase formation as observed earlier for CP1 upon complexing with DP1. In Figure 4.3B, we observe the smooth decay in intensity of band I at 415 nm as compared to the band II at 436 nm, until $f+ = 0.30$. This gradual stretching and planarizing of the polyfluorene backbone shows that BT units incorporated

in the PF backbone do not alter the optical response of the mechanosensor polymer in dilute condition.

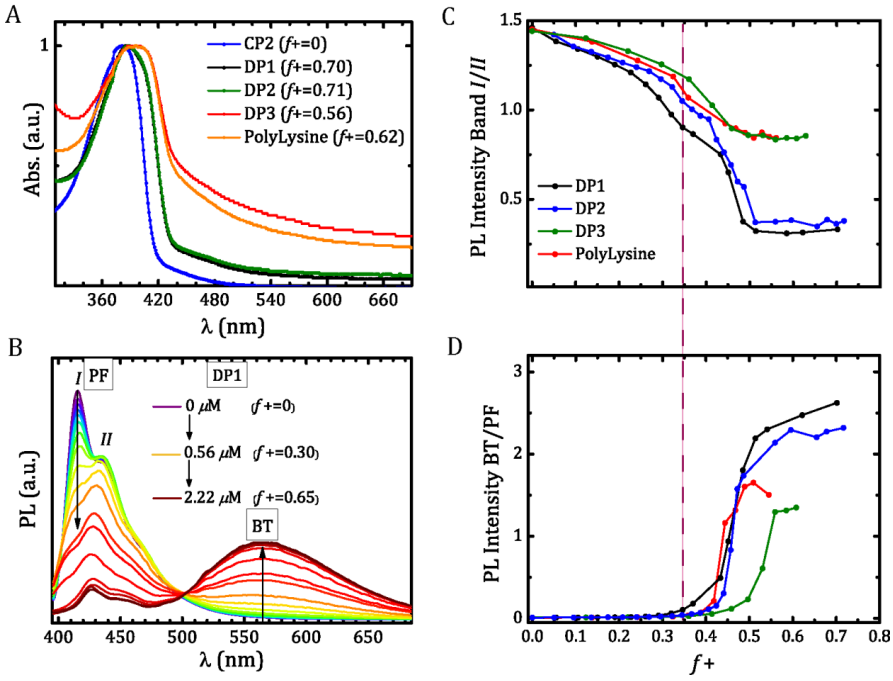

Figure 4.3 Absorption spectra of CP2 with DPs and polylysine homopolymer at high $f+$ (A); Normalized PL spectra of bare CP2 and of the complex formed with DP1 at different $f+$, arrows indicating the intensity change of vibronic bands I and II of PF and BT band (B); The ratio of band I over band II intensity to probe chain stretching (C) and the corresponding FRET ratio of BT over PF intensity which probes chain proximity (D) of complexes formed with DPs and polylysine as a function of mixing ratio.

The binding-induced stretching commences at the very first addition of diblock copolymer; this highlights that at low $f+$, complexation already takes place. However, below $f+ = 0.3$, no FRET signal is observable. Thus, these soluble complexes formed at low mixing ratios are single molecules of CPE coated with the diblock.However, exactly above $f+ = 0.3$, where we previously observed the featureless low energy band, we now see a distinct emergence and growth of the FRET peak at 560 nm, while the PF bands decay simultaneously. This shows that a distinct transition occurs from single-molecular complexes, at low $f+$, to multimolecular complex coacervate core micelles close to charge compensation.

Binding is expected to halt when all charges have been compensated; indeed, we see a plateau in the BT band growth at $f+ \geq 0.5$, where it has become the prominent emission band. We conclude that the molecular engineering of the sensor to include the FRET indeed allows chain proximity to be detected at high mixing ratios and thereby shapes the optical response of the system. We observe a very similar sequence of event for all complexes formed with the other diblock copolymers, and the polylysine (Figure A4.4-A4.6), indicating that the observed transitions are universal during this multimolecular micelle formation.

At low mixing ratios, $f+ < 0.30$, binding leads to the formation of small, soluble complexes of single conjugated polymers coated by a few diblocks which carry a net charge. The side chains on the backbone creates a bottlebrush architecture that cause stretching of the conjugated polymer backbone by reducing its rotational degrees of freedom, as illustrated in Figure 4.4. As a result of this mechanical stretching, the intensity ratio of emission band I to band II continuously drops (Figure 4.3C).

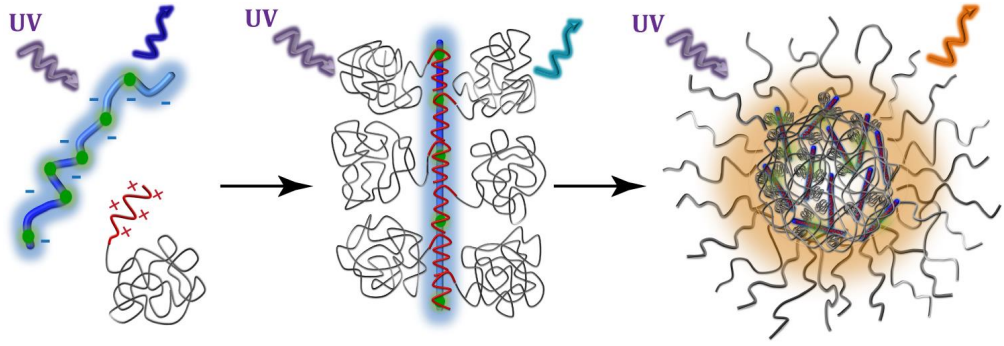

Figure 4.4 Schematic illustration of the sequence of electrostatic co-assembly with diblock copolymers and mechanochromic sensor (left), yielding soluble complexes of individual CP after binding multiple diblocks below charge stoichiometry (middle) which convert to condensed coacervate micelles containing multiple CPs in a coacervate core at mixing ratios close to stoichiometry $f+ \sim 0.5$ (right).

As charge stoichiometry is approached ($f+ = 0.4 - 0.5$), the objects become close to charge neutral and undergo a condensation transition into a microphase-separated coacervate micelle composed of many polymer chains. Experiments on other complex coacervate

micelles have indicated aggregation numbers as large as 20 - 100.[2] As the local concentration of conjugated chains increases, interchain interactions enhance the intermolecular energy transfer process between PF and BT segments. This gives rise to a strong increase in FRET signal which we see as a growth in the ratio of BT to PF emission (Figure 4.3D). There is a final question which cannot be answered by employing our mechanochromic sensors: is the transition from single molecule complexes to micelles abrupt or gradual? In the PL spectra, we see the FRET band emerge gradually, which could originate either from gradual transformation of soluble complexes to micelles, or by gradual condensation of the micellar core as $f+$ approaches 0.5. To answer this question we perform light scattering experiments on complexes formed by CP1 with DPs (Figure A4.7) and by CP2 with DPs and polylysine (Figure A4.8). As an example, we show the scattering intensity, corrected for dilution, as a function of mixing ratio for micelles formed by CP2 with DP2, and the corresponding number-averaged hydrodynamic radius (R_h) in Figure 4.5A.

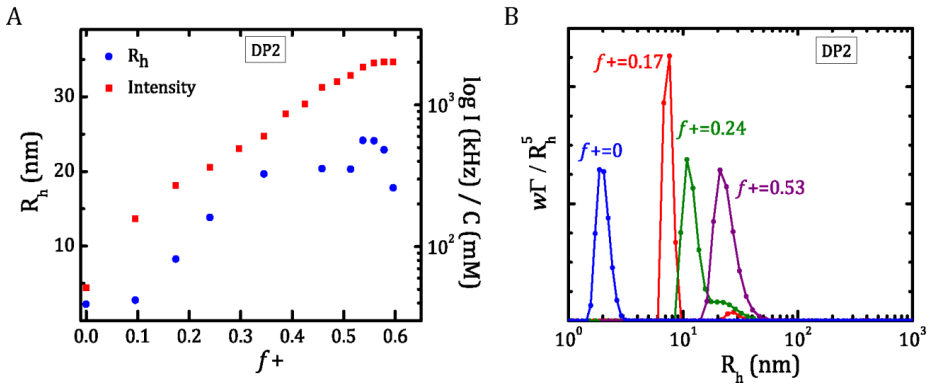

Figure 4.5 Light scattering intensity, corrected for dilution, obtained from DLS measurements of micelles formed by CP2 with DP2 and corresponding number-averaged hydrodynamic radius as a function of mixing ratio, at pH = 9.0 and an ionic strength of 0.01 mM (A); number-weighted size distributions at different mixing ratios from CONTIN analysis (B).

The immediate increase in scattering intensity upon addition of DP2 confirms that interpolyelectrolyte complexation occurs already at low $f+$. The scattering intensity reaches a plateau at $f+ \approx 0.5$, which indicates a saturation of binding at full charge compensation and confirms the results obtained from PL spectroscopy.

The number-weighted size distribution of complexes at different mixing ratios (obtained from CONTIN analysis of correlation functions) we see two populations during co-assembly (Figure 4.5B). Apparently, the transition from a unimodal distribution of CP2 at $f+ < 0.17$ to a bimodal distribution at $0.17 < f+ < 0.53$, confirms the gradual nature of the transition from a single-backbone bottlebrush-like complex to a condensed micelle composed of multiple chains. For this system we find objects with a hydrodynamic radius of 24 nm; similar values are found for complexes formed with DP1 (22 nm) and DP3 (38 nm). The large radius obtained for the CP2-DP3 complex is due to the longer N_{PM2VP} binding block, and the shorter N_{PEO} stabilizing blocks, which results in a stronger driving force for micelle growth.[41] These radii are in good agreement with previously reported values for micelles formed from same diblock copolymers with different anionic polyelectrolytes.[34-35] Complexes formed by CP2 with polylysine, which lack the PEO block that arrests growth of demixed coacervate droplets, do not show well-defined nanophase separation as expected, but rather the formation of large aggregates with $R_h \approx 2.5$ μm at $f+ \approx 0.45$, eventually leading to macroscopic phase separation.

4.2.5 Micelle disintegration

Finally, to explore the reversibility and responsiveness of the electrostatic complexation, we investigate the effect of adding indifferent electrolyte to the system. Electrostatic interactions are the driving force for complex formation in our system. As a result, the critical micelle concentration increases when charge interactions become screened as indifferent electrolyte is added. We find that this leads to a reversal of the process we demonstrated above (Figure 4.6A).

Initially, weakening the electrostatic bonds shifts the dynamic association equilibrium to the unimer state in the bulk; the micelles take up more water in their core, but the overall amount of molecules participating in micelles reduces.[35] At some salt concentration, the multimolecular micelles disintegrate and transform back into the intermediate state of a stretched rod-like, single molecule complex. Further increase of the ionic strength makes the interactions vanish and the conjugated polyelectrolyte returns back to its uncoated state. We observe this process very clearly in PL spectra of the complexes formed by CP2 and DP1 at $f+ = 0.45$, upon gradually titration with NaCl. In Figure 4.6A, the initial PL

spectra of the complex clearly show the quenched PF band and dominant BT band, so the complex emits yellow instead of blue.

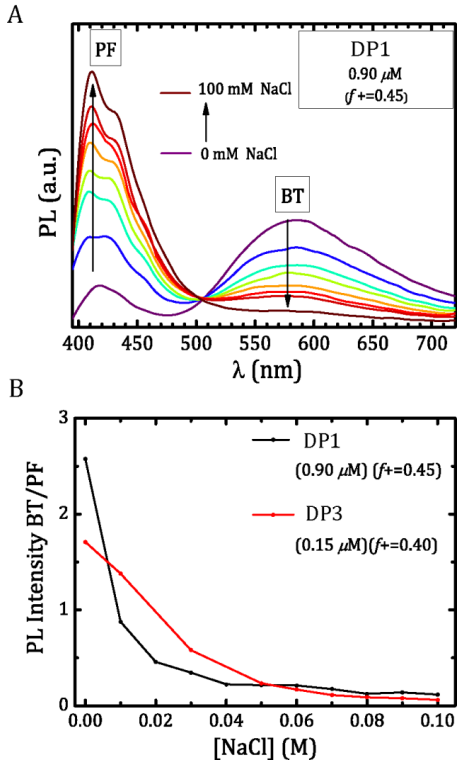

Figure 4.6 Salt induced disassembly of micelles: normalized PL spectra of micelles formed by CP2 and DP1 at $f+ = 0.45$ shows the recovery of PF emission over the BT emission upon titrating with NaCl (A); The corresponding PL intensity of BT /PF ratio for micelles formed by CP2 with DP1 and with DP2 as a function of NaCl concentration (B).

Addition of NaCl quenches the BT emission band and simultaneously restores the PF band (Figure 4.6B). As the ionic strength increases, vibronic bands of PF also return back to their original state. This illustrates that micelle disassembly follows the same pathway as the ($f+$)-dependent assembly: first the multimolecular micelles decompose into soluble, single-molecule complexes, which subsequently decay into the mixture of two, non-interacting, macromolecular species.

4.3 Conclusion

In this chapter we have shown how mechanochromic polymer sensors can be used to shed light onto the intra- and intermolecular changes which occur during electrostatic polyelectrolyte complexation. By molecular engineering of water-soluble conjugated polymers, we develop molecular fluorescence sensors that not only detect chain stretching but also proximity to neighboring polymers. In this way, we show how electrostatic complexation occurs in two distinct stages. At asymmetric charge ratios between oppositely charged polymers, single-molecule soluble complexes form. These complexes carry excess charges and repel too strongly for correlation effects to take effect. As the charge ratio approaches stoichiometry, the repulsion dies out and the single-molecule complexes gradually transform into larger, condensed, complex coacervate micelles which contain many molecules. These results give new insight into the sequence of events that unfolds when co-assembled nanostructures spontaneously form through supramolecular interactions.

4.4 Experimental Section

4.4.1 Materials and Methods

The monomer 2,7-Dibromo-9,9-bis(3-(*tert*-butyl propanoate)) fluorene was purchased from SageChem, China. The monomer 4,7-dibromobenzo[c]-1,2,5-thiadiazole (95%) was purchased from Sigma-Aldrich. Poly(L-lysine) hydrochloride ($PLKC_{20}$) with (M_w=3300 g/mol and PDI=1.05) was purchased from Alamanda Polymers, USA. Various poly(2-vinylpyridine)-b-poly(ethylene oxide) diblock copolymers were purchased from Polymer Source. All reagents were purchased from Sigma-Aldrich or Biosolve and were used as received unless otherwise stated. Mill-Q water (18.2 MΩ) was used to prepare all polymer solutions. All the measurements were performed at 22 ^{o}C. NMR spectra were obtained on a Bruker Avance III 400MHz spectrometer.

4.4.2 Photophysical Experiments

UV-vis absorption spectra of the solutions were obtained from Shimadzu UV-2600 Spectrophotometer. Steady-state fluorescence emission measurements were performed on Edin-

burg Instruments Fluorescent Spectrophotometer FLS920 with 450W xenon lamp for solutions of CP1 and Cary Eclipse Fluorescent Spectrophotometer with a xenon lamp for solutions of CP2.

4.4.3 Light Scattering Titration Experiments

Dynamic light scattering experiments were performed at detection angle of 90 ° with an ALV instrument equipped with a 400 mW argon ion laser operating at a wavelength of 660 nm, a Thorn-Emi RFIB263KF photomultiplier detector, connected to an external ALV7002 multiple tau digital correlator. For the light scattering experiments, all solutions are filtered through 0.2 μm syringe filters to remove trace quantities of dust. After every addition of titrant, the light scattering intensity (I) is recorded in 20 independent runs of 30 seconds. From standard ALV software analysis, decay rates (Γ) are obtained and later used to calculate diffusion coefficients (D). By using Stokes-Einstein equation, apparent hydrodynamic radii (R_h) are obtained. Size distributions of complexes are obtained by performing inverse Laplace transformation with CONTIN software.

4.4.4 Conjugated Polymer Synthesis

Poly[9,9′-bis(tert-butyl-3″-propanoate)fluoren-2,7-yl](PF3(tert)): The synthesis of homopolymer PF3(*tert)* via the nickel(0)-mediated polymerization reaction, Yamamoto polymerization, has been slightly modified from a previously described method.[33] $Ni(COD)_2$ (550 mg, 2 mmol) and 2,2′-bipyridyl (312 mg, 2 mmol) were placed in a 50 mL two neck round- bottom flask in the glove box. Dry dimethylformamide (3.5 mL) was added into the flask and purged with nitrogen at 75 °C. COD (245 μL, 2 mmol) was added dropwise and the mixture was stirred for 1 hour. Monomer 2,7-dibromo-9,9-bis(3-(*tert*-butyl propanoate)) fluorene (Mon-1) (0.55 g, 1 mmol) was dissolved in anhydrous toluene (6 mL) in a separate flask and purged with nitrogen, later it was added into the reaction vessel dropwise. The mixture was stirred under nitrogen for 9 hrs. The endcap agent, 1-bromo-4-ethynylbenzene (97%) (181 mg, 1 mmol) was dissolved in anhydrous toluene (2 mL) and injected into the reaction vessel dropwise. The mixture is stirred overnight under the same conditions. For the purification of the polymer, crude product is stirred in a solvent mixture (methanol: acetone: HCl (0.1M) = 1:1:1) for 2 h. The precipitate is filtered and Soxhlet extracted subsequently with

Methanol, Acetone, DCM and obtained as yellow solid (310 mg, 56 %). The molecular weight of obtained homopolymer is determined by gel-permeation chromatography (GPC) against polystyrene standards. The molecular weight (M_w) is corrected[42] for the overestimation due to the semirigid-rod nature of the polymer and obtained as M_w =16.7 kgmol^{-1} and PDI = 2.4. ^{1}H NMR (400 MHz, $CDCl_3$, δ): 7.79-7.66 (m, 6H), 2.46 (s, 4H, $-CH_2-$), 1.57 (s, 4H,$-CH_2-$), 1.22 (s, 18H) ppm.

Poly[9,9′-bis(tert-butyl-3″-propanoate)fluorene-co-4,7-(2,1,3-benzothiadiazole)$_{20}$] (PF3(tert)-BT$_{20}$): The synthesis of copolymer was obtained with the same protocol described above for homopolymer PF3(*tert).* Monomer Mon-1 (442 mg, 0.8 mmol) and monomer 4,7-dibromobenzo[c]-1,2,5-thiadiazole (Mon-2) (58.8 mg, 0.2 mmol) were incorporated in the polymer backbone at mole ratio 4:1. The endcap agent used in this synthesis was 4-bromo-2,1,3-benzothiadiazole (21.5 mg, 0.1 mmol). After purification the copolymer was obtained as brownish yellow solid (430 mg, 84%) with M_w = 12.0 kgmol^{-1} (after correction against polystyrene standards) and PDI = 2.2. ^{1}H NMR (400 MHz, CD_2Cl_2, δ): 7.84-7.74 (m, 6H), 2.49 (s, 4H, $-CH_2-$), 2.00 (s, 4H,$-CH_2-$), 1.23 (s, 18H) ppm.

Poly[9,9′-bis(3′′-propanoate)fluoren-2,7-yl] Sodium Salt (PF3)(CP1): PF3(*tert)* (60 mg) was dissolved in DCM (50 mL) in a 100 mL round bottom flask. Trifluoroacetic acid (TFA) (5 mL) was added dropwise into the reaction flask and the mixture was stirred overnight at room temperature. After the removal of solvent with rotavap, the residue was refluxed with Na_2CO_3 solution (0.5 M, 50 mL) for 24 hrs. The polymer was purified through dialysis units (M_w cutoff: 1000) against Mill-Q water for 3 days. CP1 is obtained after freeze-drying as fibrous yellow solid (31.3 mg, 52 %). ^{1}H NMR (400 MHz, MeOD, δ): 7.83-7.73 (m, 6H), 2.51 (s, 4H), 1.54 (s, 4H) ppm, 1.22 (s, 18H).

Poly[9,9′-bis(3′′-propanoate)fluorene-co-4,7-(2,1,3-benzothiadiazole)$_{20}$]Sodium Salt (PF3-BT$_{20}$) (CP2): The hydrolysis and dialysis of copolymer was achieved with the same protocol described above. After freeze-drying, CP2 was obtained as brownish yellow solid (400 mg, 93%). ^{1}H NMR (400 MHz, MeOD, δ): 7.90-7.82 (m, 6H), 2.59 (s, 4H), 1.62 (s, 4H) ppm, 1.29 (s, 18H).

4.4.5 Diblock Copolymers

Poly (N-methyl-2-vinyl-pyridinium iodide)-b-poly(ethylene oxide) ($PM2VP_x$-*b*-PEO_y)(DP): The specifications of diblock copolymers are given in Table 1. For the quaternization of poly(2-vinylpyridine)-b-poly(ethylene oxide) ($P2VP_x$-*b*-PEO_y), a previously described protocol is followed.[34]

Table 4.1 Specifications of diblock copolymers

Diblock copolymer	Annotation	M_n kgmol^{-1}	N	M_w/M_n	DQ*
$P2VP_{41}$-*b*-PEO_{204}	DP1	9.6-*b*-9.0	41-*b*-204	1.05	89%
$P2VP_{128}$-*b*-PEO_{477}	DP2	29.8-*b*-21.0	128-*b*-477	1.10	89%
$P2VP_{249}$-*b*-PEO_{134}	DP3	56.5-*b*-5.9	249-*b*-134	1.05	86%

*denotes the degree of quaternization

4.4.6 Complex Formation

Solutions of DPs (1 mgmL^{-1}), poly(L-lysine) (1 mgmL^{-1}), CP1 (0.01 mgmL^{-1}) and CP2 (0.01 mgmL^{-1}) were prepared in Mill-Q, pH is adjusted to pH = 9.0 for all diblock copolymers and to pH = 8.6 for poly(L-lysine), using NaOH. This gives a minimum ionic strength in all experiments of approximately 0.01 mM. Samples were mixed by vortexing for few seconds. Sonication was only used for DP stock solutions for 10 mins. For the salt experiments, complexes were titrated with 5M NaCl to the desired ionic strength.

References

[1] M. A. Cohen Stuart, B. Hofs, I. K. Voets, A. De Keizer, *Curr Opin Colloid Interface Sci* **2005**, *10*, 30-36.

[2] I. K. Voets, A. De Keizer, M. A. Cohen Stuart, *Adv Colloid Interface Sci* **2009**, *147-148*, 300-318.

[3] R. Chollakup, W. Smitthipong, C. D. Eisenbach, M. Tirrell, *Macromolecules* **2010**, *43*, 2518-2528.

[4] J. F. Gohy, S. K. Varshney, R. Jérôme, *Macromolecules* **2001**, *34*, 3361-3366.

[5] D. V. Pergushov, E. V. Remizova, J. Feldthusen, A. B. Zezin, A. H. E. Müller, V. A. Kabanov, *J Phys Chem B* **2003**, *107*, 8093-8096.

[6] V. Bütün, A. B. Lowe, N. C. Billingham, S. P. Armes, *J Am Chem Soc* **1999**, *121*, 4288-4289.

[7] A. Harada, K. Kataoka, *Prog Polym Sci (Oxford)* **2006**, *31*, 949-982.

[8] Y. Bae, K. Kataoka, *Adv Drug Deliv Rev* **2009**, *61*, 768-784.

[9] J. V. D. Gucht, E. Spruijt, M. Lemmers, M. A. Cohen Stuart, *J Colloid Interface Sci* **2011**, *361*, 407-422.

[10] J. Wang, A. De Keizer, R. Fokkink, Y. Yan, M. A. Cohen Stuart, J. Van Der Gucht, *J Phys Chem B* **2010**, *114*, 8313-8319.

[11] J. Wang, A. H. Velders, E. Gianolio, S. Aime, F. J. Vergeldt, H. Van As, Y. Yan, M. Drechsler, A. De Keizer, M. A. Cohen Stuart, J. Van Der Gucht, *Chem Commun* **2013**, *49*, 3736-3738.

[12] A. B. Kayitmazer, S. P. Strand, C. Tribet, W. Jaeger, P. L. Dubin, *Biomacromolecules* **2007**, *8*, 3568-3577.

[13] E. Kizilay, A. B. Kayitmazer, P. L. Dubin, *Adv Colloid Interface Sci* **2011**, *167*, 24-37.

[14] S. Chodankar, V. K. Aswal, J. Kohlbrecher, R. Vavrin, A. G. Wagh, *Phys Rev E: Stat, Nonlinear, Soft Matter Phys* **2008**, *78*.

[15] I. A. Levitsky, J. Kim, T. M. Swager, *J Am Chem Soc* **1999**, *121*, 1466-1472.

[16] J. W. Hong, W. L. Hemme, G. E. Keller, M. T. Rinke, G. C. Bazan, *Adv Mater* **2006**, *18*, 878-882.

[17] B. Liu, G. C. Bazan, *J Am Chem Soc* **2004**, *126*, 1942-1943.

[18] K. Y. Pu, L. Cai, B. Liu, *Macromolecules* **2009**, *42*, 5933-5940.

[19] D. Yu, Y. Zhang, B. Liu, *Macromolecules* **2008**, *41*, 4003-4011.

[20] A. Satrijo, T. M. Swager, *J Am Chem Soc* **2007**, *129*, 16020-16028.

[21] L. An, Y. Tang, F. Feng, F. He, S. Wang, *J Mater Chem* **2007**, *17*, 4147-4152.

[22] F. He, Y. Tang, M. Yu, S. Wang, Y. Li, D. Zhu, *Adv Funct Mater* **2006**, *16*, 91-94.

[23] B. Yoon, S. Lee, J. M. Kim, *Chem Soc Rev* **2009**, *38*, 1958-1968.

[24] K. P. R. Nilsson, A. Herland, P. Hammarström, O. Inganäs, *Biochemistry* **2005**, *44*, 3718-3724.

[25] S. Seo, J. Lee, E. J. Choi, E. J. Kim, J. Y. Song, J. Kim, *Macromol Rapid Commun* **2013**, *34*, 743-748.

[26] T. L. Nelson, C. O'sullivan, N. T. Greene, M. S. Maynor, J. J. Lavigne, *J Am Chem Soc* **2006**, *128*, 5640-5641.

[27] H. A. Ho, M. Boissinot, M. G. Bergeron, G. Corbeil, K. Doré, D. Boudreau, M. Leclerc, *Angew Chem Int Ed* **2002**, *41*, 1548-1551.

[28] H. A. Ho, M. Leclerc, *J Am Chem Soc* **2004**, *126*, 1384-1387.

[29] H. E. Cingil, I. M. Storm, Y. Yorulmaz, D. W. Te Brake, R. De Vries, M. A. Cohen Stuart, J. Sprakel, *J Am Chem Soc* **2015**, *137*, 9800-9803.

[30] M. Grell, D. D. C. Bradley, G. Ungar, J. Hill, K. S. Whitehead, *Macromolecules* **1999**, *32*, 5810-5817.

[31] A. J. Cadby, P. A. Lane, H. Mellor, S. J. Martin, M. Grell, C. Giebeler, D. D. C. Bradley, M. Wohlgenannt, C. An, Z. V. Vardeny, *Phys Rev B: Condens Matter Mater Phys* **2000**, *62*, 15604-15609.

[32] R. Zhang, B. I. Shklovskii, *Phys A* **2005**, *352*, 216-238.

[33] S. Y. Cho, A. C. Grimsdale, D. J. Jones, S. E. Watkins, A. B. Holmes, *J Am Chem Soc* **2007**, *129*, 11910-+.

[34] A. M. Brzozowska, B. Hofs, A. De Keizer, R. Fokkink, M. A. Cohen Stuart, W. Norde, *Colloids Surf, A* **2009**, *347*, 146-155.

[35] H. M. Van Der Kooij, E. Spruijt, I. K. Voets, R. Fokkink, M. A. Cohen Stuart, J. Van Der Gucht, *Langmuir* **2012**, *28*, 14180-14191.

[36] D. W. Bright, F. B. Dias, F. Galbrecht, U. Scherf, A. P. Monkman, *Adv Funct Mater* **2009**, *19*, 67-73.

[37] U. Scherf, E. J. W. List, *Adv Mater* **2002**, *14*, 477-487.

[38] M. Knaapila, A. P. Monkman, *Adv Mater* **2013**, *25*, 1090-1108.

[39] F. K. Wang, G. C. Bazan, *J Am Chem Soc* **2006**, *128*, 15786-15792.

[40] B. Bao, L. Yuwen, X. Zheng, L. Weng, X. Zhu, X. Zhan, L. Wang, *J Mater Chem* **2010**, *20*, 9628-9634.

[41] J. Sprakel, F. a. M. Leermakers, M. A. Cohen Stuart, N. a. M. Besseling, *Phys Chem Chem Phys* **2008**, *10*, 5308-5316.

[42] M. B. Grell, D.D.C.; Long, X.; Chamberlain, T.; Inbasekaran, M.; Woo, E.P.; Soliman, M., *Acta Polymerica* **1998**, *49*, 439-444.

APPENDIX

PM2VP$_x$-*b*-PEO$_y$ (DP)

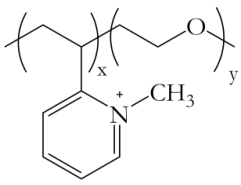

Scheme A4.1 Molecular structure of diblock copolymer poly(N-methyl-2-vinylpyridinium)-*b*-poly(ethylene oxide) (DP)

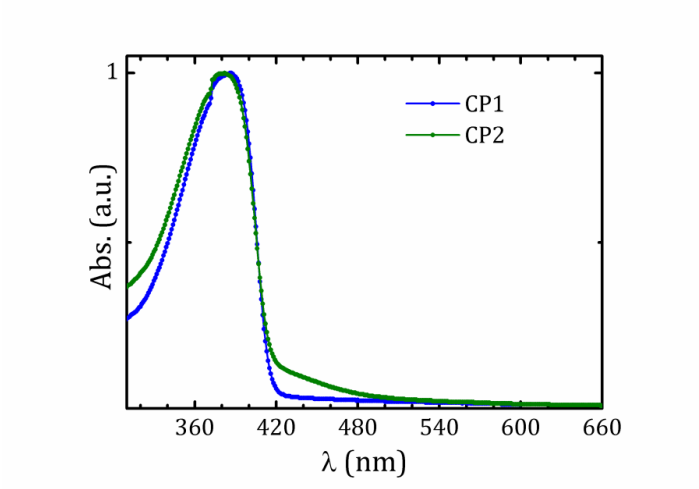

Figure A4.1 Normalized absorption spectra of PF3 (CP1) (c = 0.6 μM) and PF3-BT$_{20}$ (CP2) (c = 0.8 μM) at pH 8.5.

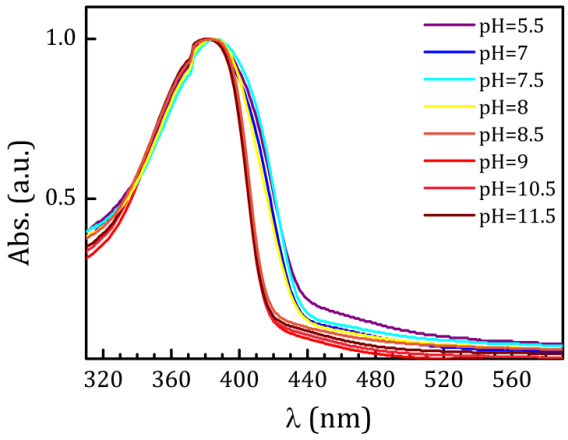

Figure A4.2 Normalized absorption spectra of CP2 (c = 0.8 μM) at various pH conditions.

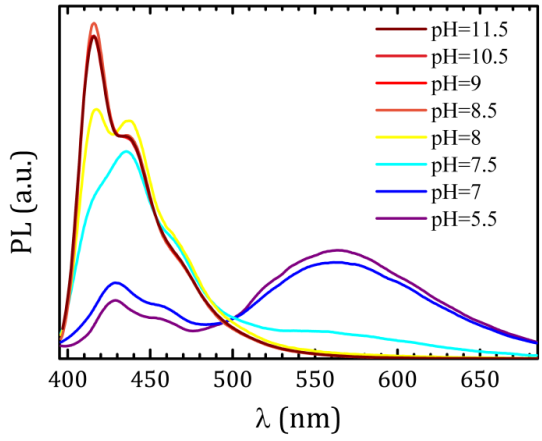

Figure A4.3 Normalized photoluminescence spectra of CP2 (c = 0.8 μM) at various pH conditions.

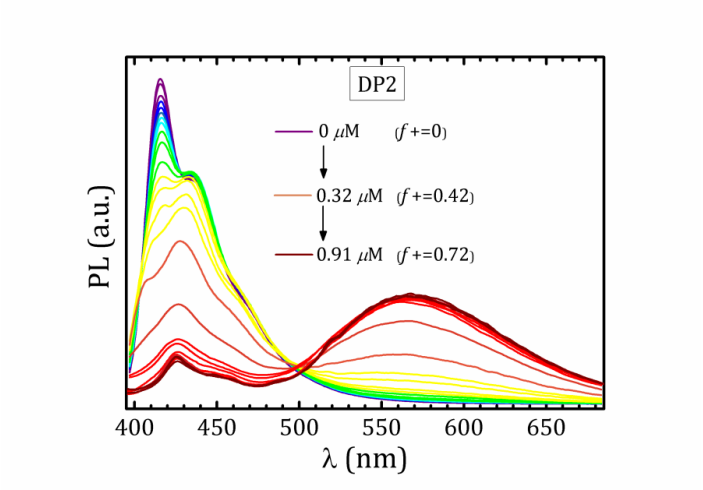

Figure A4.4 Photoluminescence spectra of CP2 (c = 0.8 μM) upon addition of DP2 in water at pH 9 with no added salt. The excitation wavelength is 380 nm. The initial, middle and final concentrations and corresponding charge ratios ($f+$) are indicated with legends for clarity.

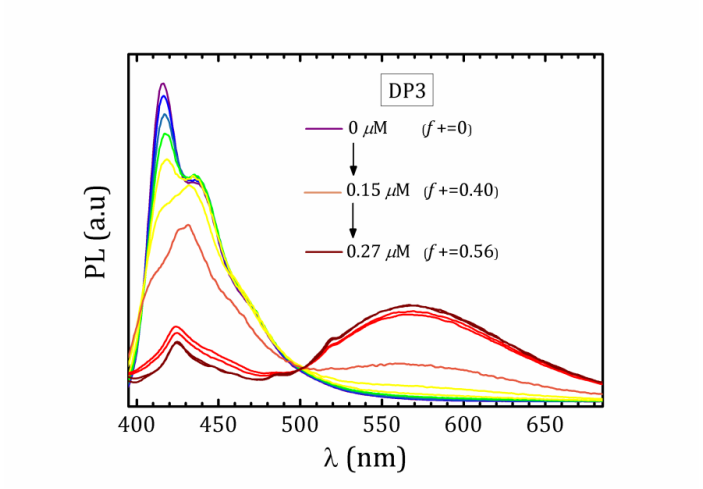

Figure A4.5 Photoluminescence spectra of CP2 (c = 0.8 μM) upon addition of DP3 in water at pH 9 with no added salt. The excitation wavelength is 380 nm. The concentration range and corresponding charge ratios ($f+$) are indicated with legends for clarity.

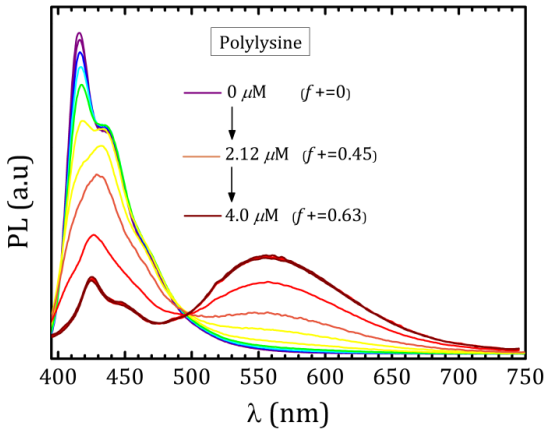

Figure A4.6 Photoluminescence spectra of CP2 (c = 0.8 μM) upon addition of Polylysine in water at pH 8.5 with no added salt. The excitation wavelength is 380 nm. The concentration range and corresponding charge ratios ($f+$) are indicated with legends for clarity.

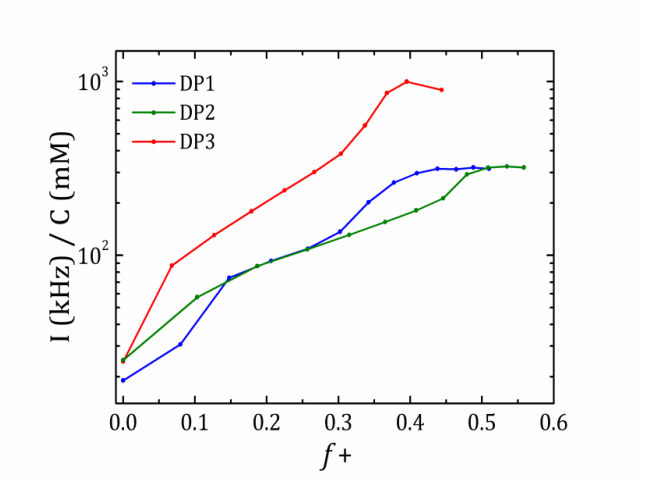

Figure A4.7 Light scattering intensity, corrected for dilution, detected at 90° for CP1 (c = 6 μM) titration with various diblock copolymers at pH 9 is plotted as a function of mixing ratio ($f+$).

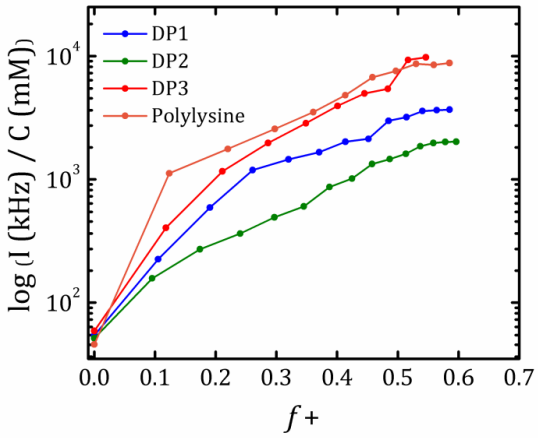

Figure A4.8 Light scattering intensity, corrected for dilution, detected at 90° for CP2 (c = 8 μM) titration with various diblock copolymers at pH 9 is plotted as a function of mixing ratio ($f+$).

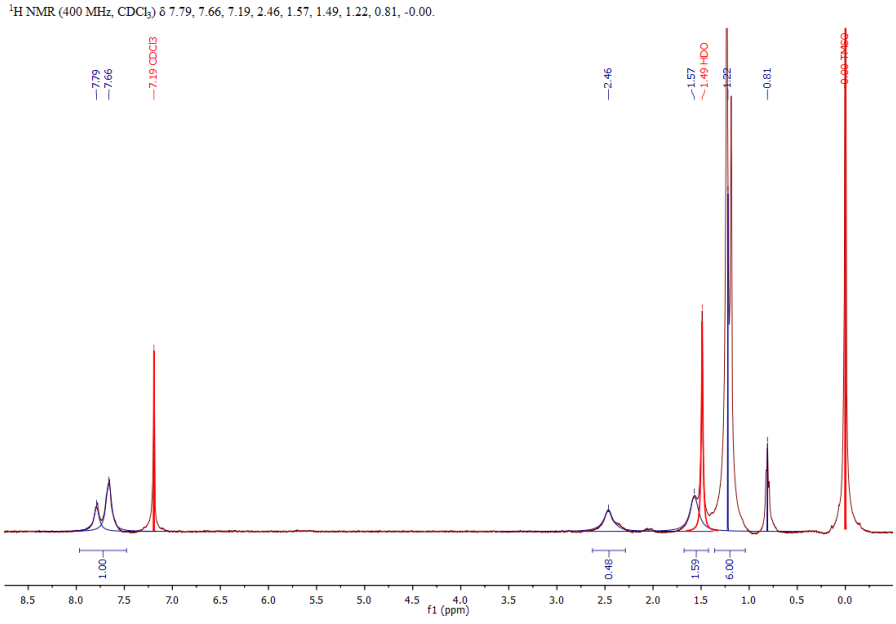

Figure A4.9 ^{1}H NMR spectrum of PF3-*tert*

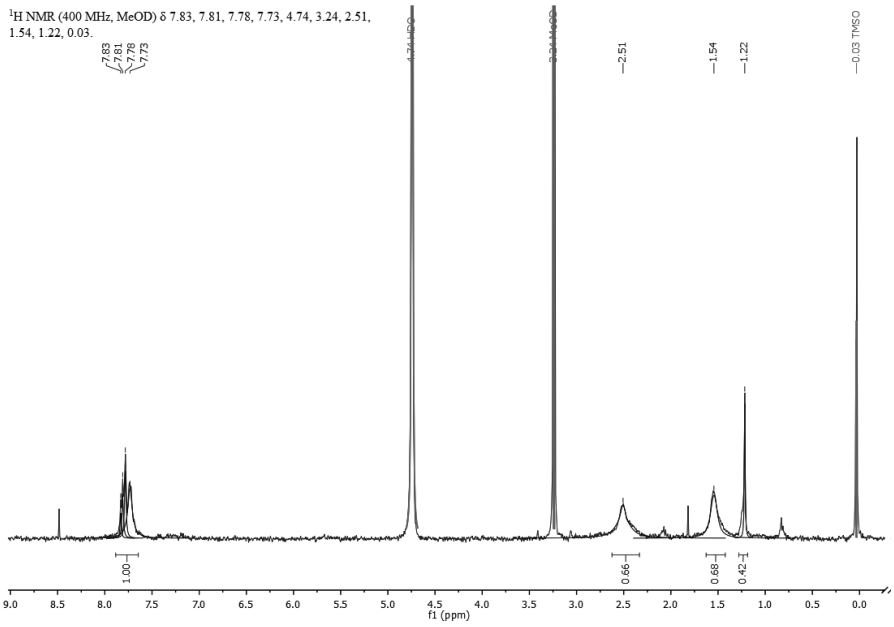

Figure A4.10 ¹H NMR spectrum of CP1

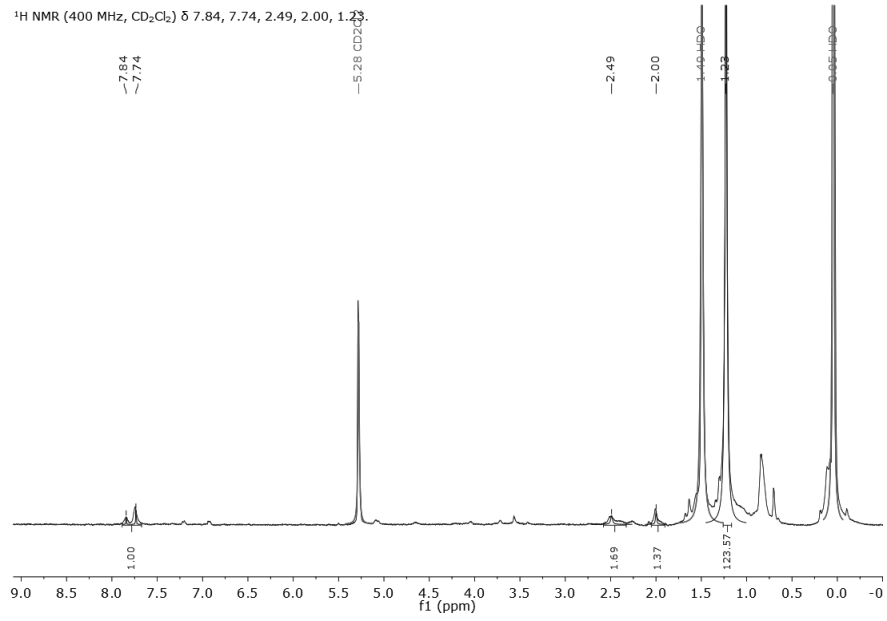

Figure A4.11 ¹H NMR spectrum of PF3(tert)-BT_{20}

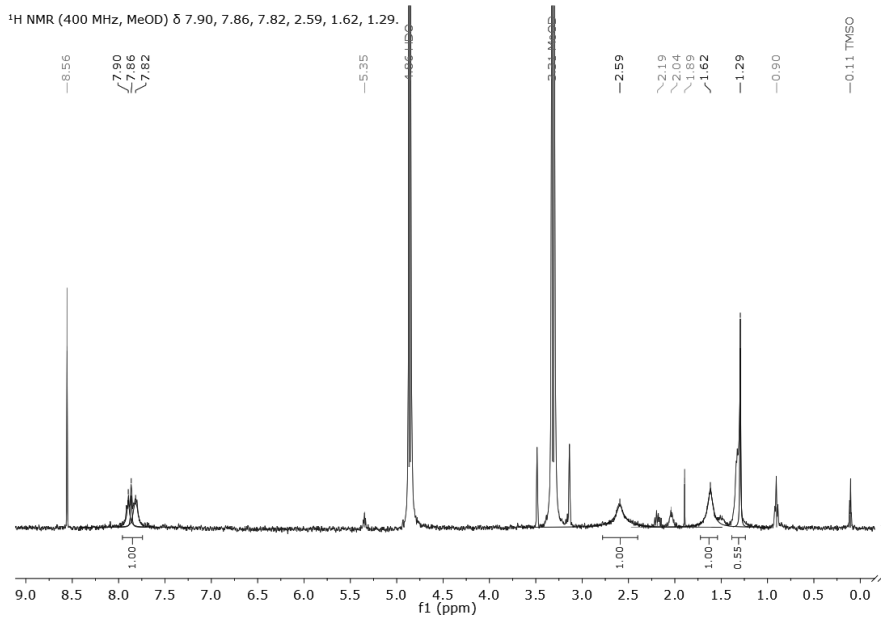

Figure A4.12 ¹H NMR spectrum of CP2

CHAPTER 5

Mechanochromic molecular sensors reveal complexity in the self-assembly of virus-like particles

Mechanochromic conjugated polymers act as sensors for changes in their own conformation upon mechanical perturbation. They report the change with altered photoluminescence spectra and different emission color. Here we show how polyfluorene-based mechanochromic sensors can be used as a template, replacing of DNA, to study the kinetics of binding and self-assembly of a designer protein which forms virus-like particles. Mechanochromic sensors allow the noninvasive monitoring of such a complex system in aqueous media with high temporal resolution. We follow the process starting from the initial electrostatic binding of protein to the template, capsid formation along the template while inducing polymer chain stretching, and even bundling in the final stages. We report a distinct nucleation-and-growth mechanism for virus-like particle formation, with a nucleation lag time that depends strongly on concentration. Moreover, we provide evidence for the competition between co- and self-assembly, demonstrating how complexity emerges when orthogonal interactions are combined within a single system.

Manuscript is in preparation

Hande E. Cingil, Emre B. Boz, Renko de Vries, Martien A. Cohen Stuart, Joris Sprakel

5.1 Introduction

Supramolecular interactions provide cohesion to a wide variety of biological structures and man-made materials.[1-2] In many cases, especially in nature, several orthogonal interaction mechanisms are at play within the same system. High-fidelity self-assembly in such systems which feature competing and orthogonal interactions, requires that a plethora of highly specific motifs can act independently, despite of their proximity. Yet, the competition between different interactions at the molecular level can give rise to multiple pathways, which lead to multiple self-organized structures, some of which may represent metastable configurations, from the same initial building blocks.[3-4] This gives rise to an intriguing complexity in the process of spontaneous structure formation.

Unravelling how this complexity manifests itself at the molecular scale in the kinetics of self- or co-assembly remains a major challenge to date; in particular when the changes in molecular conformations are subtle and difficult to ascertain with conventional analytical methods. A prototypical example of complex self-assembly in nature is the formation of virus-like particles from coat proteins templated by DNA or RNA strands.[5-7] Well-defined geometric structures, with specific functionality, form through cooperative assembly of relatively simple capsid protein building blocks.[8-10] To first order, viral coat proteins exhibit three main functionalities:[11] *i)* a binding block, responsible for binding to the template DNA or RNA chains, by means of electrostatic interactions, *ii)* a cooperativity block, that can adopt a secondary structure to ensure lateral self-assembly of multiple coat proteins along the template, and *iii)* a stabilizing block, such as a random coil motif, that shields the DNA from enzymatic degradation and provides colloidal stability to the virus particle. The competition between self-assembly guided by the cooperativity block, and co-assembly of the same proteins with a template, driven primarily by the binding block, can be expected to lead to complex self-assembly kinetics and pathways. Yet, to date these have been difficult to unravel in non-invasive experiments designed to follow virus particle formation.

In this chapter, we study the assembly kinetics of a (recombinant) coat protein which features all three essential functionalities and acts as an artificial virus capsid. To probe how this designer protein forms the virus-like structure, we replaced the DNA by semiconducting polymers as the template; vibronic luminescence spectra of the latter exhibit distinct

shifts when they become encapsulated within the protein capsid. This unique mechanochromism exhibited by these conjugated polyelectrolytes allows us to monitor non-invasively and with high temporal resolution how the designer proteins bind to the template, form a rigid capsid which stretches the chains and induces their bundling in the final stages of capsid formation. These experiments unveil a distinct nucleation-and-growth mechanism for virus-like particle formation, with a nucleation lag time that depends strongly on concentration. Moreover, we provide evidence for the competition between co- and self-assembly, demonstrating how complexity emerges when orthogonal interactions are combined within a single system.

5.2 Results and Discussion

5.2.1 Mechanochromic sensors

We use a specific class of conjugated polyelectrolytes (CPEs) as molecular sensors to probe the kinetics of virus-like self-assembly. CPEs combine the unique optoelectronic properties of the delocalized electronic backbone of conjugated polymers, with charged side groups which both render the chain water-soluble and allow it to interact with oppositely charged biological molecules via electrostatic interactions.[12-16] Any change that happens at a site along the conjugated backbone due to environmental disturbances such as analyte binding, affects the optoelectronic properties of the entire polymer by causing signal amplification, because excited states migrate along the conjugated backbone.[17]

The optoelectronic response to changes can easily be probed in the fluorescence spectra of CPEs as an enhancement,[18-19] a quenching[20-25] or wavelength shift[19] depending on the molecular design and type of interaction. Here we use the phenomenon known as mechanochromism, seen in e.g. polydiacetylenes[26-28], polythiophenes[29-32] and polyfluorenes[33] as a distinct change in emission color upon mechanical perturbation of the polymeric chain; thus, mechanochromic CPEs function as sensors for changes in their own conformation.

Our sensor of virus-like self-assembly is a carboxylated poly[9,9'-bis(3'-propanoate) fluoren-2,7-yl] sodium salt (App. Figure 5.1), with M_w = 16.7 kgmol^{-1} and PDI = 2.4, which has been synthesized via Yamamoto coupling[34] from the monomer 2,7-dibromo-9,9-bis(3-(*tert*-

butyl propanoate)) fluorene. We have previously demonstrated how this polyfluorene-based anionic CPE, here denoted as CP1, can be used to monitor co-assembly by the spectral changes which occur due to supramolecular binding-induced chain stretching.[33] These molecular sensors exhibit three distinct vibronic bands in their photoluminescence (PL) spectrum in native state (Figure 5.1A), where the backbone exhibits significant rotational degrees of freedom, which restrict its conjugation length.[35]

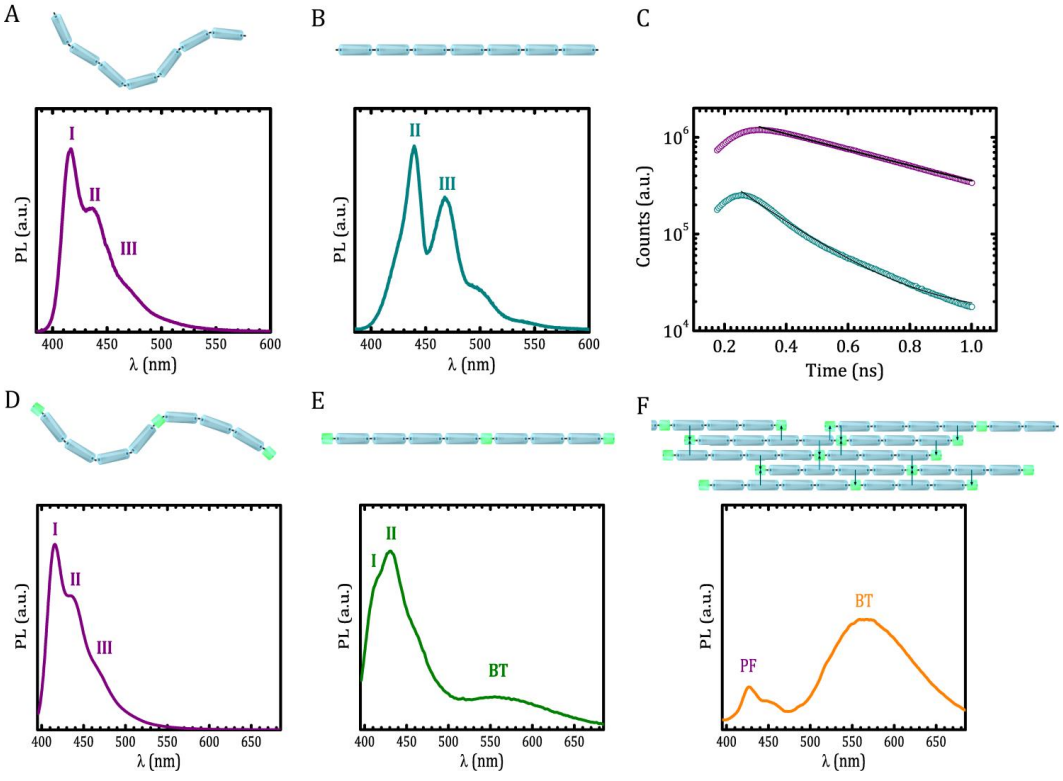

Figure 5.1 Schematic illustration of structure and corresponding photoluminescence (PL) spectra of polyfluorene based mechanochromic sensors CP1 and CP2: in its native, semi-flexible conformation, CP1 (A); in *β*-phase, planarized and extended conformation, CP1 (B); time-resolved fluorescence emission decays of native (top), *β*-phase (bottom) polyfluorene, CP1, with laser excitation at 373 nm (C); in native conformation, CP2 (D); in *β*-phase, CP2 (E); in aggregate (bundled) phase, CP2 (F).

Upon stretching the conjugated backbone, e.g., by creating a physical bottlebrush,[33] the twisted conformation is forced into a planarized one, and the PL spectrum exhibits distinct changes in vibronic band structure: while the 1-0 vibronic transition at 418 nm decays and

almost vanishes, the higher order transitions, such as the 2-0 and 3-0 bands at 436 and 465 nm, respectively, grow in intensity (Figure 5.1B). This distinct sequence of events upon chain planarization is known in the solid state of polyfluorenes as the β-phase, a partially-ordered state in which intermolecular interactions cause chain alignment and extension.[36-37] Our mechanochromic sensor exhibits exactly the same properties, but in solution and in response to mechanical cues; the ratio of vibronic band intensities that changes as these transitions occur can be used to quantitatively detect chain stretching, as was demonstrated previously.[33] Interestingly, this single molecule manifestation of the well-known beta-phase also shows the corresponding reduction in excited state lifetime. While we find an average PL lifetime ~ 500 ps for the flexible and twisted native configuration of the polyfluorene-derivative; this decreases to ~ 200 ps when it is stretched into planarization (Figure 5.1C). The reduction in lifetime with chain alignment is also observed in solid films of polyfluorene, and may be related to the increased efficiency of exciton migration along the conjugated chain when out-of-plane rotations are restricted.[38-39]

In addition, we use a second polyfluorene-based anionic CPE (CP2) which features the same basic chemical structure, but includes 20 mol% of benzothiadiazole (BT) sub-units, randomly doped into the backbone. By incorporating this efficient energy acceptor unit, we introduce a colorimetric response to chain bundling or folding, by means of Förster resonance energy transfer (FRET) from fluorene to BT units.[12-15] CP2 in its fully dissolved state exhibits the same three vibronic bands, with a ~ 2 nm blue-shift (Figure 5.1D). Also this sensor chain can undergo a transition from twisted to a planarized conformation (Figure 5.1E) in solution, with a similar response in vibronic bands; however, we see that the 3-0 transition diminishes due to overlap with the absorption band of the BT units within the same chain. Nevertheless, CP2 still acts as a mechanosensor and reports for conformational changes. Interestingly, upon inducing the bundling or aggregation of these chains, an additional optical response is triggered; the entire fluorene vibronic bands diminish while the BT emission band ~ 550 nm grows due to the more efficient three-dimensional interchain FRET (Figure 5.1F). Thus, CP2 is not only a mechanosensor that detects stretching of chains but also a colorimetric sensor that detects chain proximity.

5.2.2 Artificial viral coat protein

To explore the kinetics of biologically-inspired and complex self-assembly we use a designer protein which acts as building block of an artificial virus capsid. This recombinant protein, $C_4S_{10}B^{K12}$, has been designed to closely mimic the properties of natural rod-like viruses from nature, featuring all three essential functionalities in a triblock segmented configuration. The colloidal stability block (C_4) consists of 407 mostly hydrophilic amino acids and maintains a random coil structure which is weakly-zwitterionic; the self-assembly block (S_{10}) is an octapeptide repeat with silk-like sequence $(GAGAGAGQ)_{10}$, which folds and stacks into a characteristic β-roll conformation; the cationic binding block (B^{K12}) consists of 12 lysine residues (Figure 5.2).

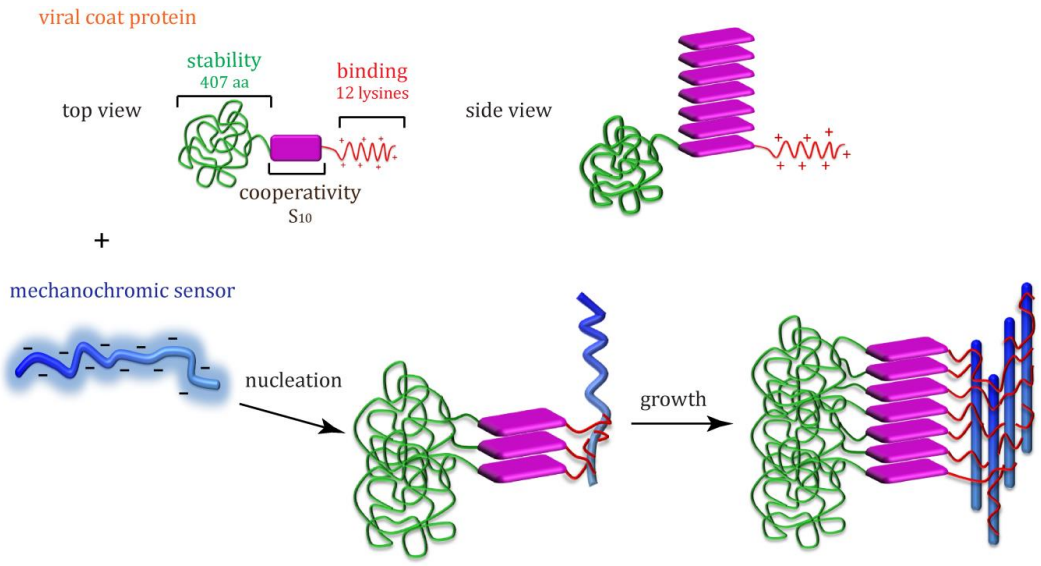

Figure 5.2 Schematic illustration of polyfluorene-based mechanochromic sensor CP1, the viral coat protein $C_4S_{10}B^{K12}$ and the capsid formation.

It was previously shown that this coat protein is capable of mimicking several key aspects of natural rod-like viruses, such as tobacco mosaic virus. It exhibits nucleation-and-growth self-assembly onto a templating DNA chain; the artificial capsid protects the genetic information from attack by DNA-cleaving enzymes.[40] The design and production of this recombinant protein and its highly cooperative self-assembly onto DNA templates is described in detail elsewhere.[40]

5.2.3 Capsid formation kinetics

Upon adding the anionic template polymer to the cationic coat protein, electrostatic interactions first cause weak binding of protein molecules on the template. This binding enhances the local protein concentration, which then triggers folding into the secondary structure, and formation of a rigid capsid. In this latter stage, the template chain becomes stretched and elongated, and the rod-like geometry encoded in the virus design appears (Figure 5.2). We expect that this leads to the same sequence of vibronic shifts we have observed previously upon planarizing CP1 and CP2. Hence, we record fluorescence spectra every 6 minutes during approximately 3 days, in tightly sealed cuvettes, starting directly after mixing CP1 and $C_4S_{10}B^{K12}$. In these experiments we deliberately work at dilute conditions, to suppress the formation of "empty" capsids by self-assembly of the protein alone. We express the mixing ratio of the two species as the molar ratio of cationic charges on the binding block to the total number of polymer charges in the system: $f+= [+]/([+] + [-])$. Four cases are studied: $f+= 0.25, f+= 0.40, f+= 0.50, f+= 0.70$. In all cases, we observe a gradual shift in the luminescence spectra: The initial spectrum shows a large peak for the 1-0 transition and minor peaks for 2-0 and 3-0; with time, the first transition band diminishes while the second and third band grow (Figure 5.3A-D).

This optical response is the same as that observed for the same mechanochromic chains, when they are forced into an elongated conformation either in the solid state[37, 41-42], or by means of bottlebrush formation[33]. This indicates that over time, the coat proteins bind to the template, begin to assemble laterally, and eventually form a rigid capsid in which the CPE must adopt a planar configuration. The initial electrostatic binding is diffusion-limited; for these relatively fast diffusing short polymeric objects this should be virtually instantaneous as compared to the time between two recorded spectra. This can be seen by the rapid quenching of total emission intensity after mixing, when the first proteins bind to the CPE.[23-24] The extent of this initial quenching caused by binding depends on the mixing ratio. This can be clearly seen by comparing the absolute intensity of the first recorded spectrum in each plot in Figure 5.3; these data are for identical concentrations of CP1 but various concentrations of protein. While initial binding is fast, the subsequent lateral self- as-

sembly of the attached proteins resulting in capsid formation and chain stretching is very slow.

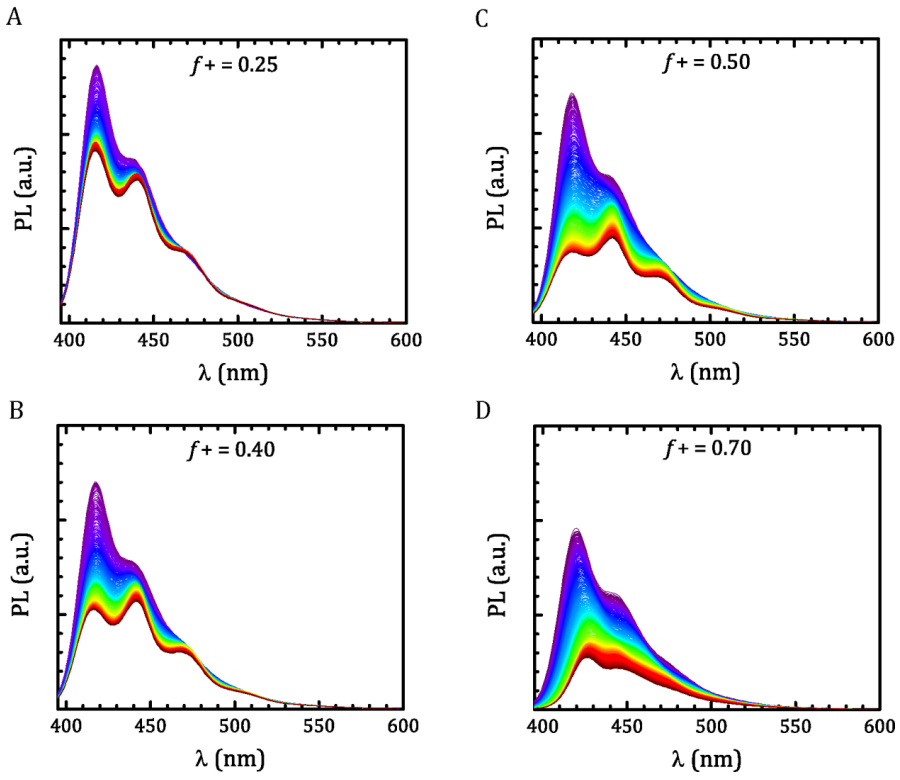

Figure 5.3 Time dependent changes in PL spectra of CP1 (0.6 μM) with $C_4S_{10}B^{K12}$ (22.2 μM) at mixing ratio ($f+$) of 0.25 (A); 0.40 (B); 0.50 (C); 0.70 (D) during the course of nucleation and growth for 70 hours.

We monitor this second stage in the assembly pathway by inspecting the ratio of vibronic bands, which are uniquely sensitive to the extent of chain planarization.[33] When the protein is present in a large under-dose ($f+ = 0.25$), we see mild changes of the 2-0 and 3-0 bands, which gradually become slightly more pronounced (Figure 5.3A). However, as the mixing ratio approaches the point of charge compensation ($f+ = 0.50$), we observe a smooth decay of the intensity of the lowest vibronic transition, 1-0, while the 2-0 transition becomes the prominent emission band. We observe here the time-dependent transition from a semi-flexible conjugated backbone to a coated and stretched one which is a direct manifestation of the self-assembly of coat protein on the CP1 template.

To quantify the capsid formation process as seen by the molecular sensors, we realize that at each point in time-sections of uncoated template coexist with segments of conjugated chain, which are encapsulated and stretched within a viral capsid. As time progresses, the nucleated section of capsid will grow until full coverage is reached. The normalized intensity of the i^{th} vibronic band in these evolving systems is thus a convolution of contributions from coated and uncoated sections of the sensor chain. In a two-state approximation, this can be expressed as: $I^i = I_n^i(1-\alpha) + I_c^i\,\alpha$, in which I_n^i and I_c^i are the normalized intensities of uncoated and coated states, respectively, α is the fraction of the chain that is coated, the quantity of interest, and $1-\alpha$ is the fraction of bare chain. Note that we observe a gradual decrease in quantum efficiency as the viral coat protein binds to the mechanosensor CP1. We determine the quantum efficiency of the bare CP1, against an anthracene standard, to be 69.1%, which decreases to 38% at $f+=$ 0.1 and saturates at approximately 9.8% for the fully encapsulated chain at $f+=$ 0.5. This binding-induced quenching was employed previously for other conjugated polyelectrolytes as a biosensor. [23-24] However, here we do not need these quantum efficiencies, as we extract ratios of vibronic peak intensities taken within one spectrum, such that the change in quantum efficiency divides out. Our most sensitive measure of the coating-induced stretching is the ratio of vibronic band intensities between the 2-0 and 1-0 transitions. Within the two-state model, this ratio can be expressed as:

$$r_{ij} = \frac{I^i}{I^j} = \frac{I_n^i(1-\alpha) + I_c^i\alpha}{I_n^j(1-\alpha) + I_c^j\alpha} \tag{5.1}$$

This allows us to directly relate the measured time-dependence of the intensity ratio $r_{ij}(t)$ to the fraction of the template chain that is encapsulated at time *t*:

$$\alpha = {r_{ij}I_n^j - I_n^i}\Big/{\left(r_{ij}\left(I_n^j - I_c^j\right) - I_n^i + I_c^i\right)} \tag{5.2}$$

The reference intensities, $I_n^{1,2}$ and $I_c^{1,2}$, are constants that can be measured experimentally from spectra for a chain in absence of any protein, and for a chain which is fully coated. For the later, we choose a sample at exact charge compensation ($f+=0.5$) and low overall concentration (0.06 μM of CP1 or 0.08 μM of CP2) after equilibration for 80 h. This analysis

gives rise to a weakly non-linear relationship between the measured vibronic intensity ratio r_{12} and the degree of coating α.

Eq. 5.2 allows us to monitor the capsid formation process quantitatively. We first applied this method on the dilute system which contains 0.06 μM CP1 with 2.22 μM $C_4S_{10}B^{K12}$, the time-dependent changes in the PL spectra of this system can be seen in Figure A5.1. We see that at this very dilute condition, a distinct nucleation-and-growth kinetics is found (Figure 5.4A). Initially, the degree of chain encapsulation is very low, until after a lag time of approximately 30 hrs, capsids begin to nucleate and grow over the course of a few hours to reach completion. When insufficient protein is present to encapsulate all chains fully ($f+ < 0.5$), we indeed observe only partial encapsulation (Figure 5.4A).

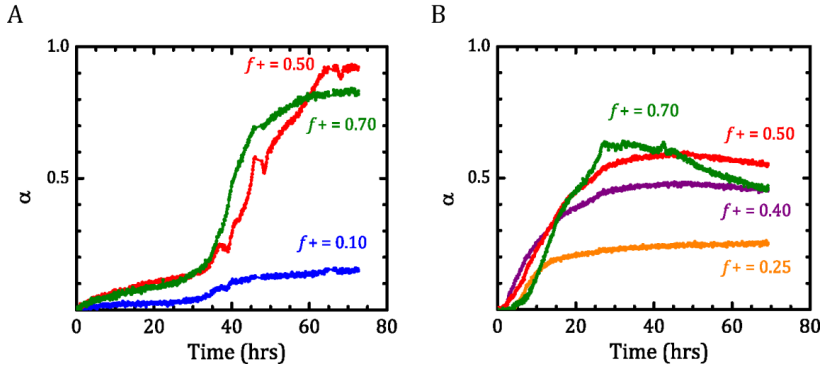

Figure 5.4 Time dependent changes of the coated fraction ($\boldsymbol{\alpha}$) of CP1 chains during the course of nucleation and growth for 70 hrs for CP1 (0.06 μM) with $C_4S_{10}B^{K12}$ (2.22 μM) (A) and CP1 (0.6 μM) with $C_4S_{10}B^{K12}$ (22.2 μM) (B) at various mixing ratio ($f+$).

If the self-assembly of the viral capsids indeed occurs through a classical nucleation mechanism, as proposed by recent theory for rod-like virus assembly,[40] this distinct nucleation lag time should be very sensitive to the protein concentration, which effectively sets the oversaturation. We therefore applied this method to a more concentrated system 0.6 μM CP1 with 22.2 μM $C_4S_{10}B^{K12}$ (10x higher), Figure 5.3. Interestingly, while the nucleation lag time has decreased from 30 hrs to only 5 hrs, the rate of growth remains unchanged. This is in full agreement with the idea that the rate of nucleation is set by the relative degree of oversaturation, while the growth is governed by the rate at which protein folding can

propagate along the template, which should be much less sensitive to the overall concentration.

5.2.4 Competition between co- and self-assembly

When the protein is in excess with respect to the template, ($f+ > 0.5$) we surprisingly observe that the capsid initially forms almost to completion, but after some time reverses somewhat into a partially-coated state (Figure 5.4B). It is known that $C_4S_{10}B^{K12}$ can also self-assemble, in absence of a template, into empty rod-shaped capsids. Thus, at mixing ratios higher than charge stoichiometry, there are two competing mechanism acting in the system. On the one hand there is the initial co-assembly of the anionic template with the protein, guided by binding through the B^{K12} block of the protein. This locally increases the protein concentration, which triggers the nucleation of a filled capsid around the oppositely charged chain. Yet, due to the strong interactions between the S_{10} blocks, structures can also form in the bulk, which are invisible to our mechanochromic sensors. This second mechanism is triggered only when there is an excess of protein in solution and at sufficient concentration. Our results suggest that as a result of this competition, some protein can be scavenged from filled capsids by means of slow equilibration due to thermally-activated protein dissociation, leading to the non-monotonic behavior we observe for sample $f+ = 0.7$ in Figure 5.4B. At a much lower protein concentration, the critical association threshold of the protein in the bulk is not exceeded, such that even at $f+ > 0.5$ this competition between co- and self-assembly, and the resulting scavenging, is not observed on the experimental time scale (Figure 5.4A).

5.2.5 Chain bundling within the capsid

The results above demonstrate how the combination of electrostatic co-assembly and silk-domain guided self-assembly in the formation of artificial virus capsids gives rise to complex kinetics. To evaluate whether the capsid is filled with a single conjugated template chain, or whether multiple, or folded, chains occupy the capsid void; we finally employ a second molecular sensor CP2 which features a FRET-based colorimetric response when multiple chains are in close proximity. In isolation, the fluorescence spectra of CP2 exhibit the same response as those of CP1. However, when chains bundle or fold, a significant in-

crease in luminescence at 550 - 600 nm should be observed due to FRET between fluorene and benzothiadiazole units on neighboring chains. In a fully aggregated state, the emission of the fluorene units in the blue is almost completely suppressed in favor of emission from the FRET acceptors (Figure 5.1F). With this sensor we repeat the experiments discussed above. The luminescence spectra show a similar change in the vibronic band structure as observed for CP1 (Figure 5.5).

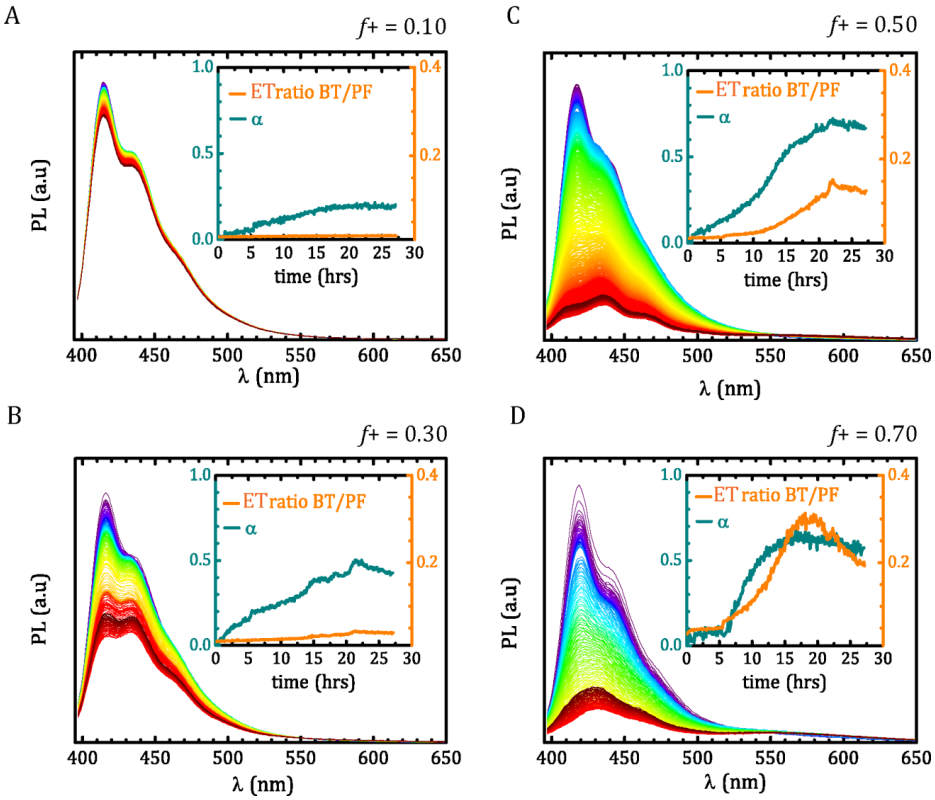

Figure 5.5 Time dependent changes in PL spectra of CP2 (0.08 μM) with $C_4S_{10}B^{K12}$ (2.22 μM) at mixing ratio ($f+$) of 0.10 (A); 0.30 (B); 0.50 (C); 0.70 (D) during the course of nucleation, growth and retraction for 28 hours. Insets show the time dependent changes of the coated fraction (α) of CP2 chains (left axis) and ratio of PL intensity of BT band over the PF band (right axis).

We can use the ratio of vibronic bands to directly quantify the fraction of template that is coated (insets Figure 5.5); we find the highest fraction of coated template at around 70% for $f+= 0.50$. This is slightly lower than for the homopolymer sensor CP1, which we attribute

to the 20% reduction in anionic charge density upon introducing uncharged BT moieties at the expense of dicarboxylic acid fluorene units. At charge stoichiometry and above we see a subtle increase in intensity of the FRET peak at 560 nm. To quantify this we determine the energy transfer (ET) ratio by dividing the intensity of the BT peak by that of the fluorene donor. Even though the amount of bundling do not reach the ratio obtained for aggregated sensor chains in the core of a charge-drive micelle[43] we observe significant FRET in the protein capsids. This indicates that the void of the viral capsid is occupied by more than one template chain. Interestingly, the FRET signal that reports chain proximity does not emerge until the final stages of capsid formation.

This indicates that a capsid first nucleates and begins to grow around a single isolated chain after which this chain folds, or the object recruits neighboring chains, to achieve full charge compensation within the capsid which is rich in cationic lysine residues from the B^{K12} blocks. Also here we see the non-monotonic behavior in time when an excess of coat protein is present (Figure 5.5D), which provides further evidence for the dynamic equilibrium between filled and empty capsids due to the competition between co- and self-assembly.

5.3 Conclusion

In this chapter, we have shown that the presence of two competing association motifs within a single coat protein gives rise to complex assembly kinetics, of forming a protein coat around a template and a competition between co-assembly with a template chain and self-assembly. The pattern observed is very similar to that of formation of natural (rod-like) viruses like tobacco mosaic virus. Using novel mechanochromic polymer sensors as the anionic templates for protein assembly, the nucleation-and-growth kinetics, and protein scavenging by empty capsids can be followed in detail. Moreover, inclusion of additional functionality in the sensor through incorporation of acceptor units allows us to show that the core of the co-assembled particles shows significant chain overlap, due to either folding of single chains, or bundling of multiple chains. These results highlight how competing and orthogonal supramolecular interactions within a single macromolecular building block can give rise to complex kinetic pathways of molecular-assembly.

5.4 Experimental Section

5.4.1 Photophysical Experiments

Steady-state fluorescence spectroscopy was performed on a Cary Eclipse Fluorescent Spectrophotometer with a xenon lamp. The temperature was regulated at 22 ^{o}C by a temperature controller mounted to the spectrophotometer. Fluorescence lifetime measurements were performed on an Edinburg Instruments Fluorescent Spectrophotometer FLS920 with picosecond pulsed diode laser (PDL 800-B) at an excitation wavelength of 373 nm, photoluminescence quantum efficiency (PLQE) measurements were performed on the same instrument, against an anthracene standard.

5.4.2 Conjugated Polymers

The synthesis of homopolymer *poly[9,9′-bis(tert-butyl-3″-propanoate)fluoren-2,7-yl], (PF3(tert))* via the nickel(0)-mediated polymerization reaction, Yamamoto polymerization, has been slightly modified from a previously described method.[34] $Ni(COD)_2$ (550 mg, 2 mmol) and 2,2′-bipyridyl (312 mg, 2 mmol) were placed in a 50 mL two neck round- bottom flask in a glove box. Dry dimethylformamide (3.5 mL) was added into the flask and purged with nitrogen at 75 ^{o}C. COD (245 µL, 2 mmol) was added dropwise and the mixture was stirred for 1 hour. Monomer 1 (Mon1) 2,7-dibromo-9,9-bis(3-(tert-butyl propanoate)) fluorene (0.55 g, 1 mmol) was dissolved in anhydrous toluene (6 mL) in a separate flask and purged with nitrogen, after which it was added to the reaction vessel dropwise. The reaction was allowed to proceed for 9 hrs under inert atmosphere. The chains were end-capped by injecting 1-bromo-4-ethynylbenzene (97%) (181 mg, 1 mmol) dissolved in anhydrous toluene (2 mL) into the reaction vessel. The product is purified by precipitation and Soxhlet extraction after which it is obtained as a yellow solid (310 mg, 56 %); from GPC we find M_w =16.7 kgmol^{-1} and PDI = 2.4. ^{1}H NMR (400 MHz, $CDCl_3$, δ): 7.79-7.66 (m, 6H), 2.46 (s, 4H,− CH_2-), 1.57 (s, 4H,− CH_2−), 1.22 (s, 18H) ppm.

To obtain the carboxylated water-soluble polymer *poly[9,9′-bis(3′′-propanoate)fluoren-2,7-yl] sodium salt (PF3) (CP1)*, the side chains were hydrolyzed using TFA in DCM followed by a second hydrolysis step using Na_2CO_3 in water. The polymer was purified through dialysis

against Mill-Q water for 3 days. CP1 is obtained after freeze-drying as fibrous yellow solid (31.3 mg, 52 %) with near complete hydrolysis of the propanoate side chains into their carboxylic acids. ^{1}H NMR (400 MHz, MeOD, δ): 7.83-7.73 (m, 6H), 2.51 (s, 4H), 1.54 (s, 4H) ppm, 1.22 (s, 18H).

The synthesis of copolymer, *poly[9,9′-bis(tert-butyl-3″-propanoate)fluorene-co-4,7-(2,1,3-benzothiadiazole)$_{20}$], (PF3(tert)-BT$_{20}$)* was performed using the same procedure as above: monomer Mon1 (442 mg, 0.8 mmol) and monomer 4,7-dibromobenzo[c]-1,2,5-thiadiazole (Mon2) (58.8 mg, 0.2 mmol) were incorporated in the polymer backbone at a 4:1 molar ratio. The endcap agent used in this synthesis was 4-bromo-2,1,3-benzothiadiazole (21.5 mg, 0.1 mmol). After purification the copolymer was obtained (430 mg, 84%) with M_w = 12.0 kg mol^{-1} and PDI = 2.2. ^{1}H NMR (400 MHz, CD_2Cl_2, δ): 7.84-7.74 (m, 6H), 2.49 (s, 4H, $-CH_2-$), 2.00 (s, 4H,$-CH_2-$), 1.23 (s, 18H) ppm.

Using the same protocol as above we obtain the polyelectrolyte *CP2: poly[9,9′-bis(3′′-propanoate)fluorene-co-4,7-(2,1,3-benzothiadiazole)$_{20}$] sodium salt (PF3-BT$_{20}$)* as a brown- yellow solid (400 mg, 93%). ^{1}H NMR (400 MHz, MeOD, δ): 7.90-7.82 (m, 6H), 2.59 (s, 4H), 1.62 (s, 4H) ppm, 1.29 (s, 18H).

5.4.3 Artificial viral coat protein

The artificial viral coat protein ($C_4S_{10}B^{K12}$) is prepared using recombinant *Pichia pastoris* yeast strains that carry the artificial genes for the desired amino acid sequence. We follow previously established protocols [11, 40] for the design, biosynthesis and purification. $C_4S_{10}B^{K12}$ (M_w = 45 kDa) (Figure A5.2) consists of *i)* a stabilizing (C_4) block of 407 amino acids with the same composition as collagen but a randomized sequence to create an inert and hydrophilic random coil structure with a radius of gyration of 7 nm;[11] *ii)* a electrostatic binding block (B^{K12}) that has 12 lysine residues which are located at the C-terminus of the protein polymer and *iii)* a central block that consists of a silk-like sequence S_{10}= (GAGAGAGQ)$_{10}$ that provides cooperativity by folding and stacking into stiff filamentous structures with a characteristic *β*-roll structure, in which the glutamine residue (Q) resides at the corners of the folded turns.

5.4.4 Sample Preparation

Solutions of CP1 (1 or 10 μgml^{-1}), CP2 (1 μgml^{-1}), $C_4S_{10}B^{K12}$ (0.1 or 1 mgml^{-1}) were prepared in deionized water whose pH was adjusted to 8.6 with NaOH. $C_4S_{10}B^{K12}$ solutions are kept at 60 ^{o}C for 10-15mins to ensure a purely unimeric state prior to mixing with CPs. Samples were mixed by vortexing for few seconds. Solutions were immediately transferred into quartz cuvettes and sealed to prevent evaporation during the course of the experiment.

References

[1] J. M. Lehn, *Rep Prog Phys* **2004**, *67*, 249-265.

[2] G. M. Whitesides, B. Grzybowski, *Science* **2002**, *295*, 2418-2421.

[3] I. V. Baskakov, G. Legname, M. A. Baldwin, S. B. Prusiner, F. E. Cohen, *J Bio Chem* **2002**, *277*, 21140-21148.

[4] P. A. Korevaar, S. J. George, A. J. Markvoort, M. M. J. Smulders, P. a. J. Hilbers, A. Schenning, T. F. A. De Greef, E. W. Meijer, *Nature* **2012**, *481*, 492-U103.

[5] F. Boato, R. M. Thomas, A. Ghasparian, A. Freund-Renard, K. Moehle, J. A. Robinson, *Angew Chem Int Ed* **2007**, *46*, 9015-9018.

[6] Y.-B. Lim, E. Lee, Y.-R. Yoon, M. S. Lee, M. Lee, *Angew Chem Int Ed* **2008**, *47*, 4525-4528.

[7] K. Matsuura, K. Watanabe, T. Matsuzaki, K. Sakurai, N. Kimizuka, *Angew Chem Int Ed* **2010**, *49*, 9662-9665.

[8] J. B. Bancroft, *Adv Virus Res* **1970**, *16*, 99-134.

[9] H. D. Nguyen, V. S. Reddy, I. C. L. Brooks, *Nano Lett* **2007**, *7*, 338-344.

[10] D. Philp, J. Fraser Stoddart, *Angew Chem Int Ed* **1996**, *35*, 1154-1196.

[11] A. Hernandez-Garcia, M. W. T. Werten, M. A. Cohen Stuart, F. A. De Wolf, R. De Vries, *Small* **2012**, *8*, 3491-3501.

[12] B. Liu, G. C. Bazan, *J Am Chem Soc* **2004**, *126*, 1942-1943.

[13] K. Y. Pu, B. Liu, *Macromolecules* **2008**, *41*, 6636-6640.

[14] D. Yu, Y. Zhang, B. Liu, *Macromolecules* **2008**, *41*, 4003-4011.

[15] J. W. Hong, W. L. Hemme, G. E. Keller, M. T. Rinke, G. C. Bazan, *Adv Mater* **2006**, *18*, 878-882.

[16] C. Chi, A. Mikhailovsky, G. C. Bazan, *J Am Chem Soc* **2007**, *129*, 11134-11145.

[17] T. M. Swager, *Acc Chem Res* **1998**, *31*, 201-207.

[18] A. Satrijo, T. M. Swager, *J Am Chem Soc* **2007**, *129*, 16020-16028.

[19] S. W. Thomas, G. D. Joly, T. M. Swager, *Chem Rev* **2007**, *107*, 1339-1386.

[20] L. Chen, D. W. Mcbranch, H. L. Wang, R. Helgeson, F. Wudl, D. G. Whitten, *Proc Natl Acad Sci U S A* **1999**, *96*, 12287-12292.

[21] B. S. Gaylord, S. Wang, A. J. Heeger, G. C. Bazan, *J Am Chem Soc* **2001**, *123*, 6417-6418.

[22] C. H. Fan, S. Wang, J. W. Hong, G. C. Bazan, K. W. Plaxco, A. J. Heeger, *Proc Natl Acad Sci U S A* **2003**, *100*, 6297-6301.

[23] S. Kumaraswamy, T. Bergstedt, X. B. Shi, F. Rininsland, S. Kushon, W. S. Xia, K. Ley, K. Achyuthan, D. Mcbranch, D. Whitten, *Proc Natl Acad Sci U S A* **2004**, *101*, 7511-7515.

[24] K. E. Achyuthan, T. S. Bergstedt, L. Chen, R. M. Jones, S. Kumaraswamy, S. A. Kushon, K. D. Ley, L. Lu, D. Mcbranch, H. Mukundan, F. Rininsland, X. Shi, W. Xia, D. G. Whitten, *J Mater Chem* **2005**, *15*, 2648-2656.

[25] M. Liu, P. Kaur, D. H. Waldeck, C. Xue, H. Liu, *Langmuir* **2005**, *21*, 1687-1690.

[26] J. Lee, H. J. Kim, J. Kim, *J Am Chem Soc* **2008**, *130*, 5010-5011.

[27] S. Seo, J. Lee, E. J. Choi, E. J. Kim, J. Y. Song, J. Kim, *Macromol Rapid Commun* **2013**, *34*, 743-748.

[28] B. Yoon, S. Lee, J. M. Kim, *Chem Soc Rev* **2009**, *38*, 1958-1968.

[29] K. P. R. Nilsson, A. Herland, P. Hammarström, O. Inganäs, *Biochemistry* **2005**, *44*, 3718-3724.

[30] H. A. Ho, M. Boissinot, M. G. Bergeron, G. Corbeil, K. Doré, D. Boudreau, M. Leclerc, *Angew Chem Int Ed* **2002**, *41*, 1548-1551.

[31] H. A. Ho, M. Leclerc, *J Am Chem Soc* **2004**, *126*, 1384-1387.

[32] T. L. Nelson, C. O'sullivan, N. T. Greene, M. S. Maynor, J. J. Lavigne, *J Am Chem Soc* **2006**, *128*, 5640-5641.

[33] H. E. Cingil, I. M. Storm, Y. Yorulmaz, D. W. Te Brake, R. De Vries, M. A. Cohen Stuart, J. Sprakel, *J Am Chem Soc* **2015**, *137*, 9800-9803.

[34] S. Y. Cho, A. C. Grimsdale, D. J. Jones, S. E. Watkins, A. B. Holmes, *J Am Chem Soc* **2007**, *129*, 11910-+.

[35] M. Knaapila, M. J. Winokur, in *Adv Poly Sci, Vol. 212*, **2008**, pp. 227-272.

[36] M. Grell, D. D. C. Bradley, X. Long, T. Chamberlain, M. Inbasekaran, E. P. Woo, M. Soliman, *Acta Polym* **1998**, *49*, 439-444.

[37] M. Grell, D. D. C. Bradley, G. Ungar, J. Hill, K. S. Whitehead, *Macromolecules* **1999**, *32*, 5810-5817.

[38] A. L. T. Khan, P. Sreearunothai, L. M. Herz, M. J. Banach, A. Köhler, *Phys Rev B: Condens Matter Mater Phys* **2004**, *69*, 852011-852018.

[39] A. K. Bansal, A. Ruseckas, P. E. Shaw, I. D. W. Samuel, *J Phys Chem C* **2010**, *114*, 17864-17867.

[40] A. Hernandez-Garcia, D. J. Kraft, A. F. J. Janssen, P. H. H. Bomans, N. a. J. M. Sommerdijk, D. M. E. Thies-Weesie, M. E. Favretto, R. Brock, F. A. De Wolf, M. W. T. Werten, P. Van Der Schoot, M. A. Cohen Stuart, R. De Vries, *Nat Nanotechnol* **2014**, *9*, 698-702.

[41] A. J. Cadby, P. A. Lane, H. Mellor, S. J. Martin, M. Grell, C. Giebeler, D. D. C. Bradley, M. Wohlgenannt, C. An, Z. V. Vardeny, *Phys Rev B: Condens Matter Mater Phys* **2000**, *62*, 15604-15609.

[42] U. Scherf, E. J. W. List, *Adv Mater* **2002**, *14*, 477-487.

[43] H. E. Cingil, E. B. Boz, J. Wang, M. A. Cohen Stuart, J. Sprakel *Adv Funct Mater* **2016**, *in press*.

APPENDIX

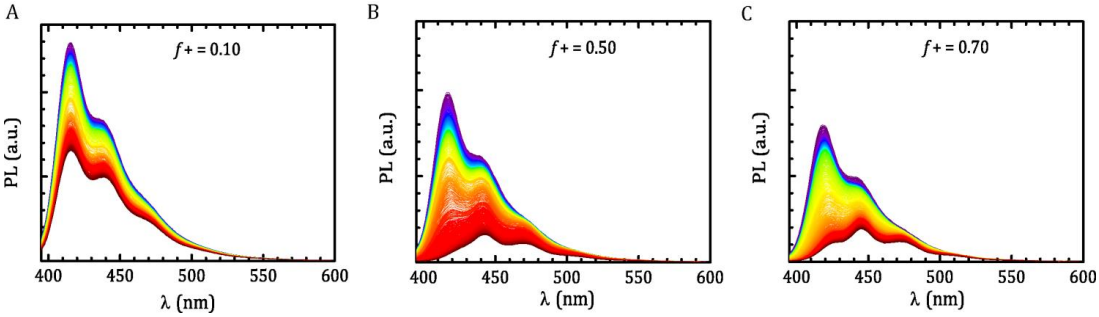

Figure A5.1 Time dependent changes in PL spectra of CP1 (0.06 μM) with $C_4S_{10}B^{K12}$ (2.22 μM) at mixing ratio ($f+$) of 0.10 (A); 0.50 (B); 0.70 (C) during the course of nucleation and growth for 70 hours.

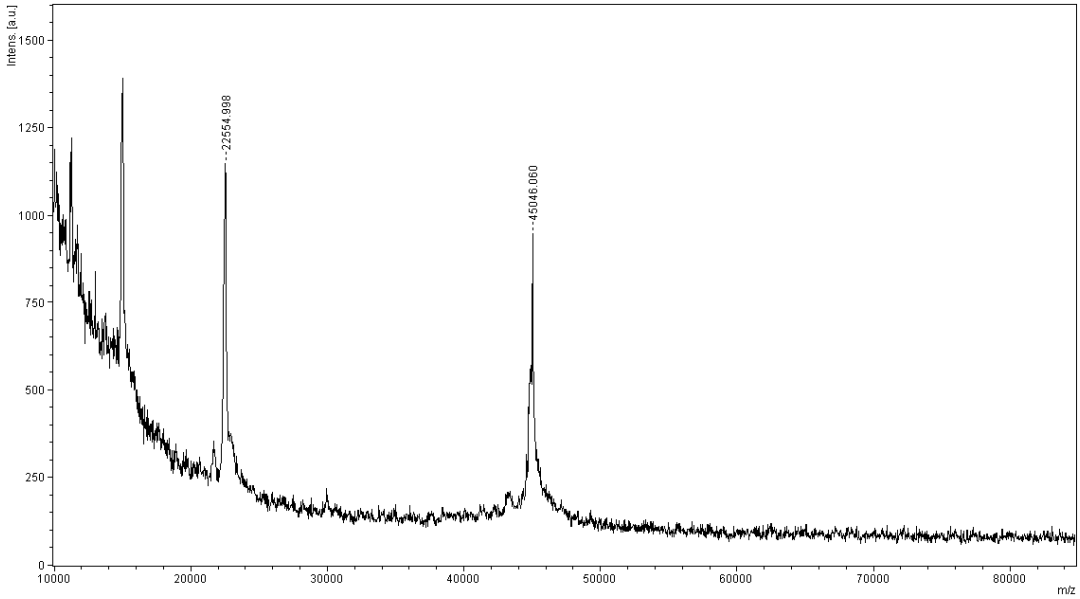

Figure A5.2 MALDI-TOF (Matrix Assisted Laser Desorption/Ionization Time-of-Flight Mass Spectroscopy) spectrum of $C_4S_{10}B^{K12}$.

CHAPTER 6

General Discussion

This thesis consists of four experimental chapters based on studies conducted on four distinct supramolecular systems. Our aim was to push our understanding of supramolecular assembly at the nanoscale with *(i)* a technique that was developed earlier but had never been applied to a thermodynamically reversible system and *(ii)* a novel approach based on multi-responsive mechanochromic polymer sensors, designed, developed and optimized to shine new light onto charge driven co-assembly.

In this chapter we will place the outcome of this thesis in a broader perspective. We will first discuss the mechanochromism of polyfluorenes by specifically focusing on the factors which affect its transition to the β-phase. In addition to the examples from the literature, we will also discuss some preliminary experiments not shown in the previous Chapters. We will conclude this section with prospects for future research using the experimental technique of single molecule spectroscopy, which may have the answers to the questions related with the origin of β-phase formation in polyfluorene. Finally, we will emphasize the potential use of mechanochromic polyfluorene in high complexity supramolecular systems to probe local viscoelastic changes (spectroscopic microrheology) with experimental results obtained from an asymmetric triblock protein which combines the properties of proteins used in Chapter 2 and Chapter 3.

The morpho-chromic relationship between the chain conformation of conjugated polymers (CPs) and their spectral response is well-known. Structurally, CPs almost invariable exhibit a semi-flexible backbone which is not easily soluble in common solvents due to the strong tendency for π-π interactions. The insoluble nature of CPs limits their processability and thus potential applications. A common approach to resolve this limitation is to substitute the backbone with flexible side chains to provide steric hindrance against π-π stacking. The structure of CPs with grafted side chains is often described as a semi-flexible hairy-rod architecture whose side "hairs" ensures the solubility of aromatic backbone. The type of the side chain influences polymer solubility in different types of solvents. Moreover, it alters the phase behavior of polymer which directly affects the optoelectronic properties. To date, these effects have been most extensively studied in polyfluorenes, due to the relative ease with which they can be synthesized and functionalized, and their distinct spectral response in the visible range of the electromagnetic spectrum. In addition, polyfluorenes are among

the most studied conjugated polymers due to their unique application characteristics for optoelectronic devices, such as having a low band gap, efficient blue light emission, excellent stability and easy processability.[1]

6.1 The *β*-phase of polyfluorene

In this thesis we demonstrated how supramolecular binding could induce a conformational change in individually dissolved conjugated polyelectrolytes, which in turn resulted in a distinct mechanochromic response. We have attributed this to the planarization of the backbone and the resulting increase in effective conjugation length. These phenomena are also observed to occur during the planarization of alkyl-substituted polyfluorene chains in the solid state during a transition between amorphous and partially-crystalline phases. To explore the origins of this mechanochromism, we thus explore the *β*-phase in some detail below.

The *β*-phase of polyfluorene was first reported in 1998 as an "aggregate" state of poly(9,9-dioctylfluorene), where chains adopts an extended conformation when placed in a poor solvent.[2] The detection of this structural change in the backbone conformation of polyfluorene was possible only because this new phase had distinct spectral features appearing in the absorption spectra, as a new low energy band ~ 436 nm, and more pronouncedly in the emission spectra as a red-shift with well-resolved vibronic bands. In response, detailed studies were performed to understand the origin of *β*-phase formation in polyfluorene. We must emphasize here that most of this research was performed on polyfluorene substituted with di-*n*-alkyl side chains prepared in thin films in the solid state. Primarily, polyfluorene films were subjected to thermal treatment or exposed to solvent vapor which resulted in mechanical stress or swelling stress on polymer chains, respectively.[3] More recently, *β*-phase of polyfluorene was observed when polymer chains were physically confined inside an ionogel or in nanoparticles.[4-5] The proposed driving force for *β*-phase formation in this system was a combination of various "possible" contributors such as π-π stacking and hydrophobic interactions. Even though the efforts made to find out the origin of *β*-phase formation of polyfluorene chains do not yield a straightforward answer, the studies have revealed one commonality that this new phase appears in conditions where the polyfluorene

chains are subjected to stresses in any form, such as mechanical, thermodynamic or supramolecular.

Meanwhile, details about the morphology of the β-phase of polyfluorene were being studied by various *x*-ray scattering methods, such as fiber diffraction, small angle and wide angle scattering.[3, 6] The results showed that chains in the β-phase of polyfluorene exhibit a significantly longer effective conjugation length than those in an amorphous conformation. Thus, the β-phase of polyfluorene relates to a planarized and stretched conjugated backbone. This intrachain (within-the-chain) planarization with chain stretching can be considered as a one-dimensional (1D) crystallization process, rarely observed in nature.[7] Even though the initial studies related the β-phase formation of polyfluorene to intrachain ordering under applied stress, it was later discovered that with the appropriate alkyl-chain substitution, β–phase formation can occur spontaneously from the glassy state.[6, 8] This highlights the critical contribution of interchain (between-the-chains) interactions on this phase transition in the bulk.

6.1.1 Alkyl side-chain length dependence

The effect of alkyl-chain length on the β-phase formation of polyfluorene has been studied in detail with optical spectroscopy (absorption, emission and excitation) and *x*-ray scattering (small- and wide- angle) methods for linear side chains consisting of 6 - 10 carbon atoms.[6, 8] There has been no report on β-phase formation with branched side chains yet, but we may expect the bulkiness of branched side chains to have a significant effect on the formation of the partially ordered phase. Thus, we will focus on the linear side chains, only. Polyfluorenes substituted with different lengths of linear alkyl side chains exhibit different phase behaviors when exposed to the same thermal treatment or dissolved in same solvent. Results indicate that the *octyl* (8C) chain length is the most favorable to induce β-phase polyfluorene, followed by heptyl and nonyl substitutions. Interestingly, no β-phase formation is observed in polyfluorenes with side chains of 6 and 10 carbons. Two possible factors were proposed for such a specific effect of side chain length: (1) "Aggregate formation efficiency" which is considered to be weak due to increased disorder for long chain lengths (10 carbons) and (2) "van der Waals bond energy" which is required to planarize the back-

bone by overcoming the steric repulsion, is considered to be insufficient for short chain lengths (6 carbons).

The polyfluorene-based mechanochromic sensors which were used in this thesis are substituted with linear side chains of only 3 carbon atoms with a terminal carboxylic acid. There is no information on β-phase formation of polyfluorene with this side chain length (or any other length < 6 carbons). We suspect this is due to the very limited solubility of polyfluorenes with only short alkyl side chains due to π-π stacking in solution. Interestingly, our results presented in this thesis have shown the phase transition from amorphous to β-phase occurring in short side chain substituted polyfluorenes, both in solution (Chapters 3-5) and the solid-state by pH-triggered precipitation (Figure A3.2 in Chapter 3). We also prepared similar conjugated polyelectrolytes (PF2), synthesized via the same, nickel (0)-mediated Yamamoto coupling, but with a side chain of only 2 carbons (Figure 6.1A). Note that this sample exhibited an almost 4 times higher molecular weight of the polymer (M_w= 68.5 $kgmol^{-1}$) and slightly improved polydispersity (PDI=2.2). PF2 is an anionic homopolymer which is highly soluble in aqueous solution under basic conditions. When we introduced the cationic-neutral diblock polypeptide C_4B^{K12} (the coat protein used in Chapter 3) to an aqueous solution of PF2 (0.15 μM), electrostatic interactions ensure the binding of positively charged molecules which then leads to spectral changes in the photoluminescence (PL) spectra of PF2 (Figure 6.1B). Upon coating of the PF2 backbone with protein we observe again the same distinct spectral changes in emission bands which were attributed to β-phase of polyfluorene, similarly as those shown in Chapter 3.

For these supramolecularly-stretched polyelectrolytes, the side-chain length thus appears to be relatively unimportant. This can be understood by recognizing the contribution of the bulky neutral block (400 amino acids) of the protein to the stress applied on the polymer backbone. The coil radius of this neutral block is ≈ 6-7 nm.[9] There must be multiple diblock proteins attached to a single polyfluorene chain, hence, when the spacing between each neutral block becomes much smaller than their coil radius, strong entropic repulsion between neighboring neutral blocks will lead to side chain stretching.[9-10]

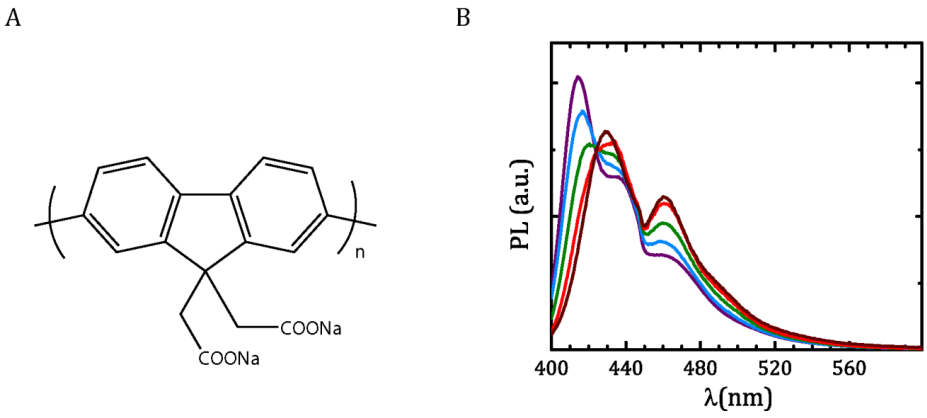

Figure 6.1 The chemical structure of PF2 (A); Normalized PL spectra of uncoated PF2 (violet) and of the gradually coated PF2 with diblock C_4B^{K12}, showing the decrease in main band I and gradual increases in band II and III (β-phase of polyfluorene) (B).

Moreover, since this co-assembly results in the formation of a self-assembled bottle-brush structure, there is also the possibility of side chain induced main chain stiffening[11-12] onto which the opto-mechanical calibration curve in Chapter 3 is based.

All these indicate that there is a major effect of interchain interactions on the stress felt by the conjugated backbone of polyfluorene, thus the β-phase formation. Results of other reports in the literature support our claim. A recent study used a polyfluorene homopolymer with carboxylated side chains (3 carbons in length), the same polymer as we have used in Chapter 3 - 5, to selectively detect mono- and divalent metal ions, such as Cu^{+} and Cu^{2+} ions.[13] The PL spectra only exhibited quenching due to binding, which we also observe (Figure A3.1, Chapter 3), but no β-phase formation. Moreover, also experiments on complexation with a homopolymer, which lacks the neutral side chains, reported in Figure 3.2C in Chapter 3, show no appreciable chain planarization. Apparently, the interaction between side grafts is required to mechanically force the chain into an extended conformation. Finally, another study considered the use of poly(fluorene-*co*-benzothiadiazole), structurally similar to the CP2 used in Chapter 4 - 5, except the carboxylated side chains which had 4 carbons instead of 3 carbons, to detect diamines and biogenic polyamines at very low concentrations via FRET.[14] This study also only monitored the quenching in emission intensity to detect binding, but reports no signs of β-phase formation. These data are strong evidence

that the origin of single-molecule β-phase formation in solution is not due to charge neutralization itself but the result of a mechanical stress induced by various supramolecular interactions.

6.1.2 Conjugated backbone design

Over the past decade, we have seen an increased interest in the development of biological recognition systems based on a multicolor sensor response from a single polyfluorene (or other conjugated) polymer chain. The conjugated backbone of polyfluorene has been *(i)* tailored with donor-acceptor units to achieve a colorimetric response via energy transfer; and *(ii)* substituted with water-soluble anionic or cationic side chains to ensure the binding of specific biomolecule. Even though various polyfluorene-based colorimetric sensors have been reported to detect and quantify even low concentrations of biomolecules, none of them were reported to exhibit the specific mechanosensor property, *i.e.* stress induced change in conjugated backbone conformation, we have utilized in Chapters 3 - 5 in this thesis. This may seems surprising as the vibronic changes we observe are so strong. However, the conjugated backbone of the previously used colorimetric polyfluorenes has a small difference in chemical composition. Even though the acceptor unit was almost always chosen to be 2,1,3-benzothiadiazole (BT) moiety that we have also used (with exceptions)[15-16], it was introduced into poly(fluorene-*co*-phenylene) chains (Figure 6.2) instead of pure polyfluorene chains.[17-20]

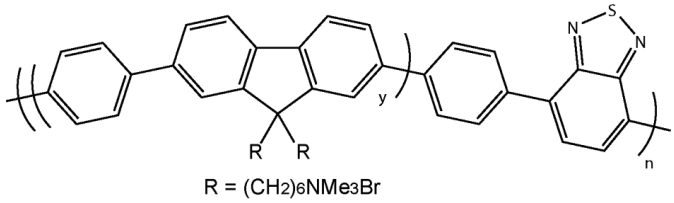

Figure 6.2 The chemical structure of frequently used poly(fluorene-*co*-phenylene) based colorimetric sensors. Reproduced with permission from ref 10. Copyright 2006 Wiley-VCH Verlag Gmbh & Co. KGaA.

This design variations have been studied extensively for their effective reporting of multicolor detection of biomolecules via Förster resonant energy transfer (FRET). However, even a very bulky biomolecule, *i.e.* DNA, could not induce backbone planarization in these pol-

ymers, hence no β-phase formation is reported. Apparently, this design variations changed the ability of the conjugated chain to form the 1D crystal required to create the specific vibronic mechanosensor response. Additionally, in a study which shows the pH dependence of a similarly designed poly(fluorene-*co*-phenylene-*co*-benzothiadiazole), only enhanced FRET at low pH due to aggregation-induced increases in interchain contacts is reported, but also here no β-phase formation is observed.[20] By contrast, for pure polyfluorene chains with BT doping, we observe the mechanochromic response also in the aggregated state (Chapter 4).

To confirm these data within our experimental approach, we have synthesized a polymer (PFpBT) with a similar design in which we also included a phenylene unit into the backbone (Figure 6.3A). We show the changes in PL spectra of PFpBT when the pH is lowered from 11 to 5 in Figure 6.3B. Also here, we observe enhanced FRET from the fluorene units to BT, which occurs when chains become increasingly insoluble. However, as can be clearly seen, the relative intensities of the vibronic transitions remain unaltered, hence there is no sign of chain planarization which can be utilized for molecular force sensing, in stark contrast to what we reported in Figure A3.2.

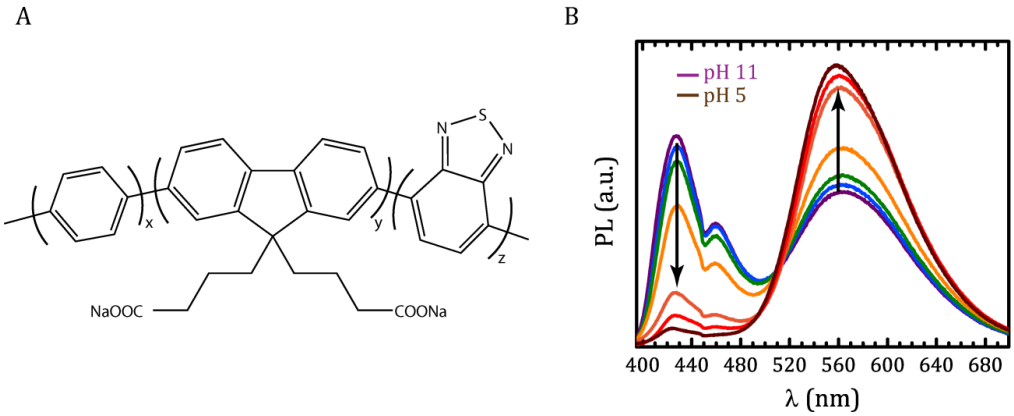

Figure 6.3 The chemical structure of PFpBT (A) and normalized PL spectra of PFpBT as a function of decreasing pH (as indicated by the arrow) from 11 (violet) to 5 (brown) (B).

We speculate that the alternating phenylene units in the backbone increase the rotational degrees of freedom along the conjugated chain. In turn this increases the flexibility of the backbone and may aid in relieving stresses applied to the backbone. Moreover, the phe-

nylene units increase the inter-monomer spacing between adjacent fluorene units between which energy is transferred in the planarized chain conformation, characteristic of the beta-phase. The combination of these effects appears to suppress the characteristic vibronic response at the heart of the mechanochromic sensing described in Chapters 3 - 5.

6.1.3 Single molecule spectroscopy

Single molecule spectroscopy (SMS) is a relatively new technique to study the structure, position and environment of single fluorescent objects at the nanometer scale.[7] It allows the optical detection of single molecules and eliminates for the ambiguities that may arise due to ensemble-averaged responses collected by conventional spectroscopy methods in heterogeneous systems such as conjugated polymers, proteins and biological light-harvesting complexes. As discussion in the previous section, still many questions remain regarding the nature of the β-phase formation in polyfluorene and its mechanochromic response. To utilize the mechanochromism of polyfluorene in further studies in sensing or for other future applications, it is crucial to understand the exact nature of the stretching-induced vibronic shifts at the single molecule level. We know that chain planarization, in the solid state or in solution, results in the distinct beta-phase signature in the luminescence spectra. We also have evidence for the contributions of side chains and binding complexes on the stresses created and transduced onto the polyfluorene backbone. But, not all binding events lead to the apparent β-phase formation. Moreover, how subtle structural differences between a homopolymer polyfluorene chain and a poly(fluorene-*co*-phenylene) chain result in the emergence or lack of mechanochromism, e.g. upon complexation with our neutral-cationic diblock protein C_4B^{K12}, remains unclear. Moreover, while we have determined the optical response of the whole medium, we do not know how each single chain actually contributes to that collective response. Can thermal fluctuations in the density of analyte bound to a chain be detected as fluctuations in vibronic peaks? Can the resolution of force detection be increased by detecting single molecules in which the vibronic peaks are expected to become significantly more pronounced? The only experimental technique currently available to address these questions and gain more insight into β-phase formation in polyfluorene chains is SMS. Thus, based on the findings in this thesis, we believe this is the most logical direction to continue this work. Application of single-molecule detection in

combination with super-resolution imaging, as in Stochastic optical reconstruction microscopy (STORM) or photo-activated localization microscopy (PALM) methods, could enable a novel microrheology type of method using mechanochromic chains as molecular rheological stress sensors.

6.2 Co-/ Self- assembly kinetics

Throughout this thesis we have shown that polyfluorene-based mechanochromic sensors, due to their robust and characteristic optical response, can be used to study various supramolecular self-assembly processes, such as the charge driven co-assembly of coat proteins forming a physical bottlebrush structure, micelle formation of synthetic polymers and the competition between templated and non-templated assembly of virus-mimicking proteins. In successive chapters, *(i)* we have either improved or optimized our mechanochromic sensor to achieve a deeper level of understanding of the specific system of interest; and *(ii)* we have gradually increased the level of complexity; going from single molecular objects in Chapter 3, a condensation transition to multimolecular micelles in Chapter 4, to competing pathways in cooperative self-assembly in Chapter 5. We realize that these sensors have great potential to probe local environmental changes at the nanometer scale and in this way they can be considered as a spectroscopic sort of microrheology.

To realize this, we combined a biosynthetic asymmetric triblock protein (TR4K) produced in a recombinant *Pichia pastoris* host (Figure 6.4A), by using established protocols[21] with our simplest mechanochromic sensor CP1. TR4K consists of an end block (T) which self-assembles into triple-helices at low temperature and forms an elastic network, a random coil middle block (R4) that consists of 400 amino acids and acts as hydrophilic spacer, and a cationic end block (K) consisting of 6 lysines to ensure binding. This system is thus a hybrid of the thermoreversible polypeptide gelator which was probed in Chapter 2 for its melting and gelation dynamics and the simple coat protein which was monitored during its encapsulation of our mechanochromic sensor, CP1, in Chapter 3.

We addressed two preliminary questions by studying this system: (1) can we control the stress-induced backbone planarization of CP1, when the charge ratio between TR4K and

CP1 is kept low to prevent β-phase formation, so that only thermo-reversible triple-helices are formed by the end blocks as illustrated in Figure 6.4B; and (2) can we use the mechanochromic sensor to probe local changes in viscoelastic properties in the system, similar to the microrheology method used in Chapter 2?

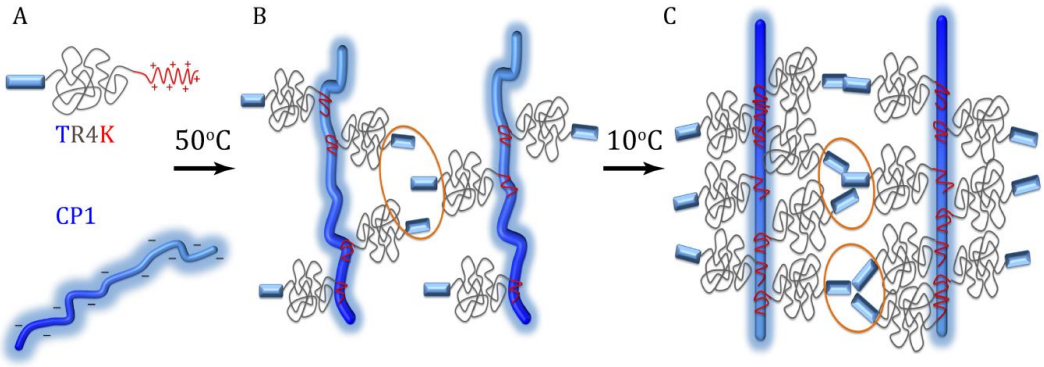

Figure 6.4 Highly illustrated schematics of asymmetric triblock polypeptide (TR4K) and anionic homopolymer polyfluorene (CP1) (A); charge-driven electrostatic binding of TR4K on CP1 backbone at high temperatures (B); and thermo-reversible triple-helices formation of T blocks at 10°C (C).

The experiments require pre-heating of TR4K at 50 °C for 30 mins to ensure the full dissociation of pre-formed triple helices in the system before introducing it into CP1 solution at pH = 8.6. Immediately after mixing the CP1 and TR4K, we quenched the temperature to 10 °C and started recording the photoluminescence spectra over the next 22 hours (1 scan/30 mins) while keeping the temperature fixed at 10 °C inside the fluorescence spectrophotometer. A control sample, which only contains CP1 with no protein, is shown in Figure 6.5A and shows no appreciable change in vibronic band structure. However, samples with protein at two different mixing ratios, $f+= 0.1$ and $f+= 0.2$, shown in Figure 6.5B – C, exhibit immediate quenching due to binding of TR4K to CP1as well as some changes in vibronic bands indicating a partial transition towards β-phase formation due to backbone coating by TR4K. As we decided to keep the mixing ratio low, we minimized the contribution of TR4K coating to backbone planarization. In Figure 6.5B - C, we therefore monitor the changes in band I and II (indicative for β-phase formation) which occur as a result of stress induced on CP1 by triple helices formation of self-assembling blocks at low temperature. Gradually in

time, we observe the characteristic changes in vibronic spectra due to the planarization and stretching of the CP1 backbone.

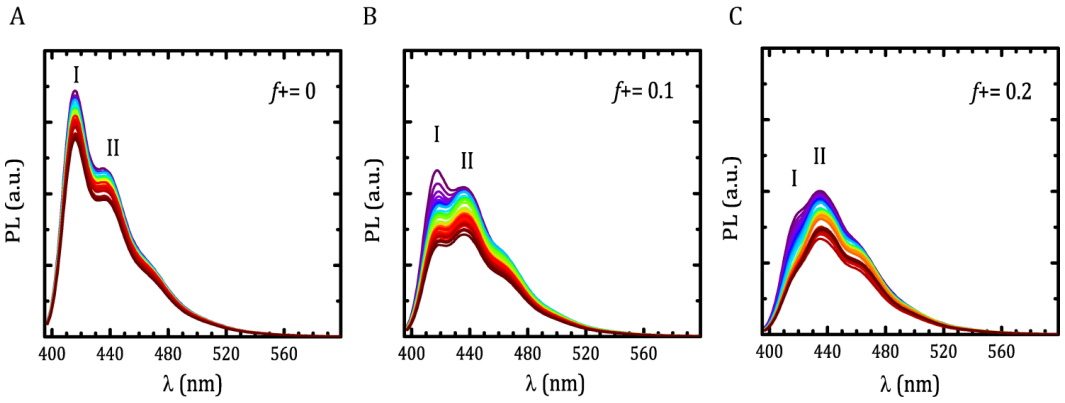

Figure 6.5 Time dependent changes in PL spectra of CP1 (0.6 μM) with no TR4K as control sample (A); with (1.10 μM) TR4K at mixing ratio $f+ = 0.1$ (B); and with (2.50 μM) TR4K at mixing ratio $f+ = 0.20$ (C) during the course of triple-helices formation of T block of TR4K for 22 hours at 10 °C.

After 22 hours at 10 °C, we increased the temperature to 30 °C and then recorded the reverse process. When sufficient time is given, all the triple helices should disassemble and the stress on the CP1 backbone should be released. The characteristic progression of the vibronic shifts due to encapsulation-induced chain planarization can be followed in detail by plotting the ratio of the intensities between the 1-0 and 2-0 bands in Figure 6.6. This clearly shows that at low temperature, where triple helices form between self-assembly blocks, there is backbone planarization to an extent. If we subsequently increase the temperature again (indicated by the dotted line in Figure 6.6), the co-assembled objects dissociate again and the spectra return to that of the bare, native, conjugated polymer.

We know from an earlier rheological study done on TR4K system[21] that the protein concentration which was used in these experiments is too low to induce a complete sol-gel transition via cross-link formations throughout the entire system. Nevertheless, we confirm from the comparison of spectra shown in Figure 6.5 A - C that vibronic band changes occur, merely due to the presence of TR4K in the system leading to elevated stress on the CP1 backbone when the temperature is low. Hence, this increased stress most likely originates from the triple-helices formed at low temperature even though the total protein concentra-

tion is too low to induce a macroscopic effect. We know that CP1 acts as a template for TR4K, due to electrostatic interactions between the anionic side chains of CP1 and the cationic binding block of TR4K. This can easily increase the local concentration of proteins around CP1 chains and bring triple-helices-forming T blocks in close proximity. The observations with our mechanochromic sensor, Figure 6.6, very likely originate from that local increase in elasticity which enhances the stress on CP1 backbone.

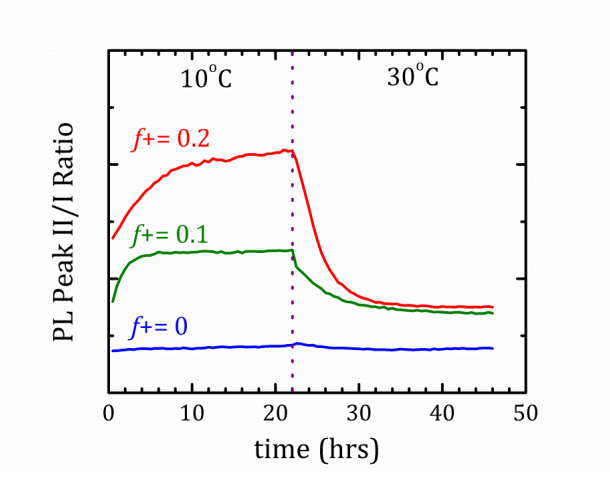

Figure 6.6 The ratio of vibronic bands II/I as a function of time after mixing sensor polymer CP1 with triblock protein TR4K at 10 °C and subsequent dissociation of co-assembled objects at 30 °C

These results highlight how mechanochromic polyfluorenes have great potential to be used as versatile, non-invasive sensors to probe local changes at nanometer scale. In this sense, they are tools like probe particles in microrheology, but their response is spectroscopic. They have the flexibility to be designed and tailored for monitoring specific interactions in various co-and self-assembled systems formed spontaneously via supramolecular interactions. They still present many challenges concerning the origin of mechanochromism which might be best addressed with single molecule spectroscopy experiments and molecular simulations, but they open up a 'bright' future for nanoscience.

Acknowledgement

We would like to thank Thao T. H. Pham for providing us the biosynthetic asymmetric triblock protein (TR4K); Diane W. te Brake for providing us the GPC data of CP2; Yelda Yorulmaz for the help during the synthesis of CP2 and finally to Emre B. Boz for the help during the fluorescence experiments of TR4K.

References

[1] M. Knaapila, M. J. Winokur, in *Adv Polym Sci* **2008**, *212*, 227-272.

[2] M. Grell, D. D. C. Bradley, X. Long, T. Chamberlain, M. Inbasekaran, E. P. Woo, M. Soliman, *Acta Polymerica* **1998**, *49*, 439-444.

[3] M. Grell, D. D. C. Bradley, G. Ungar, J. Hill, K. S. Whitehead, *Macromolecules* **1999**, *32*, 5810-5817.

[4] R. C. Evans, P. C. Marr, *Chem Commun* **2012**, *48*, 3742-3744.

[5] A. J. C. Kuehne, M. Kaiser, A. R. Mackintosh, B. H. Wallikewitz, D. Hertel, R. A. Pethrick, K. Meerholz, *Adv Funct Mater* **2011**, *21*, 2564-2570.

[6] M. Knaapila, F. B. Dias, V. M. Garamus, L. Almásy, M. Torkkeli, K. Leppänen, F. Galbrecht, E. Preis, H. D. Burrows, U. Scherf, A. P. Monkman, *Macromolecules* **2007**, *40*, 9398-9405.

[7] E. Da Como, K. Becker, J. M. Lupton, *Adv Polym Sci* **2008**, *212*, 293-318.

[8] D. W. Bright, F. B. Dias, F. Galbrecht, U. Scherf, A. P. Monkman, *Adv Funct Mater* **2009**, *19*, 67-73.

[9] A. Hernandez-Garcia, M. W. T. Werten, M. A. Cohen Stuart, F. A. De Wolf, R. De Vries, *Small* **2012**, *8*, 3491-3501.

[10] I. M. Storm, M. Kornreich, A. Hernandez-Garcia, I. K. Voets, R. Beck, M. A. Cohen Stuart, F. a. M. Leermakers, R. De Vries, *J Phys Chem B* **2015**, *119*, 4084-4092.

[11] L. Feuz, F. a. M. Leermakers, M. Textor, O. Borisov, *Macromolecules* **2005**, *38*, 8891-8901.

[12] G. H. Fredrickson, *Macromolecules* **1993**, *26*, 2825-2831.

[13] C. S. Wu, H. C. Su, Y. Chen, *Org Biomol Chem* **2014**, *12*, 5682-5690.

[14] B. Bao, L. Yuwen, X. Zheng, L. Weng, X. Zhu, X. Zhan, L. Wang, *J Mater Chem* **2010**, *20*, 9628-9634.

[15] C. H. Fan, S. Wang, J. W. Hong, G. C. Bazan, K. W. Plaxco, A. J. Heeger, *Proc Natl Acad Sci U S A* **2003**, *100*, 6297-6301.

[16] B. Liu, B. S. Gaylord, S. Wang, G. C. Bazan, *J Am Chem Soc* **2003**, *125*, 6705-6714.

[17] J. W. Hong, W. L. Hemme, G. E. Keller, M. T. Rinke, G. C. Bazan, *Adv Mater* **2006**, *18*, 878-882.

[18] B. Liu, G. C. Bazan, *J Am Chem Soc* **2004**, *126*, 1942-1943.

[19] C. Chi, A. Mikhailovsky, G. C. Bazan, *J Am Chem Soc* **2007**, *129*, 11134-11145.

[20] F. K. Wang, G. C. Bazan, *J Am Chem Soc* **2006**, *128*, 15786-15792.

[21] T. T. H. Pham, F. Snijkers, I. M. Storm, F. A. De Wolf, M. A. Cohen Stuart, J. Van Der Gucht, *Int J Polym Mater Polym Biomater* **2016**, *65*, 125-133.

Summary

In this thesis, we employ two distinct powerful methods to shed light on the dynamics of supramolecular assembly at the nanoscale *(i)* particle tracking microrheology and *(ii)* conjugated polymer sensing.

In **Chapter 2**, we employed microrheology, based on multiple particle tracking with optical microscopy, to study the melting and gelation behavior of a thermoreversible biopolymer gel. At the sol-gel transition, the mechanics of this percolating system are so weak and evolve rapidly in time such that conventional rheometry fails to give insight into the nature of the gel point. It could only be probed with a method which noninvasively provides information about the changing visco-elasticity of the medium at short intervals (0.04 Hz ≈ 25 secs), by using submicron sized beads as thermally-driven microrheological probes. The gelator, a well-defined triblock copolypeptide inspired by collagen, has the special feature of forming a gel network at low temperature; a percolated structure is built under these conditions via the assembly of its end blocks into triple helices stabilized by hydrogen bonds. During the transition from a molten liquid state to a percolated elastic network, and its reverse, we have collected video recordings of the thermal motion of tracer particles, from which their mean squared displacements (MSDs) could be reconstructed. We then applied the principle of time-cure superposition to ascertain the nature of the gel point. Although various alternative approaches exist to apply time-cure superposition, we proposed a new, straightforward method for unambiguous reshifting of the MSDs to a single master curve; i.e. we first determine the logarithmic slopes of the MSDs as a function of experimental time. Then, using theoretical predictions of the critical gel regime for a fractal like polymer growth, which resembles the self-assembly of our polypeptide network, we constructed master curves which span the entire melting and gelation process by shifting MSD curves obtained at discrete curing times. This allowed us to unequivocally identify the gel and melt regimes and, hence, the location of melting or gelation point in time. The critical exponents of both melting and gelation are the same, indicating the same pathway is followed through phase space during this inverse transformation. However, the concentration dependence of gelation is much stronger than that of melting; this formed direct experimental proof of a previously postulated kinetic model that node-formation (gelation) requires exactly three dispersed nodes to come in close proximity for a stable triple helix to form. This is a third-order diffusion limited process which is extremely sensitive to end-

block concentration. By contrast, for melting to take place, existing triple helical nodes only need to disintegrate, which is a 1st-order reaction limited process with linear concentration dependence.

In the **Chapter 3** of this thesis, we have introduced a new tool to monitor supramolecular systems during co-assembly and self-assembly. Using polymer chemistry we have subsequently (in Chapters 4 and 5) tailored this method at the monomer level to increase the functionality and sensitivity of this novel approach. The tool we have developed and explored is a polymeric mechanosensor, obtained by the synthesis of a water-soluble polyfluorene homopolymer with a high density of pendant carboxylic acid groups along the main chain. In Chapter 3, we showed how this sensor can be used to quantitatively monitor electrostatic co-assembly with a simple coat protein, consisting of a cationic-neutral diblock polypeptide produced biosynthetically in a recombinant host. Polyfluorene in its native and semiflexible (amorphous) state exhibits well known vibronic emission bands in the violet-blue region of the electromagnetic spectrum. Our charge-functionalized polyfluorene shows the same spectral features in aqueous solution, where the conjugated backbone has a coiled conformation with semi-rigid nature due to the charged side chains attached to the conjugated backbone. Upon introducing small amounts of protein into the solution of polyfluorene, we observe that the fluorescence emission intensity decreases due to binding; that binding occurs indeed is supported by light scattering experiments. Moreover, we recorded a gradual change in the vibronic bands of polyfluorene where the intensity from the lowest vibronic transition decays while the higher vibronic transition bands grow in intensity and develop well-defined peaks. These characteristic changes in the vibronic bands are attributed to a solution-equivalent of the β-phase of polyfluorene, in which the molecule adopts a planarized backbone conformation leading to increased conjugation. In our study, we have shown that the optical properties commonly found in thin films of polyfluorene can also be observed in aqueous solutions of anionic polyfluorene, when it binds cationic protein. As the protein coats the conjugated backbone, by binding with the cationic block, it creates a bottle-brush structure of neutral chains along the backbone, which stretch the chain into a planar configuration. In turn, this backbone planarization and stretching, alters the vibronic band structure of the anionic polyfluorene. By analyzing these changes in the fluorescence spectrum, we showed that it is possible to detect even low degrees of binding,

and to non-invasively measure the brush density from simple spectroscopy experiments. We confirmed the structural changes in the conjugated backbone by synchrotron small-angle *x*-ray scattering experiments where we observed a distinct transition from a semi-flexible coiled chain into a stiff ribbon-like structure. We also showed that upon adding salt the disintegration of the bottle brush occurs, with the reversal of changes in vibronic bands. Thus, these results present in Chapter 3 demonstrate the first direct use of a conjugated polymer as a mechanosensor for self-assembly processes due to its unique fluorescence sensitive to its own conformational change. In the follow-up study, presented in **Chapter 4**, we replaced the polypeptide with a synthetic diblock copolymer to create supramolecular micelles. Following the same experimental approach as in Chapter 3, we monitored the co-assembly of our polymeric sensor with a diblock copolymer. At low concentrations of diblock copolymer, we observed the same changes in structural and optical properties observed earlier for the coating with polypeptide: a transition from uncoated conjugated backbone to a coated, planarized and stretched backbone with characteristic β-phase vibronic bands. However, upon increasing the concentration, i.e., approaching charge stoichiometry, a featureless low-energy emission band emerged; we hypothesized that this could be due to a secondary structural transition which involves chain aggregation. To investigate this speculated bundling transition from single bottle brush objects into multimolecular condensed micelles, we designed a new diblock copolymer by incorporating an acceptor unit into the polyfluorene (donor) backbone. We tuned the ratio of acceptor-donor units in such a way that there is no appreciable intrachain energy transfer and resulting acceptor emission. At an optimized ratio of acceptor to donor the only change occurs when polymer chains come within close proximity and allow Förster resonant energy transfer (FRET) through the medium. By monitoring the changes in fluorescence emission bands with this new mechanosensor, we first detected the transition from isolated polyfluorene chains to coated and planarized chains, which occurs at polycation doses below charge stoichiometry. Subsequently, at high charge ratios close to complete charge neutralization, we for the first time unveiled the second step in electrostatic co-assembly toward condensed multimolecular micelle formation. While previously predicted to occur theoretically, this distinct condensation transition had not been observed in experiments. Our new mechanosensor polymer allows not only the detection of binding and disintegration of an

analyte by means of fluorescence quenching (monitoring charge driven co-assembly via the vibronic bands in fluorescence), but also probing the proximity of polymer chains inside a micelle, by the emergence of a new emission band. Thus, it is not only a vibronic mechanosensor but also a colorimetric proximity sensor.

In the last experimental chapter of this thesis, **Chapter 5**, we studied the self-assembly dynamics of a recombinant virus using our polymeric sensors. This protein is based on the same cation-neutral diblock copolypeptide as used in Chapter 3, but features an additional polypeptide block which can self-assemble laterally into stacks of β-rolls. This provides strong cooperativity to the self-assembly process, which is predicted to result in distinct nucleation-and-growth kinetics of the virus particle formation. We monitored the fluorescence emission bands of our polyfluorene sensor in time over several days after addition of coat protein at various concentrations, by recording a luminescence spectrum every few minutes. Unlike the previous supramolecular systems that we have studied, this system undergoes templated (exceptions occur) self-assembly such that the template is the sensor polymer. Once the conjugated polymer is encapsulated within this protein "capsid", the vibronic emission bands again exhibit their unique changes as observed in the previous chapters. Using a two-state model we were able to use the vibronic shifts to directly determine the fraction of template coated by the virus capsid protein This unveiled a typical nucleation-and-growth mechanism as evidenced by a nucleation lag time which strongly depends on concentration. Using the proximity sensor we were also able to provide evidence of weak chain collapse within the protein capsid. Finally, we have found experimental evidence that there is competition between templated (co-assembly) and non-templated (self-assembly) formation of virus-like particles. This complexity emerges due to the competition between electrostatic binding between protein and template, and self-binding of proteins mediated by the silk-like β-roll structures. We find out that, towards the end of the growth process, part of the protein that initially decorated the sensor polymer is scavenged by self-assembled empty capsids in solution.

About the author

Emine Hande CINGIL was born on the 30th of July, 1985 in Kayseri, Turkey. Being the latest member of a modern-day nomadic family, she had lived in various towns and cities throughout Turkey during her entire childhood. When her parents decided to settle down for a long period (7 years) in Canakkale, she finally had the feeling of a "hometown" and the first time an uninterrupted school education. At the age of 18, she moved to Istanbul to join her dream university, Sabanci University where she chose to study Materials Science and Engineering simply to make "useful materials". She worked closely with dr. Cleva Ow-Yang on the synthesis and characterization of ZnO nanoparticles. During her undergraduate education, she was selected as the only participant from Turkey to join an international nanotechnology workshop organized by Nobel laureate prof. Roald Hoffmann and lectured by prof. George Whitesides in Alexandria, Egypt. Thanks to prof. Whitesides and her nomadic blood, couple of months after the workshop she left for U.S.A to do her undergraduate internship in the research group of prof. Jennifer Lewis in University of Illinois at Urbana-Champaign. There she worked closely with dr. Jacinta Conrad to study flow behaviour of colloidal gels in microchannels using confocal microscopy. Once the nomad was awaken it was impossible to stop, so one year later Hande found herself doing her masters study in University of Sheffield in United Kingdom. She performed her MSc thesis research on conductive polymers in the Polymer Chemistry Group of prof. Steve Armes. Then she moved to the Netherlands with the decision to do a PhD. Initially she started her PhD research as a Marie Curie Fellow in the Free University of Amsterdam in Biophysics group of prof. Rienk van Grondelle to investigate energy dissipative mechanisms in photosynthetic systems of diatoms with stark fluorescence spectroscopy. After 14 months long biophysics adventure, she left Amsterdam and started her final PhD research to study biopolymers under the supervision of dr. Joris Sprakel and prof. Martien Cohen Stuart in Physical Chemistry and Soft Matter group of Wageningen University. After four years with four completed research projects, she finished her PhD research. Nowadays the nomad in her pushes her to go for new challenges in new places despite of a settled other half.

List of publications

This thesis

- Hande E. Cingil, Wolf H. Rombouts, Jasper van der Gucht, Martien A. Cohen Stuart, Joris Sprakel. Equivalent pathways in melting and gelation of well-defined biopolymer networks. *Biomacromolecules* **16** (2015), 304-310, doi: 10.1021/BM5015014.
- Hande E. Cingil, Ingeborg M. Storm, Yelda Yorulmaz, Diane te Brake, Renko de Vries, M. A. Cohen Stuart, Joris Sprakel. Monitoring protein capsid assembly with a conjugated polymer strain sensor. *Journal of American Chemical Society* **137** (2015), 9800-9803, doi: 10.1021/JACS.5b05914.
- Hande E. Cingil, Emre B. Boz, Junyou Wang, Martien A. Cohen Stuart, Joris Sprakel. Probing nanoscale co-assembly with dual mechanochromic sensors. *Advanced Functional Materials* **26** (2016), 1420-1427, doi: 10.1002/ADFM.201504632
- Hande E. Cingil, Emre B. Boz, Renko de Vries, Martien A. Cohen Stuart, Joris Sprakel. Mechanochromic molecular sensors reveal complexity in the self-assembly of virus-like particles *in preparation*.

Other work

- Md.Wahadoszamen, Hande E. Cingil, A. Ghazaryan, A. M. Ara, C. Buechel, R. van Grondelle, R. Berera. Stark fluorescence spectroscopy reveals two emitting sites in the dissipative state of FCP antennas. *Biochimica et Biophysica Acta-Bioenergetics* **1** (2014), 193-200, doi: 10.1016/j.bbabio.2013.09.001
- Hande. E. Cingil, Jennifer A. Balmer, Steven P. Armes and Paul S. Bain. Conducting polymer-coated thermally expandable microspheres. *Polymer Chemistry* **1** (2010), 1323-1331, doi: 10.1039/C0PY00108b.

Acknowledgements

Obviously doing a PhD research is a challenge; however finding the correct research topic and the group was a bigger challenge for me. To be exact in date, I spent 2 years in the "finding" process. Even though I was in Amsterdam and could find various opportunities all the way from Singapore to USA for a PhD research, I still didn't know about the existence of chemistry related groups in Wageningen University which was to my knowledge one of the top agriculture and plants science related university in the world. It was first thanks to **dr. Arzu Colak** for simply opening my eyes about Wageningen University (and being a sister not by blood but by heart) and then to **dr. Burak Eral** for encouraging me to work with prof. Martien Cohen Stuart (with his own words) in "one of the top physical chemistry groups in the Netherlands", I found myself here in Wageningen.

Starting from the day of my interview until now, my extended gratitude is for **prof.dr. Martien Cohen Stuart** and for **dr. Joris Sprakel**. Even though we had quite an exceptionally interesting interview which gave you the impression that I didn't want to get the position but nonetheless you offered and I am truly thankful that you could see the potential in me even in those days and gave me the opportunity to work with you and learn from you. Dear Martien and Joris, I was very lucky to get to work with both of you. I truly believe that you complement each other in the way you do science and handle difficulties along the way. **Martien,** I'm especially thankful for your patience, encouragement and help in the completion and publication process of my most problematic chapter, as well as for your understanding, trust and approval when Joris and I wanted to change the direction of research towards conjugated polymers. You were very open-minded for new trials, very valuable by bringing your expertise related with micelles, protein polymers and scattering methods into the brand new topic of physical chemistry group "conjugated polymers". In every project, your suggesting certainly brought up the quality of our work. Without your constant support and assurances during difficult situations and times, I could not have succeeded finishing this PhD period**. Joris,** I'm thankful to you for many things but for me the most important one is that you not only gave me a PhD position but also two years later in

this position you actually opened the doors for me to work on something I passionately like and something that could connect my previous research experience with the current PhD. It's like finding your long lost path in a jungle. Even though the time was running out and the task was very tough, we have managed to complete three very pretty and high quality research papers in one year, all thanks to your help even in your weekends and holidays. Sending you graphs and receiving a response in the midnight is not something unusual. Having you, a very hard-working supervisor, motivated me to work even harder. Despite of your young age, having broad range of research interests helped us tremendously to reach a wider audience for our polymer sensors. I will never forget this memory about the game changer comment of a professor to my first project related with polyfluorene work in Singapore workshop. The comment came at a time when we were happy with the results but not yet attributed those results to the sensor function of our polyfluorene and his question of "now what will you do with this amazing tool?" could not be interpreted until I told this comment to you. I remember your email only after couple of days, saying "yes, we have an amazing strain sensor". It was indeed a game changer and we shaped the first paper and also my further research with conjugated polymers accordingly. This memory is always vivid in my mind and your approach to that single comment by taking it very seriously, thinking about it and in the end your enthusiasm…just shows me a passionate supervisor and scientist who truly influenced my PhD research.

Dear **Cleva**, first in Sabanci then in Sheffield and later on during all the adventures in the Netherlands, more than 10 years now, you were always there…I was just an incredibly lucky person to start my journey in materials science with you, and since then you have never left me alone with obstacles but gave me the biggest support. You were in London; you were in Amsterdam even for a short trip yet arranging time to meet with me. I remember the days that I received your MIT course notes to my mail sent all the way from Istanbul or receiving CVs of brilliant undergrads after you told them Hande wanted to have a summer intern. I'm truly thankful that you have touched my life both academic and personal, without you many things wouldn't be possible.

Dear **Frank,** during the first two-years of my PhD especially the times of microrheology research, you were the biggest support by being an amazing rheology expert, helping with

the setup, helping with every single detail and problem, discussing about all the flaws of doing microrheology and most importantly being a genuine friend. I'm truly thankful. **Dimitry,** such a helpful and cheerful person you were. I remember all your help related with high-speed camera, MATLAB and particle tracking. Thanks a lot. And now my research collaborators, dear **Thao,** you were always so generous with your help. When I needed to purify proteins, when I needed ideas for the next project, for the next experiment, when I needed different proteins you were always there with your expertise in protein polymers. Thank you for being an amazing scientist who made things easier for me and many people in the lab and continued to emotionally support me even after leaving fysko. **Yelda**, I'm glad that I was your internship supervisor. During the polymer synthesis period, long hours of glove-box experiences, rota-vap sessions, light scattering titrations you never lost your positive and cheerful attitude. I will never forget your singing and dancing alone at around 7 p.m. in the light scattering room in a completely empty fysko building (except Inge of course) and an empty stomach while waiting for the next scan. **Diane,** I'm thankful for your helpful attitude both towards me and to my student Yelda during our struggle with conjugated polymer synthesis; and for all those GPC analysis. **Remco**, your expertise in scattering methods and help during the analysis were very valuable and I appreciate all the time you spent on my projects. **Junyou,** from the very first day till the last you were always very polite and helpful. It had been so long that I wanted to combine your expertise in diblock copolymers with conjugated polymers and finally in my last year we managed to collaborate. I'm glad you were still around. **Emre**, many thanks to you my dear by forcing me to carry my phone everywhere I go, just to be able to answer your questions from Whatsapp. No, seriously I'm very thankful for all your hard-work, all your smart solutions, for being focused and very organized (at a level of even criticizing my organized documents). We had a very memorable and productive summer together. And last but not the least, **Inge,** I'm not only glad to have you as a close friend but also to get to work with you, collaborate with you. Not all friends can get on well when it comes to work. But I believe we have proven it to ourselves that whatever we do together in/out of the lab, we do it with ultimate understanding, respect and support. All those long and tiring trips in the trains, sleepless nights during SAXS measurements in Grenoble, late hours in the weekdays and weekends in a completely empty fysko became bearable with your company. We

struggled, worked hard, laughed, cried and worried together yet finally managed to welcome the year 2016 together you, me and Pamuk, Thanks for always being there.

My dear **Helene,** I'm very thankful and happy to have your friendship and for all those memorable moments we shared together. You were always very thoughtful, very emotional and supportive. And I know wherever I go; you'll always be on the other side of the phone line. Dear **Goshia**, I'm glad that I relocated my office and lab space because it was only after then I got to know you better. We discussed about how to combine your work with my work for hours and we still don't know the answer; how to survive in our antisocial PhD struggle and we somehow managed; and how to handle our multinational and multilingual relationships and the work is still in progress. Thanks for your supportive friendship. **Kamuran,** we have met in fysko but we shared more out of fysko. Thank you for being a genuine friend and 155 Kamu of our lives. **Josie,** I am thankful for all the things you had done for me back in those difficult days. I will always remember your lovely laughter and motherly hug. Dear **Mara**, by being one of the most fashionable persons I have ever met, you shine like a star and that lightens up my day. Thank you for creating such a nice ambience in fysko and for all your help during the last 4 years.

I would like to also remember all the past and present members of Fysko: Jasper, Marleen, Joshua, Frans, Renko, Mieke, Hans, Anton, Christian, Yunus, Sabine, Soumi, Lennart, Wolf, Goshia W., Marcel, Monika, Natalia, Merve, Hannie, Ilse, Joanne, Lione, Hanne, Ties, Jeroen, Ruben, Pieter, Huanhuan, Maarten, Jan Maarten, Aljosha, Anita, Bert and from BioNT group: Aldrik, Vittorio, Jan Bart and Maria. Thank you all for nice memories.

My lovely **Elise,** honestly you're a sister by bond. You encouraged me to get a PhD before going for industry. After four years, I'm very thankful for your suggestion, for keeping in touch always, for your thoughtfulness about the well-beings of my family members with every bad news coming from Turkey and finally coming all the way from UK with **Stephen** for the defense ceremony of this thesis. I'm so lucky to have you both.

And finally we have reached to the VIP part of my life, **Eric**; simply, I'm very thankful that you were a very stubborn guy, very stubborn in loving me even in the most unlovable times. You brought me the cutest thing in the world, my lovely Pamuk. I hope we have many years ahead all together.

Sevgili anne ve babacığım, 30 yıldır büyük bir özveri ve sabırla beni her durumda ve her kararda koşulsuz desteklediniz. Her başarının ardındaki gerçek güç sizin sarfettiğiniz bu emeklerdir, çok teşekkür ederimç Benim bu hayattaki en büyük şansım sizlersiniz. İyi ki varsınız.

Yoncam, benimle birlikte sen de ikinci doktoranı bitirmiş oldun. Kendi deneyimlerinle saatler boyu skypetan bana yol gösterici oldun, o da yetmedi minik Pamuk u saatlerce gözlemleyip hastalık teşhisi koydun. Şimdi de binbir türlü zorluklarla bu tezin savunmasında yanımda olabilmek için geldin. Tüm bu fedakârlıkların için sana çok teşekkür ederim. **Murat ağabeyciğim**, doktora serüveni başladığından beri bıkmadan usanmadan verdiğin çok değerli öğütler, anlayış ve desteğin için çok teşekkür ederim.

Goncam, bilim aşığı ablacığım. Posterimin karşısında fotoğraflar mı çekmedin, sabırsızca protein polimer projeleri mi dinlemedin, olaylara tıpçı gözüyle yaklaşıp fikir vermeye mi çalışmadın. İyi ki varsın, her türlü desteğin için minnettarım. **Meymoşcuğum,** ablamı her Hande dediğinde fırsatları yaratıp yanıma getirdiğin, uzakları ulaşılabilir yaptığın, her konuda bitmek bilmeyen desteğin için çok minnettarım.

Pamusum, if there was one more being who felt the meaning of writing this thesis, it should have been you. Lucky to have your smiling eyes.

Overview of completed training activities

Discipline Specific

International School on Rheology	Leuven (Belgium)	2013
Advanced Soft Matter; MSc Course	Wageningen (the Netherlands)	2013
Physics at FOM*	Veldhoven (the Netherlands)	2013
The Physics of Soft and Biological Matter, IOP*	Cambridge (United Kingdom)	2014
NWO CHAINS Conference‡	Veldhoven (the Netherlands)	2014
KNCV Dutch Polymer Days‡	Lunteren (the Netherlands)	2015
Polyelectrolytes in Chemistry, Biology and Technology Workshop*	Singapore	2015
Elsevier Frontiers in Polymer Science*	Riva del Garda (Italy)	2015

General

Information literacy including EndNote introduction	Wageningen	2013
Project and time management	Wageningen	2013
Scientific publishing	Wageningen	2014
Effective behavior in your professional surroundings	Wageningen	2015
Career perspective	Wageningen	2015
Survival guide to peer review	Wageningen	2015
Brain Training	Wageningen	2015

Optionals

Preparation of research proposal	Wageningen	2012
Colloid Science; BSc Course	Wageningen	2013
PhD study trip	USA	2013
Group meetings and colloquia*	Wageningen	2012-2016

* poster presentation, ‡ oral presentation

The research described in this thesis was financially supported by European Research Council Advanced Grant Bio-Mate (ERC-267254).

Cover design: E. Hande Cıngıl & Eric M. M. Tan

Printed by GVO drukkers & vormgevers B.V., Ede, The Netherlands